Hybrid Tin Based Nanostructures Wrapped with Graphene as Efficient Anode Material for Lithium Ion Batteries

by

Qianqian Hu

A thesis
presented to the University of Waterloo
in fulfillment of the
thesis requirement for the degree of
Master of Applied Science
in
Chemical Engineering-Nanotechnology

Waterloo, Ontario, Canada, 2015

AUTHOR'S DECLARATION

I hereby declare that I am the sole author of this thesis. This is a true copy of the thesis, including any required final revisions, as accepted by my examiners.

I understand that my thesis may be made electronically available to the public.

Abstract

Recently, many developments in the electric & hybrid electric vehicles, and in the electronic devices, have resulted in an increasing demand for high power and high energy density lithium-ion batteries. The current commercial anodes based on graphite cannot meet the demand. Tin sulfide (theoretical specific capacity: 665 mAh/g) has been predicted as a potential anode material. However, its poor conductivity and large volume change during charge and discharge results in large irreversible capacity, leading to poor cycle performance. On the other hand, graphene has emerged as a new material with superior conductivity, good flexibility and extraordinary stability. In this work, we prepared tin sulfides with tuned morphology and composition which is supported by and wrapped with sulphur and nitrogen doped graphene (GSN). These nanostructures were prepared by solvothermal synthesis followed by controlled heat treatment. The as-synthesized material was found to be comprised of stannic sulfide (SnS_2) crystals grown and wrapped with doped graphene. Interestingly, the SnS_2 crystals are formed as ordered structure in the shape of hexagonal sheets. After that heat treatment the hexagonal nanosheets of SnS_2 were transformed to rod-like structure with chemical transformation to stannous sulfide (SnS). In terms of electrochemical performance, both materials have first cycle charge/discharge capacities, which exceed the theoretical values. However, the heat treated material is more durable, which was able to maintain a charge capacity of ~ 870 mAh/g for more than 100 cycles at the rate of 0.1 A/g. At a high current density of 0.5 A/g, it can also keep 1500 cycles with a reversible capacity of ~ 550 mAh/g, which showed the longest cycle life among tin based materials reported in the literature. Inspection of the results reveals that tin sulfide/graphene based nanocomposites with improved energy densities and capacities than commercial graphite can make a significant impact on the development of new batteries for electric vehicles and portable electronics applications.

Additionally, incorporating a binder into the electrode structure is vital to achieving practical lithium-ion battery performance, as it is used for improving stability. In this thesis, a new binder is introduced. Polyacrilonitrile(PAN) as a binder with no conductive additives is applied in as-prepared SnS_2/G.After low temperature heat treatment which is beyond glass transition temperature, PAN physically rearranges the construction of the electrodes. It is advantageous for volume expansion with plasticity. Synergistic effects between doped graphene and PAN does contribution to significantly enhanced cycling durability. Also, a new mechanism for chemical reaction during charge/discharge is proposed due to the obtained twice higher capacity than the calculation based on traditional principle. In terms of cycling performance and rate capability, SnS_2/G/PAN with low temperature heat treatment exhibits excellent results: there is a reversible capacity around 1200 mAh/g after 60 cycles without no obvious decrease in capacity from the initial cycle at the current density 0.1 A/g; after 150 cycles, at a higher current density of 0.25 A/g, the capacity is stable at 1000 mAh/g and the columbic efficiency is still 100%.

Acknowledgements

The work reported herein was financially supported by the Nature Sciences and Engineering Research Council of Canada and University of Waterloo.

The author would like to thank the tremendous guidance and assistance of my supervisors Dr. Zhongwei Chen and Dr. Aiping Yu in my master's studies.

Special thanks go to my colleagues including, Fathy Hassan, Xiaolei Wang, Ge Li, Ji Yan, Wook Ahn, Jingde Li, Xiaogang Fu, Xinglong Ma, Xingye Fan, Hao Liu, Drew Higgins, Hadis Zarrin, Moon Gyu Park, Ja-Yeon Choi, Ariful Hoque, Yun-seok Jun, Jared Lenos, Dongun Lee, Gaopeng Jiang, Rasim Batmaz, Raihan Ahmed, Abdul Rahman Ghannoum, Abel Sy, Gregory Lui, Guihua Liu, Min Ho Seo, Pouyan Zamani, Salah Abureden and Zhiyu Mao for their assistance and support.

Table of Contents

List of Figures

List of Abbreviations, Symbols and Nomenclature

LIBs	lithium ion batteries
DMC	dimethyl carbonate
EC	ethylene carbonate
g	gram
V	potential window
NMP	*N*-methylpyrrolidinone
SEM	scanning electron microscope
TEM	transmission electron microscope
TGA	Thermogravimetic analysis
XRD	X-ray diffraction
XPS	X-ray photoelectron spectroscopy
PAN	polyacrinitrile (PAN)
CMC	sodium carboxymethyl cellulose (CMC)
PAA	poly arctic acid
EDS	Energy –dispersive X-ray Spectroscopy
DEC	diethyl carbonate
LTHT	low temperature heat treatment
CV	Cyclic voltammetry
EIS	Electrochemical impedance spectroscopy
GO	Graphene oxide
EG	Ethylene glycol
SEI	Solid electrolyte interphase
2D	2 dimensional

Chapter 1

Introduction to lithium ion batteries

1.1 Background of lithium ion batteries (LIBs)

In the last few years, there has been tremendous industrial and technological growth, directly sparking the fast growing consumption rates of primitive energy sources like fuel. It has resulted in the whole world falling into severe energy crisis and environmental issues. In this case, batteries as renewable energy storage devices attract more and more attention as replacements of natural sources.[1, 2] LIBs as energy storage devices with certain advantages have attracted researchers' notice. Compared with other batteries, like Ni-MH, Pb-acid batteries as shown in **Figure 1**, LIBs are provided with characteristic merits: highest gravimetric and volumetric energy densities at the same scale. Furthermore, it has lower rate of discharge ,rather technical maturity and smaller size (6.94 g/mol)[3], which bring about convenience to humanity.[4, 5] It has been a long time since the first report on LIBs(LIBs),which was published by M.S. Whitingham in 1976.[6] It was demonstrated that the primary cell with lithium metal has a high theoretical capacity of 3860 mAh/g but unsafe. A breakthrough happened in 1991 when Sony Company pushed off LIBs in commerce, which used graphite as anode and $LiCoO_2$ as cathode and the operation voltage is 3.7 V, which delivered a capacity and power around 150 Ah/kg and 200 Wh/kg.[4, 7] Since then, LIBs have evolved with new material chemistry, nanotechnology, and polymer electrolytes with enhanced stability and higher energy density.

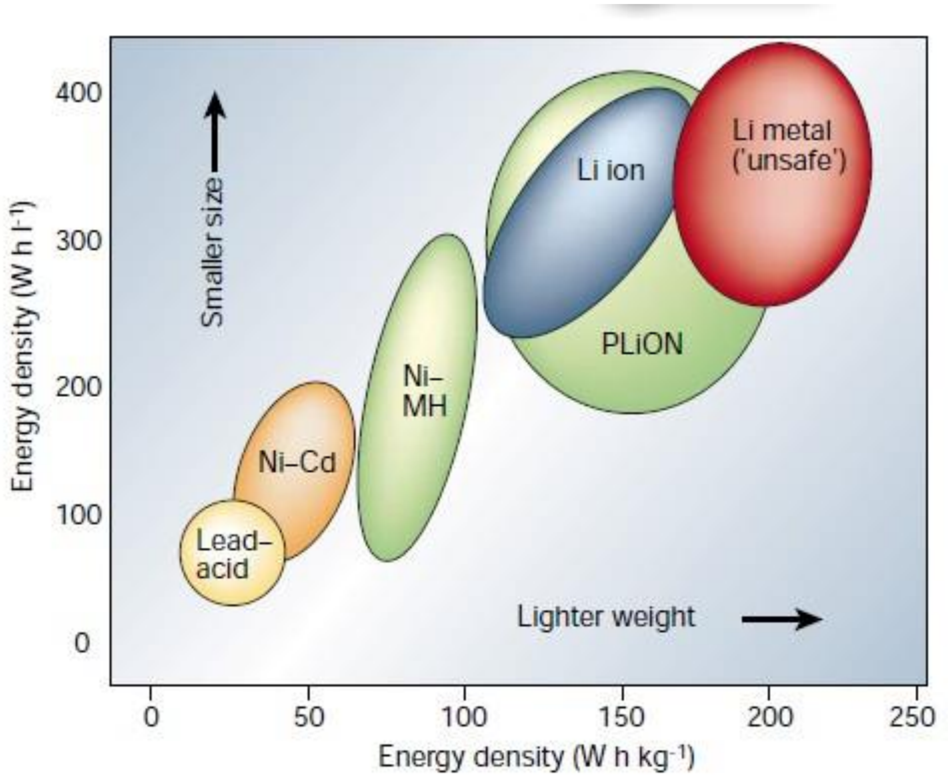

Figure 1： Comparison of different types of batteries in terms of gravimetric and volumetric energy density [3]

1.2 Current status of LIBs and next generation of LIBs

Renewable energy is essential resource for modern society for the over consumption of the fossil fuel, leading to the energy and environmental crisis. Current renewable energy like solar and wind power (**Figure 2**) is negatively impacted by the weather, which is intermittent and uncontrollable. LIBs as energy storage devices come into sight which is suggested as a major application in the widespread use of HEV and EVs in the future.

The first generation of LIBs uses $LiCoO_2$ as cathode and graphite as anode, which can store much more energy than that of nickel or lead batteries. Later, due to the demand for higher energy density, power density and lower cost energy storage devices, there are persistent achievements for the electrode materials, like $LiFeO_4$,[8] $Li_4Ti_5O_{12}$[9].Yet, the investigations for improving the battery performance still need more work on discovering the novel electrode material that is suitable for the cycling with enhanced energy density and power density. For the next generation of LIBs, it is necessary to develop low-cost, sustainable and greener LIBs with improving safety, reliability, durability, energy density and capacity.

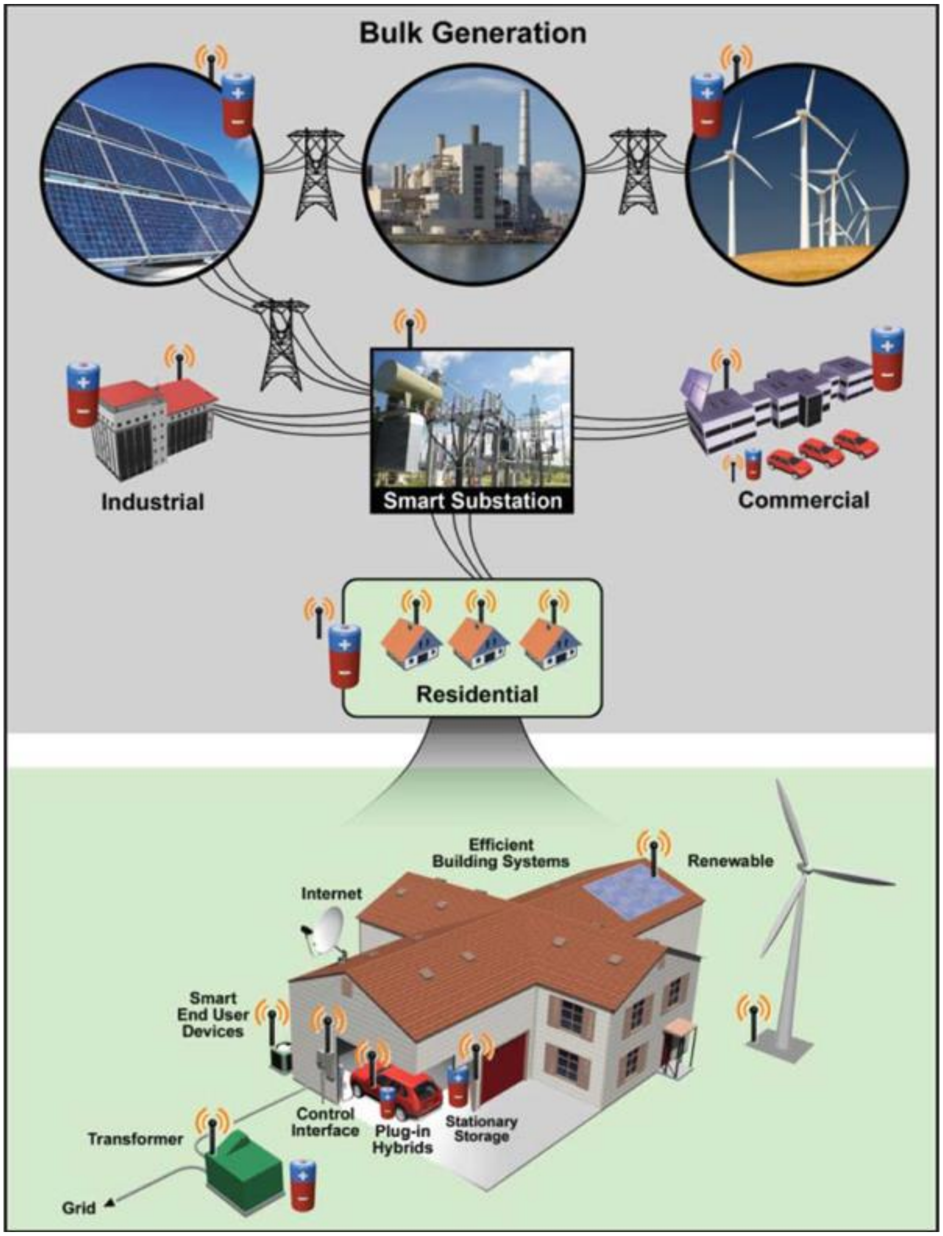

Figure 2： Electricity storage applications the future customers [10]

1.3 The principle of lithium ion batteries

Recently, over growing concerns about environmental pollution and a lack of fossil fuel have provoked a great demand for eco-friendly and renewable energy storage devices, which is important for the advancement of portable electronics and for the future guidance of electric vehicle. LIBsas one of secondary batteries, which means lithium ions moves between positive cathode and anode when LIBs are discharging and charging, have developed rapidly over the last decades. As for a complete LIB battery, it always contains an anode and a cathode, a polypropylene membrane separator used for electrical insulation and an electrolyte of $LiPF_6$ dissolved in organic solution with different ratios e.g. ethylene carbonate (EC), dimethyl carbonate (DMC). For example, in traditional applications, $LiCoO_2$ and graphite are used for cathode and anode as shown schematically in

Figure 6.[36] It can be seen that Li^+ ions leave the anode and intercalate into the crystal structure of the cathode material during the discharging process. However, during the charging process, Li^+ ions move from $LiCoO_2$ to intercalate into the graphite due to the applied electrochemical potential. Through the whole process, only Li^+ ions move between anode and cathode. The following is the chemical expression of typical lithium ion batteries:

Anode: $Li_xC_6 \longleftrightarrow xLi^+ + xe^- + C_6$

Cathode: $Li_{1-x}CoO_2 + x\,Li^+ \longleftrightarrow LiCoO_2$

Overall reaction: $LixC_6 + CoO_2 \longleftrightarrow C_6 + LiCoO_2$

To identify a reliable lithium ion battery, there are several critical requirements as the following shown:[37]

1. High energy and power density to meet the demand of the market
2. A high stability for a battery at a temperature range for operation conditions
3. The battery must have a long cycle life, which means the electrodes should be stable, at the same time, providing reversible capacity with lowest losses.
4. The battery must be safe. It represents that the battery design needs to avoid leaking.
5. In terms of the cost of electrode materials, it should be low.

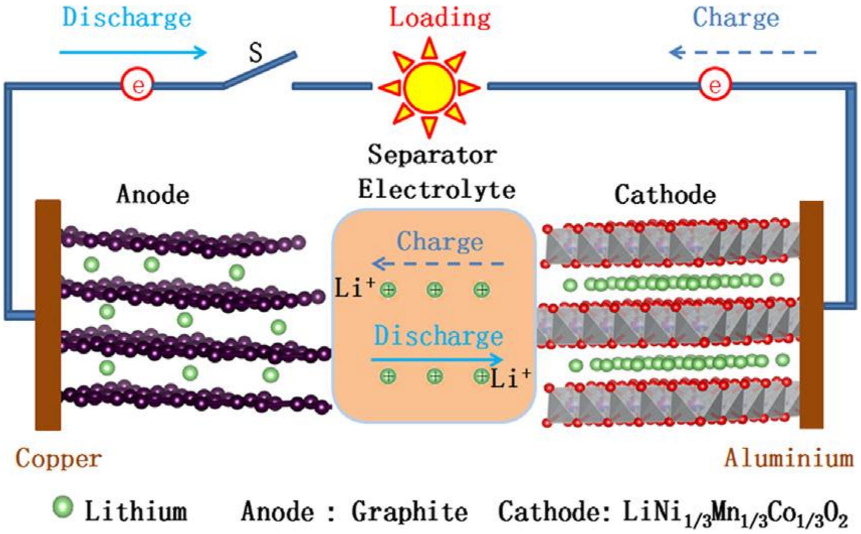

Figure 3 : Scheme of charge and discharge mechanism in lithium ion batteries.[36]

1.4 The challenges for lithium ion batteries

These days, nanomaterial used for LIBs has attracted researchers' sight due to the resistance of the electrolyte and the intrinsic diffusivity of the lithium ions in the solid state, which limits the application of LIBs. There are certain advantages and disadvantages for nanoelectrodes. By employing nanomaterial, it provides high surface area contact with the electrolyte and short paths for electron and lithium transportation. Meanwhile, compared with bulk material, nanomaterial may bring new reactions and it offers a broader space for lithium insertion/de-insertion. **Figure 4** shows the comparison between bulk and nanostructured α-Fe_2O_3 in terms of electrochemical performance. The size of large Fe_2O_3 particles is 1 to 2 μm while that of nanoparticles is 20 nm. It can be easily seen from the figure that 0.6 Li per Fe_2O_3 are reacted reversibly with nanoscale structure while only 0.05 Li per Fe_2O_3 experiences a reversible process, which demonstrates that nanomaterials sometimes undergo a reversible phase transition. Another prominent example is TiO_2, which is limited by electronic conductivity. Recent reports about enhancing the electrochemical performance are utilizing nanostructures with conductive materials, which have exhibited favorable results with the specific capacity of about 110 mAh/g at 30 C.[11]

Furthermore, except the merits that nanomaterials have exhibited, they also bring some problems in LIBs application. Generally, the synthesis of nanomaterials needs a complex process and the high surface area for nanomaterials result in unknown and unexpected reaction with electrolyte. At the same time, the apparent densities of nanomaterials are always low, which bring high loading electrodes' fabrication problems.

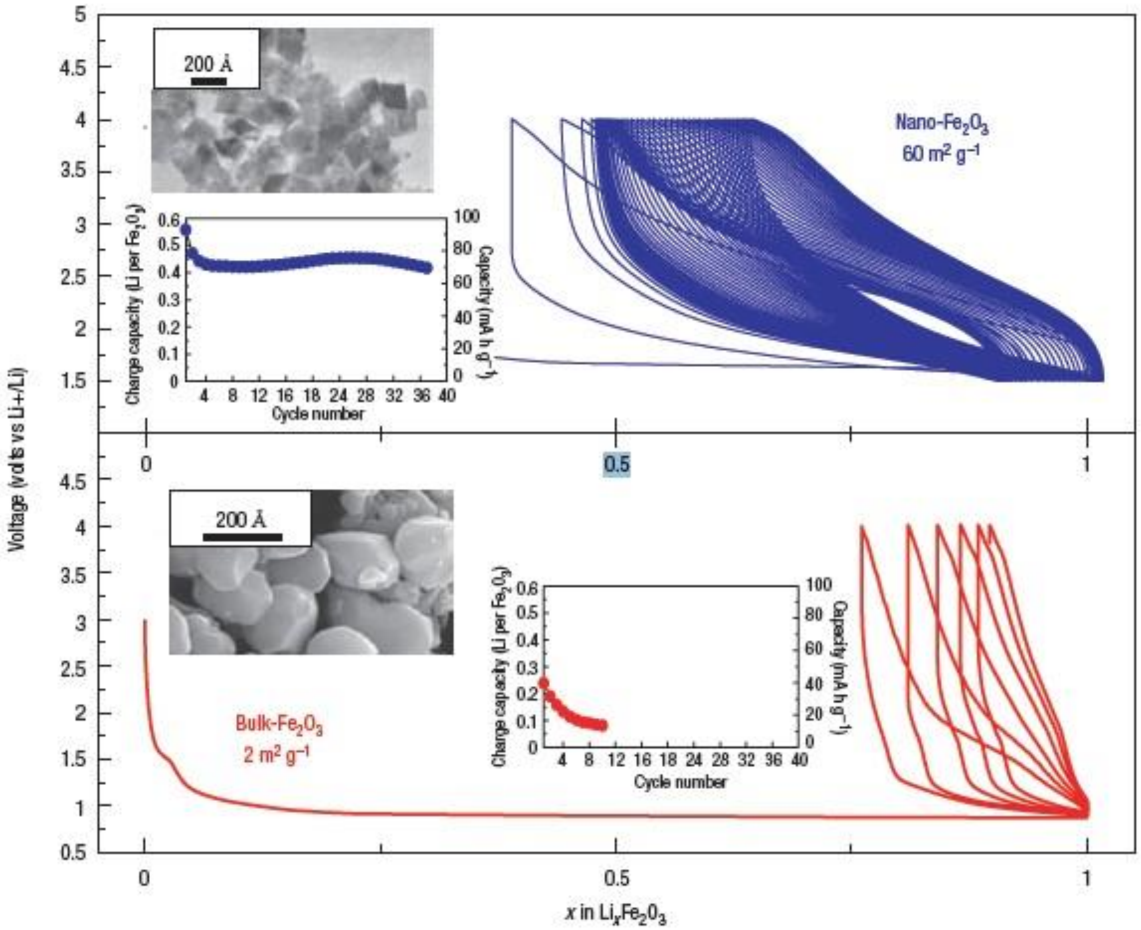

Figure 4: The comparison of bulk and nanostructured α-Fe2O3 with voltage–composition curves; the capacity retention and scanning electron micrographs of both samples are shown in the insets.[2]

Based on the mechanism of lithium ion batteries, the reversible Li^+ moves from an oxide host as the rechargeable cathode to carbon or buffered spongy silicon or tin as the anode host. During the first cycle, there is a passivating layer forming on the anode, which is referred to as solid electrolyte interphase (SEI) resulting from the reaction between the solvent of the electrolyte and lithium ions. This results in the reducing of the capacity and low current efficiency due to irreversible loss of Li^+ from the cathode. The formation process of SEI in different conditions is shown in **Figure 5.** From the process, it can be known that the SEI formation is related to the anode potential and electrolyte solvent. If the potential of graphite reaches nearly 0 V, there is a dangerous lithium metal deposition on the graphite surface as process e shown. To control it effectively, adding active additives in the solution is a good choice according to present published papers.[12-14]

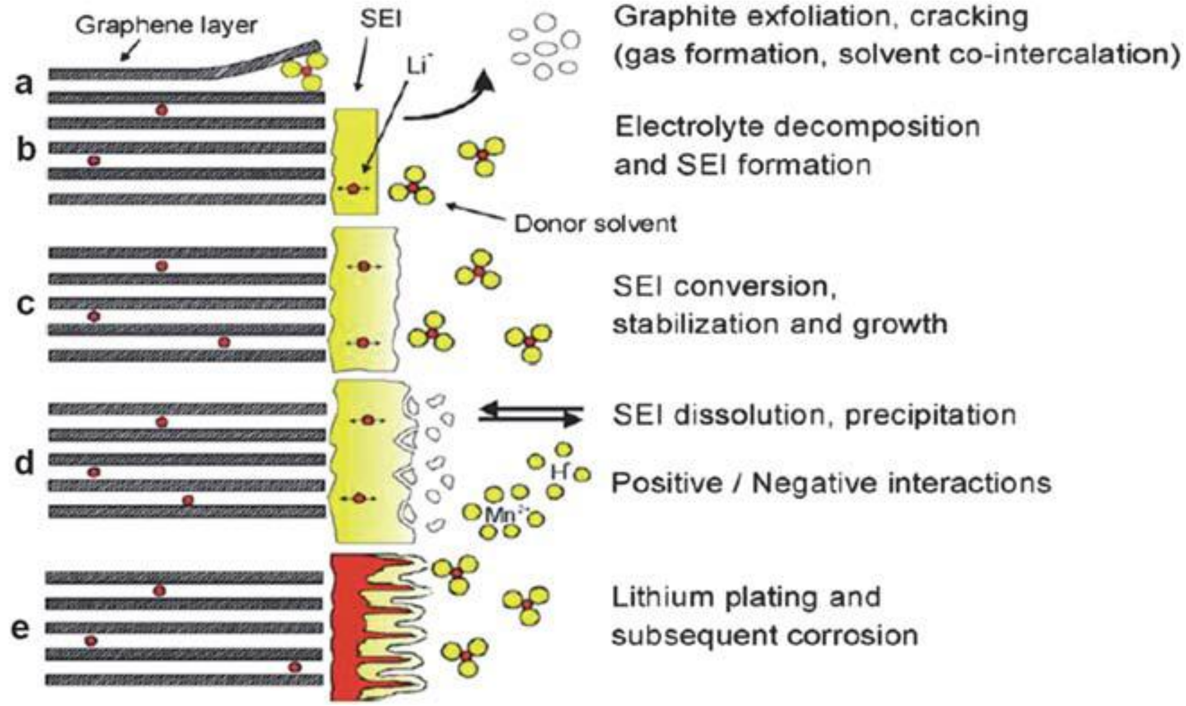

Figure 5: The mechanism of the formation of SEI and the comparison at different voltages[15]

At the same time, another challenge is that the new anode materials like Si, Sn, which show high theoretical capacities, in practical operation, undergo the volume expansion resulting in the damage of electrode and decrease of the specific capacities. Using silicon as an example, which has the highest theoretical capacity (4200 mAh/g) among the known anode materials, the volume expansion during charge / discharge process is around 420%. **Figure 6** shows the electrodes' degradation process. In the process, the volume expansion of Si electrodes results in the material pulverization and morphology change and volume change of the total electrodes, as well as the formation of SEI , which leads to electrochemical contact problems and final capacity fading .

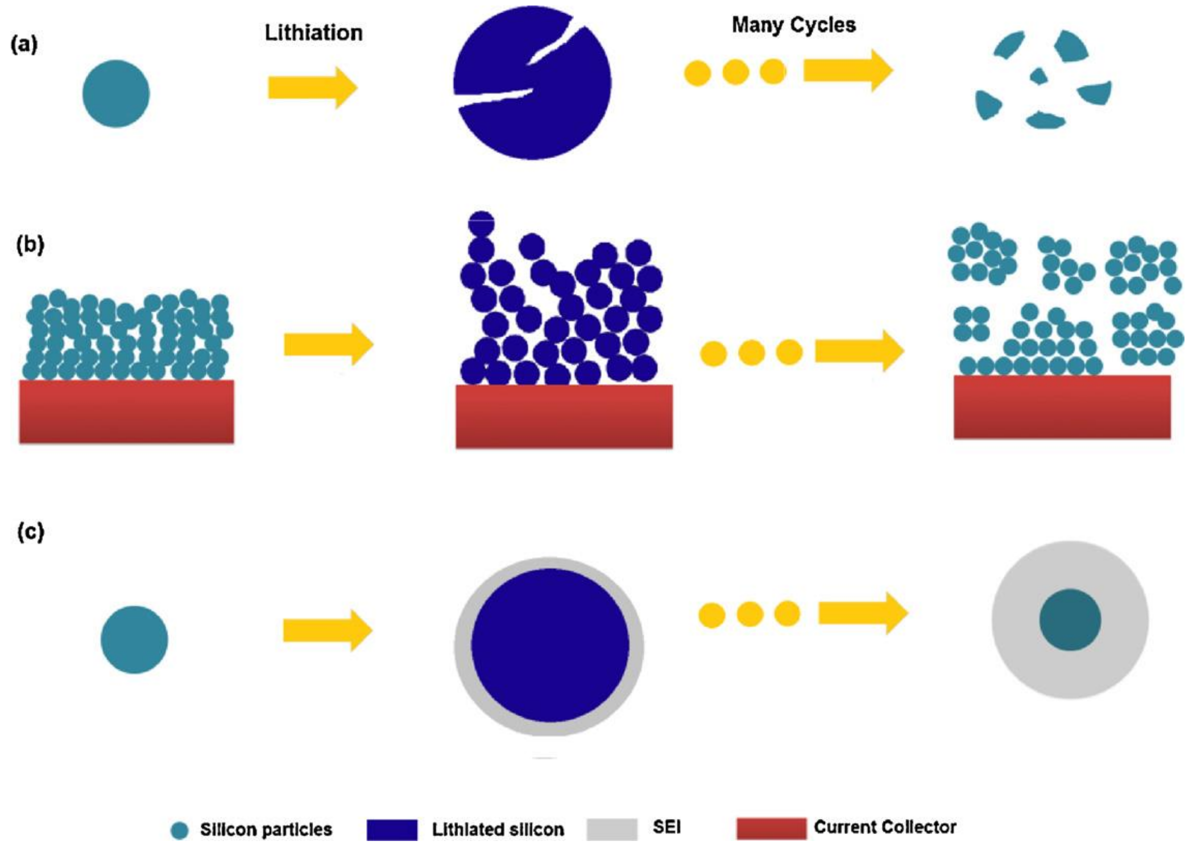

Figure 6 :The degradation for the silicon electrodes [16]

1.5 Tin based anode materials

Nevertheless, the current LIBs cannot satisfy the increasing demand for the applications of electronic products and electric vehicles.[7, 17] The researchers from the world are discovering substitutive materials in order to enhance the capacity and stability of LIBs. As for anode materials, commercially, graphite with specific capacity of 372 mAh/g leads to the limitations of practical uses. [18] The discoveries of new materials for LIBs are always continuing. Relative researches are mainly concentrated on the anode materials. Si, Sn with high theoretical capacities are appeared into the sight.[19-22] The materials during discharge/charge are both alloys and intermetallic compound, which have been explored as negative materials for LIBs for decades. Here, tin based materials are emphasized for the anode of LIBs. The specific capacity for tin based material is nearly two times higher than that of graphite even though it has relatively lower specific capacity than that of Si.[23-28] Based on tin based materials, there are still some challenges: the volume expansion and unstable solid electrolyte interphase during charge / discharge process directly results in the degradation of the electrodes, which brings adverse effect on the stability of the performance. [1, 15, 29]

Aimed at these problems, several approaches have been proposed: employing nanoscale tin based material to reduce the volume expansion; recombining the conductive material with it such as graphene, carbon nanotube.[30] Among tin based materials, tin sulfides have been a trend since they exhibited lower volume expansion and better rate capability than Si or tin material.[19, 31] Until now, several methods have been reported to optimize the structure of the tin sulfides, thus improving the electrochemical performance in LIBs. For example, combing graphene with tin sulfides offers accommodation for volume expansion during lithiation/delithiation.[32] By using hydrothermal method, SnSx nanoparticles wrapped with graphene retained a capacity of 860 mAh/g after 150 cycles.[33] A solution method with chemical vapor deposition process was used to transform tin oxide with graphene to SnS_2 directly by using H_2S as the sulphur precursor and delivered an initial capacity around 1600 mAh/g ,significantly exceeding the theoretical capacity.[34] A new solid – liquid – gas – solid (SLGS) was reported by Junjie Cai, who has prepared porous SnS nanorods on carbon. It suggested a novel hybrid nanostructure in energy storage devices.[35] The main concept on these methodologies is using conductive material to improve the capacity and stability. However, it is necessary to develop new concepts that decreases the cost and involves a novel design of the electrodes with significantly improving the electrochemical performance.

1.6 Electrode materials for anode

Nowadays, the applications of LIBs have been used in various electronic fields. Clearly, the requirements for acquiring the optimal electrodes' materials are sharply increasing. As for cathode materials, there are some limitations of new materials, which are confined by the mechanism of intercalation/ insertion of $Li^{+.}$ But for anode materials, the situation is quite different. The graphite is widely used as anode material in commercial industry, which has a limited theoretical capacity of 372 mAh g^{-1} forming LiC_6 composite. In addition to naturally occurring graphite material as anode, there are some other materials like carbon nanotubes and graphene, which have exhibited improved performance in lithium ion batteries. On the other hand, the explorations for tin, silicon and cobalt based materials in the applications of LIBs as anodes have never stopped. According to chemical reactions of negative materials with Li^+ ions, anode materials have been divided into three groups:

1) Intercalation/de–intercalation anodes. Example: Carbon based anodes such as graphite, etc.[38-40] In this type of anodes, lithium is stored between the graphitic layers. The mechanism is followed by the equation:[6, 41]

$Li^{+} + e^{-} + 6C \rightleftharpoons LiC_6$

Commercially, graphite is employed as anode material in lithium ion batteries. Actually, it is a typical layered structure, which contains graphene sheets stacking.[42] A schematic illustration of the intercalation process is shown in **Figure 7**. From **Figure 7(a),** lithium ions intercalate into graphene layers homogenously. And **Figure 7(b)** provides us an important phenomenon. The distance between the adjacent lithium ions on the graphene planes at stage 1 is √3, which is professionally called superlattice. [43-45]

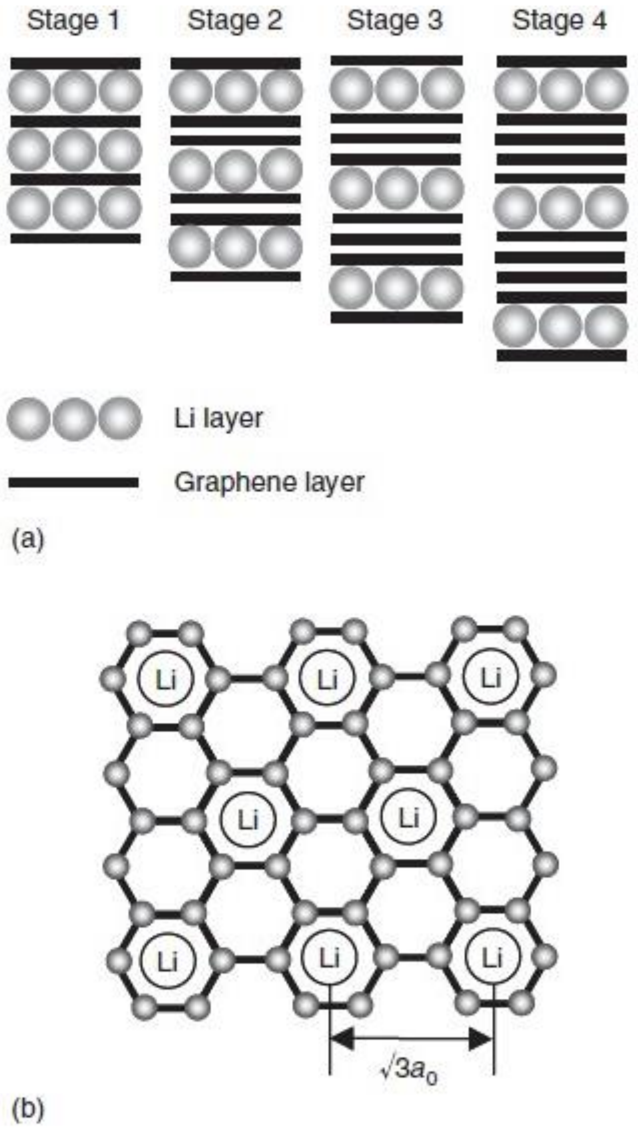

Figure 7: (a) Stage structure for lithium intercalation process; (b) Structure of stage 1 of lithium intercalation process [43]

2)Alloying/de-alloying anodes. It has been investigated that lithium can react with other elements which can take shapes of intermetallic components. For example, lithium can react with tin, forming $Li_{4.4}Sn$ that related to a gravimetric capacity of 948 mAh/g.[11, 46-52] During the discharge /charge process, Li^+ ions insert / de-insert into the material and form alloys as the following equation shown. [53, 54]

$$M + X\,Li^+ + Xe^- \rightleftarrows LixM$$

Figure 8 shows the morphology of silicon nanotubes and the electrochemical performance which is from literature.[55] Si has the highest specific capacity as anode material (4200 mAh/g), which corresponds to the formation of $Li_{4.4}Si$ during charge / discharge process. It can be seen from **Figure 8** that the obtained specific capacity for silicon nanotubes is ~600 mAh/g , which is attributed to the low conductivity for Si and large volume expansion and the formation of SEI during the charge / discharge process .

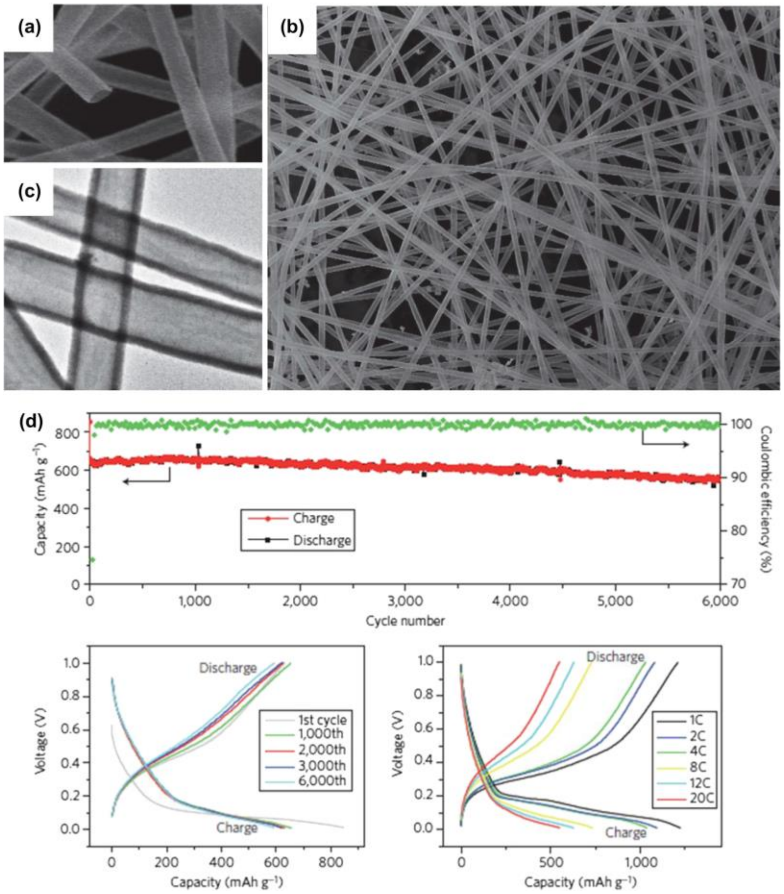

Figure 8: (a, b) SEM and (c) TEM images of double-walled Si-SiOx nanotube (DWSiNTs); (d) Electrochemical charge/ discharge cycling performance of DWSiNTs electrodes.[55]

3)Conversion reaction anode: transition-metal oxides are the typical examples like Fe_2O_3, CuO, etc. [56-61] The mechanism can be explained by the following equation :

$$2MxOy + 2y\,Li^{+} + 2ye^{-} \rightleftharpoons 2xM + 2y\,Li_2O$$

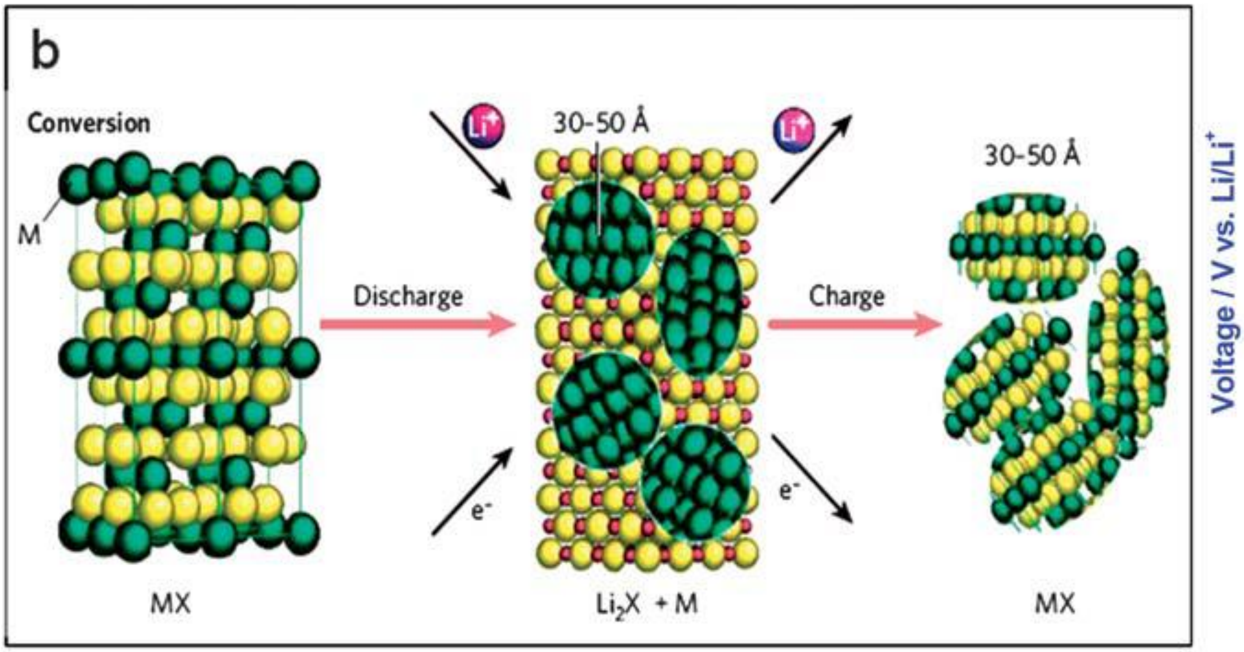

Figure 9: The illustration of conversion reaction.[15]

Our work is also focusing on the anode materials.[62] Recently, for anode materials, there are several requirements to qualify them: high capability, good stability, and excellent security. **Figure 10** displays recent anode materials with specific capacity. Compared with graphite; silicon, tin and etc. have exhibited higher specific capacity than that of commercial one. Currently, they are treated as potential anode materials for future applications in mobile electronics like laptops, mobile phones.

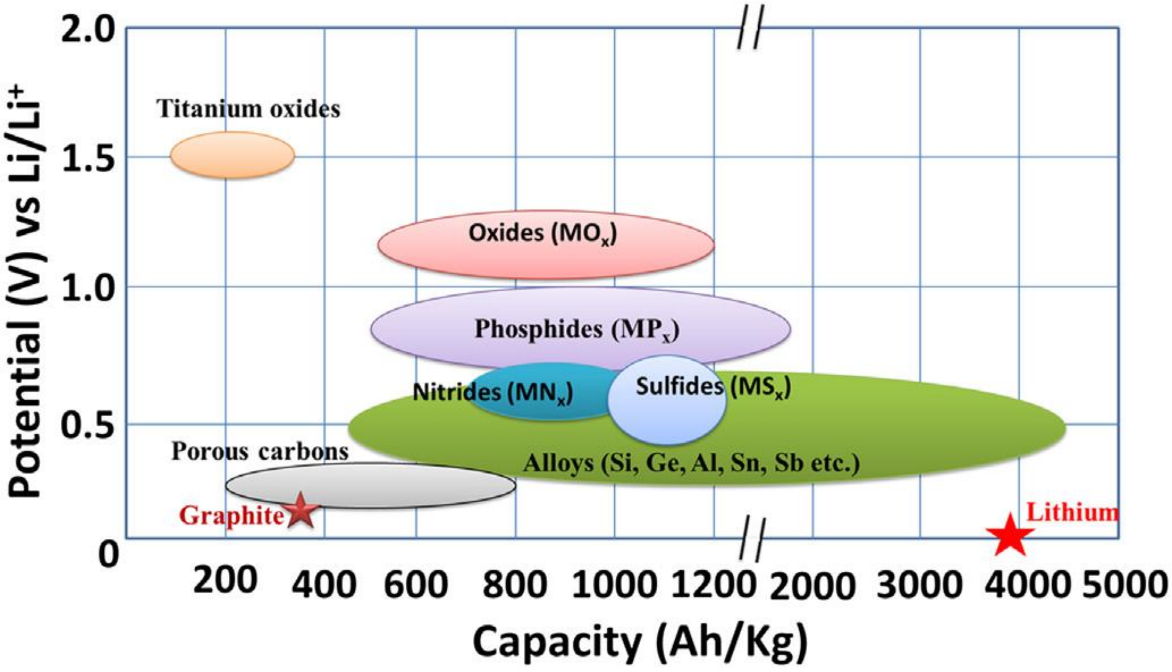

Figure 10: Schematic illustration for specific capacities comparison between the different types of anodes. [63]

And in **Figure 11**, it compares different anode and cathode materials with capacity and voltage. It can be seen that the voltage of cathode is always higher than that of anode, which results in the cell voltage. There are some potential materials whose voltage can reach more than 4.2 V, which is beneficial for new types of LIBs system.

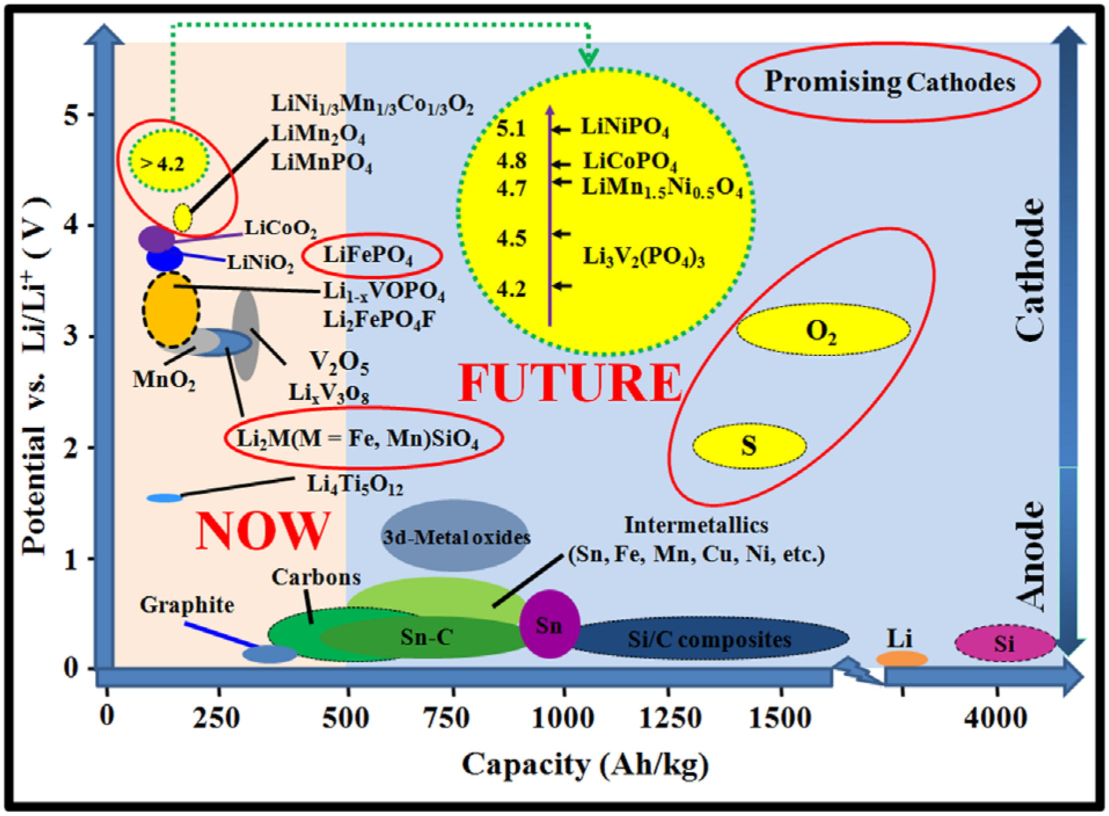

Figure 11: Illustration of electrode materials and corresponding electrochemical reduction potentials in current LIB technologies.[5]

1.7 Electrode for cathode material

Today, it is aimed to get cheaper, higher energy and more durable lithium ion batteries. Actually, cathode materials cost nearly twice higher than that of anode materials. The sluggish mechanism of Li^+ ions interaction with the cathode material has limited the number of cathode materials of significant promise. Based on the structure, it is classified the most popular cathode materials in three groups:

Layered structure: $LiMO_2$, where M is Co, Ni, and Mn, etc and compound of Li, Ni, Co, Al, O, Mn[64-67]; Orthorhombic structure ($LiFePO_4$)[68-72]; Spinel structure ($LiMn_2O_4$)[41, 45, 73-75]. These are discussed in detail as the following paragraphs.

1.7.1 Layered structure

Layered structure materials as cathode with a general formula $LiMO_2$, where M is Co, Ni, Mn, etc were discovered in 1980 by John Goodenough's group. [76] In this structure, both lithium and cobalt are octahedral coordinated by oxygen in alternating layers (**Figure 12**) where octahedrons are edge-sharing. Lithium cobalt oxide is generally used in practical applications. And when the reaction completely removes the lithium, the structure is reorganized as CoO_2.[77] When lithium cobalt oxide is charged to 4.2 V, the practical capacity is around 140 mAh/g while the theoretical capacity is around 272 mAh/g, which demonstrates that there is half lithium ions providing reversible capacity. Aimed at this phenomenon, there is one reasonable explanation: the phase transition and structure change during discharge / charge process results in the degradation of the electrode material.

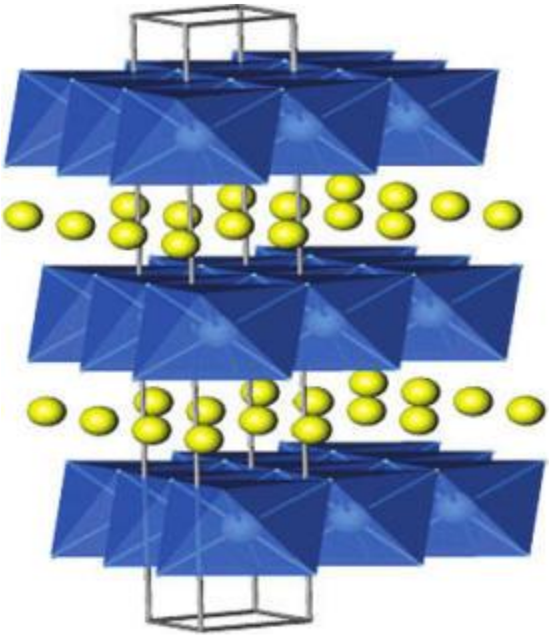

Figure 12: Layered structure of cathode material ($LiMO_2$, where M is Co,Ni,Mn,etc).[78]

1.7.2 Orthorhombic structure

$LiFePO_4$ is the most common cathode material with orthorhombic structure .In this structure, each Li and Fe is coordinated with 6 oxide ions in a octahedral structure and a tetrahedral structure of PO_4**(Figure 13).** Compared with $LiCoO_2$, it exhibits lower energy density while it discharges with a capacity of 170 mAh/g, which is even better than $LiCoO_2$. Also, it offers longer cycle life and better power density. To some extent, it is inherently safer. $LiFePO_4$ as a promising cathode material is abundant and eco-friendly. The use of phosphates stops cobalt's cost and environmental concerns, which particularly avoids care about cobalt entering the environment through improper disposal. The key barrier to allow $LiFePO_4$ to be commercialized is intrinsically low conductivity. Reducing the particle size, coating the $LiFePO_4$ particles with conductive materials like carbon have been commonly proposed to overcome this problem.[71, 79] Also, doping the results with cations of materials such as aluminum, niobium is another trend to improve conductivity. [80]

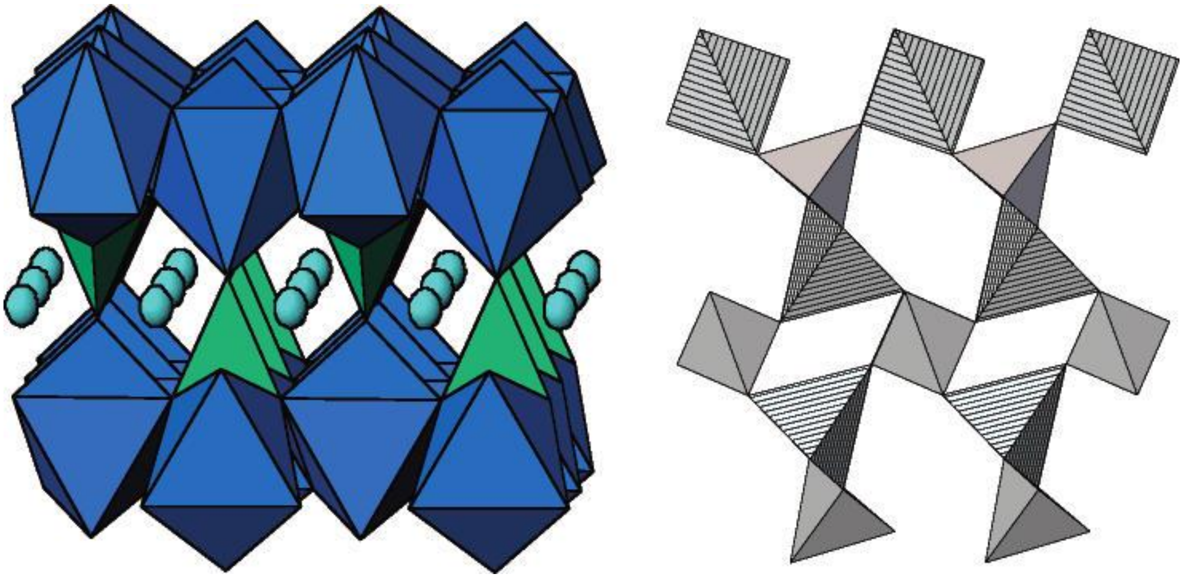

Figure 13: Structures of orthorhombic $LiFePO_4$(left) and quartz-like $FePO_4$(right).[78]

1.7.3 Spinel structure

$LiMn_2O_4$ is a typical spinel cathode material. Particularly, the Li^+ ions occupy the interstitial space which is defined by the Mn_2O_4 polyhedral frameworks with cubic closed packed structure (**Figure 14**).[53, 81-83] With $LiMn_2O_4$ as cathode material, the battery always can obtain high rate capability. The reason is that a three-dimensional framework provided by the spinel structure of $LiMn_2O_4$ for the insertion and de-insertion of Li^+ ions during discharge and charge of the battery is more advantageous for lithium ions diffusion compared with two dimensional frameworks. However, the practical capacity for $LiMn_2O_4$ is limited to 120 mAh/g, which is a little bit less than that of $LiCoO_{2.}$ This is because $LiMn_2O_4$ based batteries are recommended to avoid discharging to 3V in case that they suffer from deformation of their spinel structures. Furthermore, at higher temperatures, the $LiMn_2O_4$ spinel structure is inherently unstable in the Li-based electrolytes that are normally used in Li-ion batteries which results in dissolution of Mn ions and further capacity loss.[84, 85] It is suggested that doping transition materials like Ni, Fe, and Cu can improve the stability and cycling performance. [86-88]

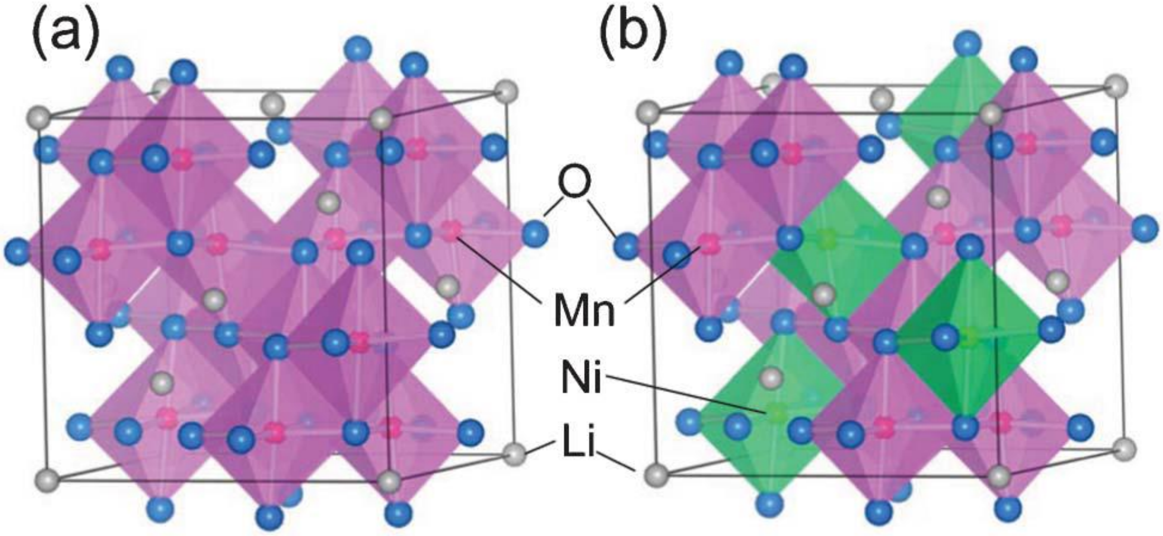

Figure 14: A typical spinel structure of $LiMn_2O_4$ and $Li[Ni_{1/2} Mn_{3/2}]O_4$ [89]

1.8 Electrolytes for lithium ion batteries

To some extent, the performance of lithium ion battery is dominated by the electrolyte material and its properties. The electrolyte is involved with battery’s safety, life, cost and power, which means that it is an indispensable part of a battery. In fact, different batteries require different electrolytes, which have an impact on the performance of a battery. Then the choice of electrolyte is a key issue. Alkyl carbonate was considered as the most suitable electrolyte for LIBs 20 years ago.[15] **Figure 15** illustrates the structure of the alkyl carbonates and the window limitation of the electrolyte for LIBs. These days, another novel electrolyte is often used in lithium ion batteries, which is a mixture of many solvents. For example, ethylene carbonate (EC) and either dimethyl carbonate (DMC), ethyl methyl carbonate (EMC) or diethyl carbonate (DEC), and the lithium salt: lithium hexafluorophosphate ($LiPF_6$) is regard as standard electrolyte solutions for Li-ion batteries.

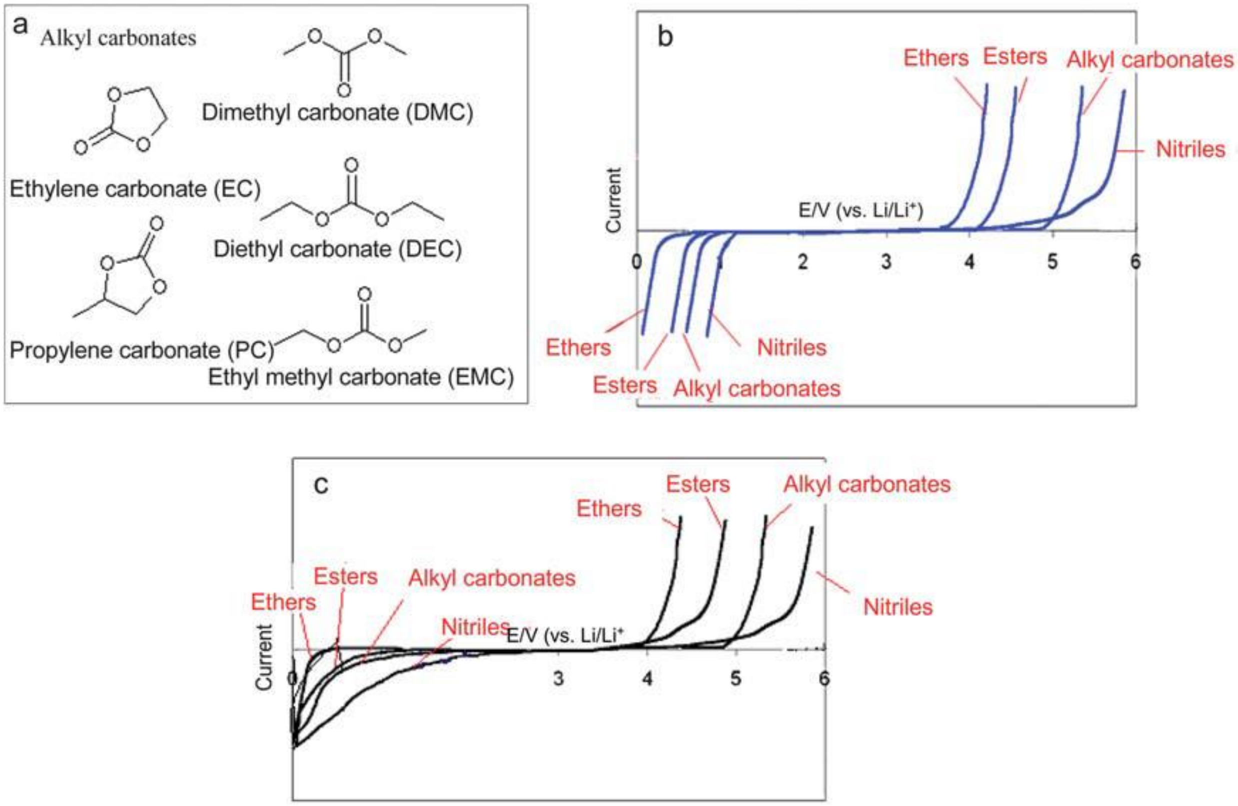

Figure 15: (a) several choices for organic solvents for dissolving electrolyte The selection of electrolyte solutions for Li-ion batteries.(b) The electrochemical windows of various solvent families with tetra-alkyl ammonium (TAA) salts. (c) electrochemical windows of Li salt solutions in different solvent families.[15]

1.9 Separators for lithium ion batteries

A separator is a porous membrane situated at the middle place between a battery's anode and cathode, whose function is to prevent electronic contact between the both electrodes, at the same time, allow the flow of the ions in the presence of current in an electrochemical cell. Although there are not so many changes in separator recently, it still occupies a critical role in lithium ion battery, which needs to keep the positive and negative sides apart. Mostly, a separator consists of a polymeric membrane forming from a microporous layer. The most significant characteristic of the separator is that it must be strong enough to prevent the damage resulting from battery construction. And it directly comes in contact with the electrolyte, so it also should be quite stable. A good separator can minimize the side effect on the battery during the discharge / charge process and it also makes a contribution to the battery's energy, power, cycle life and safety.

1.10 Binders for lithium ion battery

Binders are always used to attach the electrode composition together to prevent the electrode from collision as **Figure 16** shown. Actually, the binder is a significant part of a complete battery for battery engineering determining the battery performance. One widespread binder is poly (vinylidene) fluoride (PVDF) which has been used for both anode and cathode materials with good electrochemical stability. N – Methyl -2 –pyrrolidone (NMP) is the best solvent for it even though NMP is toxic. Today, there are also many other polymeric material as binder used for LIBs such as polyacrinitrile (PAN), sodium carboxymethyl cellulose (CMC) and poly arctic acid (PAA).

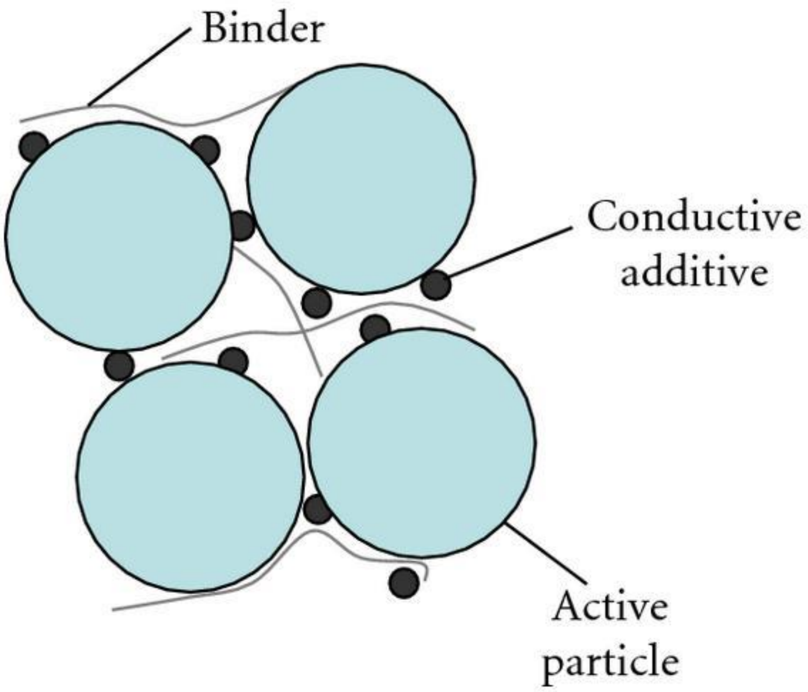

Figure 16: Illustration of a small part of an electrode, including active particles, binder, and conductive additives.

1.11 The structure of lithium ion battery (coin cells)

In general, the types of lithium ion battery cells can be divided into four; coin, clindrical, prismatic and pouch forms, whose fundamental components are the same. We are focusing on coin cells

(**Figure 17**). The most essential requirement for current collector of anode is that it cannot react with lithium ions, and copper foil meets this condition. Also, aluminum foil is always used to act as current collector for the cathode for it is easy to process. The electrodes made by combining active material with binder (CMC, PAA, PVdF) and conductive additives (Super p) for the anode while the cathode material is lithium foil in a half cell testing. In the electrode manufacturing process, active material with binder and conductive additives is mixed with solvents (DDI water， NMP) in a grinder, then it is used a doctor-blade to coat on the copper foil. The following steps contain drying, pressing and weighing. The next step involves the electrodes ‘assembly: separation with the membrane, the electrolyte injection into the battery, cathode material insertion and pressing.

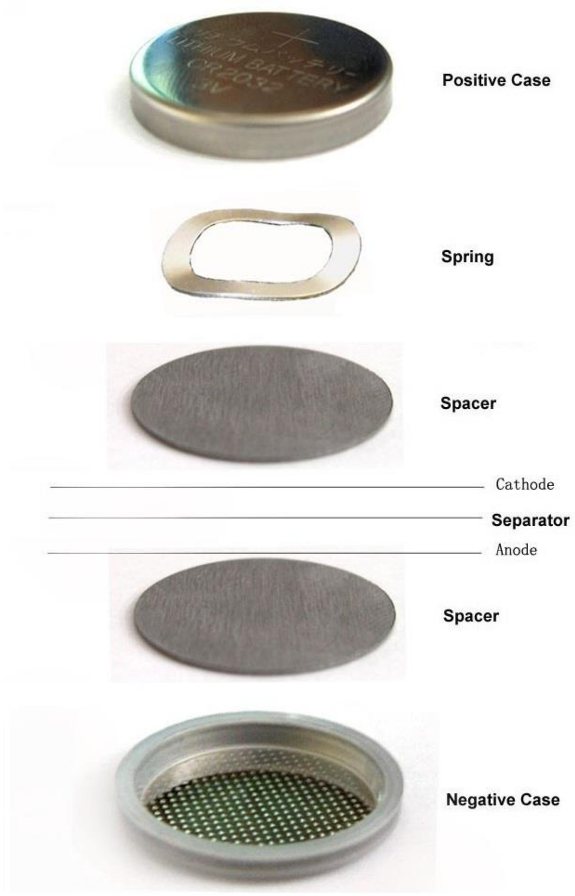

Figure 17: The structure of coin cell for lithium ion battery’s testing

1.12 Our work and goal

However, Graphite as negative electrodes (theoretical capacity: 372 mAh/g) cannot meet the demand for high power and energy density LIBs increasingly in commercial industries. In this case, a series of novel anode materials have been investigated, such as

Sn (993 mAh/g), SnS_2 (645 mAh/g), SnS (782 mAh/g) Fe_2O_3 (1005 mAh/g), whose theoretical capacities are several times higher than that of commercialized graphite. But they encounter a large volume expansion while it is discharging and charging resulting in poor cycle performance and severely confine their applications in industry. In order to solve this problem, many efforts have been investigated. In general, the objectives of this thesis are listed as the following:

1. Develop controllable nanostructures of tin sulfides with improved capacity and durability.
2. Develop simple material synthesis and electrode fabrication for LIBs
3. Investigate novel anode material with enhanced electrochemical performance

1.13 Thesis outline

In this thesis, there are several chapters. In chapter 1, an introduction including the background and literature review is included, which also provides the objectives of this thesis. In chapter 2, we introduced a brief description of the characterization tools like SEM, TEM. In chapter 3, a novel method of preparing SnS_2 via oxidizing stannous ions by graphene oxide is developed for the synthesis of SnS_2 with doped graphene nanocomposites. Then SnS nanorods are formed by controllable heat treatment of SnS_2 nanosheets. As anode material for LIBs, SnS with doped graphene nanocomposites maintained discharge capacity of about 870 mA h/ g after 100 cycles at a charge–discharge rate of 0.1 A/g. In chapter 4, it introduces a new binder with SnS_2 wrapped graphene followed by low temperature heat treatment applied in LIBs as anode materials. In this section, a new reaction mechanism is proposed. Summary and future work is shown in chapter 5.

Chapter 2

Material characterization tools

2.1 Scanning Electron Microscopy (SEM)

A scanning electron microscopy is a type of microscopy to investigate the morphology and composition of the sample. The general distribution of SEM instrument is shown in **Figure 18**. It can be clearly seen that the electron beam through several condenser lens is offered a collision with the sample and the signals which is produced by secondary electrons (SE), back scattered electrons (BSE), characteristic X-rays are received by different types of detectors, which displays the images related to the topography of the sample. SEMs have a variety of applications in industrial or scientific fields. The instruments work fast. Further, the sample preparation is easy, which always costs less than 5 minutes before placing it in the vacuum chamber. Nowadays, the resolution of SEMs can be reached to nanometer scale for the technological advances in SEMs.

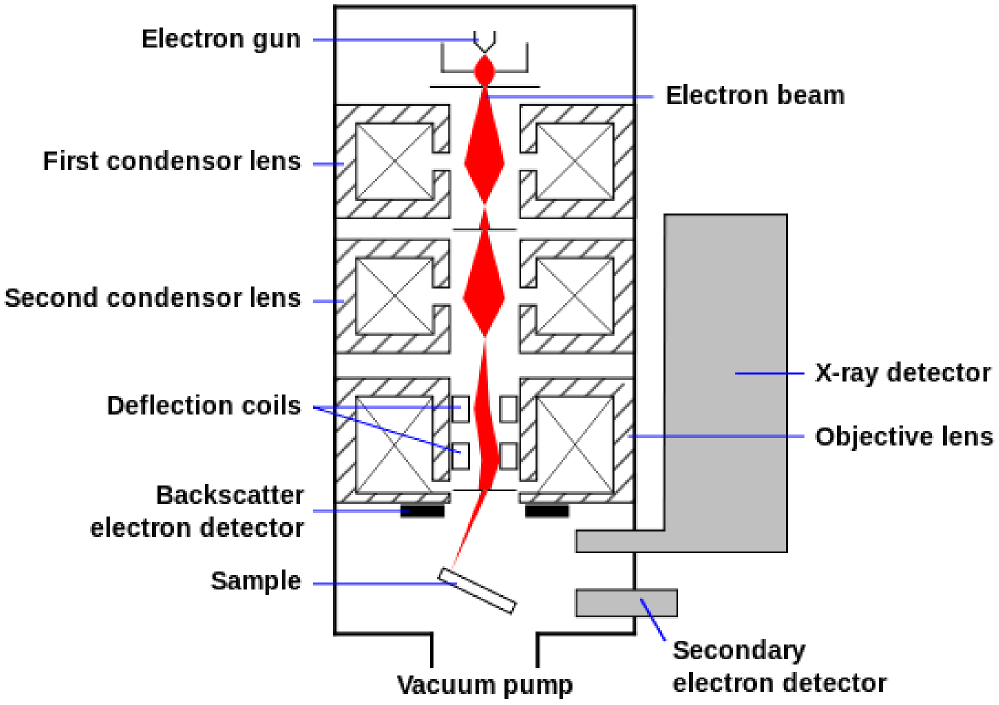

Figure 18: The layout of the SEM.

2.2 Transmission Electron Microscopy (TEM)

Transmission Electron Microscopy (TEM) is the most powerful microscopy that provides morphologic, compositional and crystallographic information about the samples. It produces high resolution, two dimensional images that applying in industry and science. The general layout is shown in **Figure 19**. The electrons through accelerated and collected along magnetic lens throw light on the surface of the thin samples. Electrons collide with the atoms of the samples, which result in three dimensional scattering. The scattering angle depends on the density and thickness of the sample. It does contribution to displaying white and black pictures for the sample. TEM can provide higher resolution than optic microscopy. Nowadays, the resolution of TEM can reach 2nm. Besides, modern TEM instrument is always used to obtain color mapping, selected area electron diffraction.

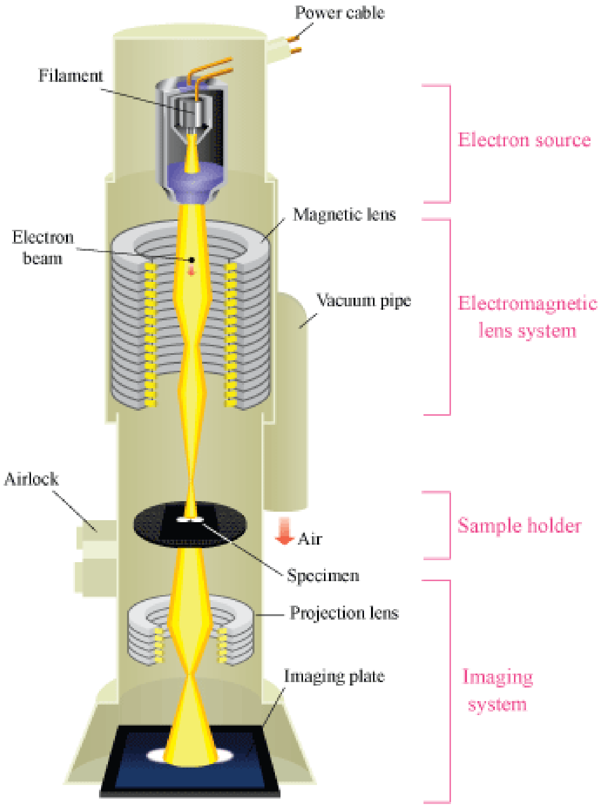

Figure 19: The layout of TEM.

Figure 20 shows high resolution images and SAED for Sn/C nanocomposites. It can be easily seen how the material looks like and the crystal structure can be determined through the order of tin atoms.

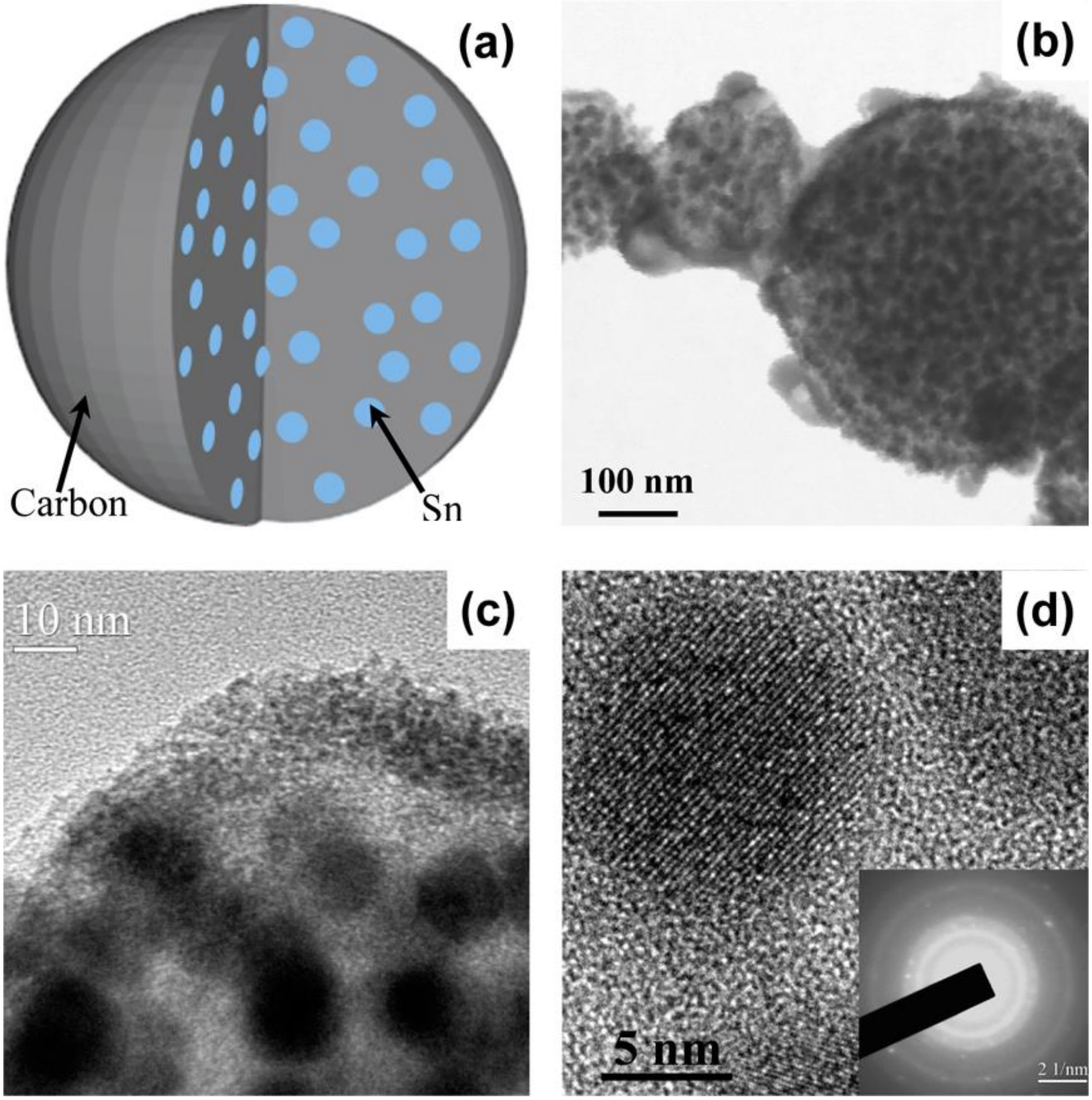

Figure 20: (a) Schematic diagram, (b) TEM image, and (c,d) high resolution images of the nano-Sn/C composite particles. Insert: SAED image.

2.3 X- Ray Diffraction (XRD)

X-ray diffraction is a common analytical technique which is primarily used for phase and composition identification of a crystalline material. **Figure 21** exhibits the fundamental principle of XRD based on Bragg’ equation. For a powder material, when the X-ray comes from the left part in **Figure 21** with certain wavelength, it is scattered by the lattice plane with separate interplanar distance d. In fact, there are two X-ray paths: constructive interference and destructive interference between the X-ray and lattice planes. When the interference is constructive, it means that the diffraction waves are strengthened in some directions. Bragg's equation is always used for describing the relationship about the interference of scattered light: $n\lambda = 2d \ \mathrm{Sin}\theta$, where n is the half of the diffraction angle, λ is the wavelength, and d is the distance of adjacent lattice planes.

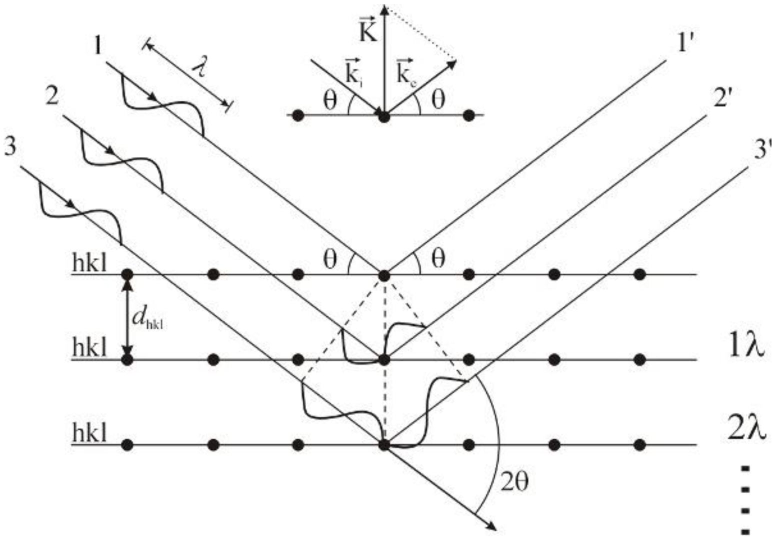

Figure 21: The schematic illustration of XRD principle.

For a complete power XRD instrument, the apparatus contains X-ray source, a stage for the sample, a monochromatic and a detector as shown in **Figure 22**. It is clear from the figure that the X-ray source is rotated from different angles with the sample in order to get ample information about the lattice plane with various directions. And the X-ray is concentrated on the sample then the scatted light is received by the detector, which provides relative information about the crystal.

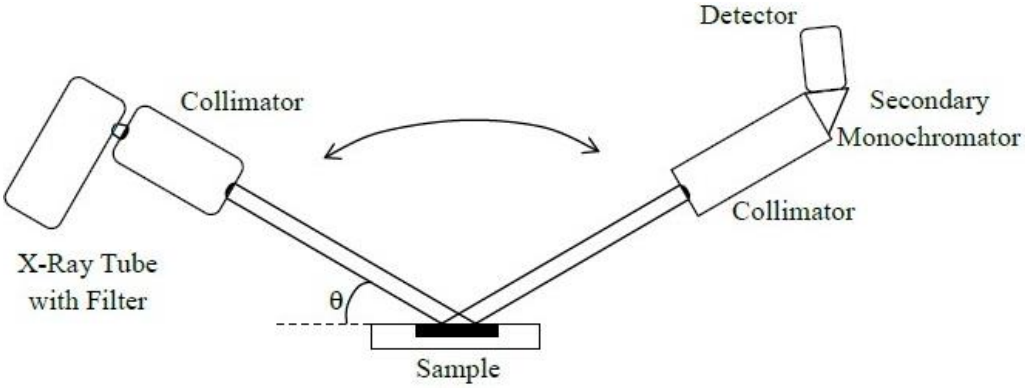

Figure 22: Schematic diagram of power XRD instrument.

2.4 Thermalgravimetric analysis (TGA)

Thermalgravimetric analysis is a method to measure the physical properties under thermal conditions in selected gas atmosphere. It can provide the information about the degradation temperature, melting points, boiling points and etc. The TGA instrument weighs the samples as it heats to a pre-set temperature. From a certain temperature, the sample should have a degradation process, which results in the loss of the total mass. The certain percentage of the composition of the sample can be acquired by the mass change. In this thesis, TGA is used to determine the percentages of the graphene and tin sulfides, which further figure out the theoretical specific capacity of the nanocomposite.

2.5 Raman

Raman is a useful tool to observe the vibrational, rotational mode of molecules. The principle of the Raman spectroscopy is based on the Raman light scattering. When a laser collides with a molecule, there are mainly two types of scattering as the following **Figure 23** shown: elastic scattering and inelastic scattering.

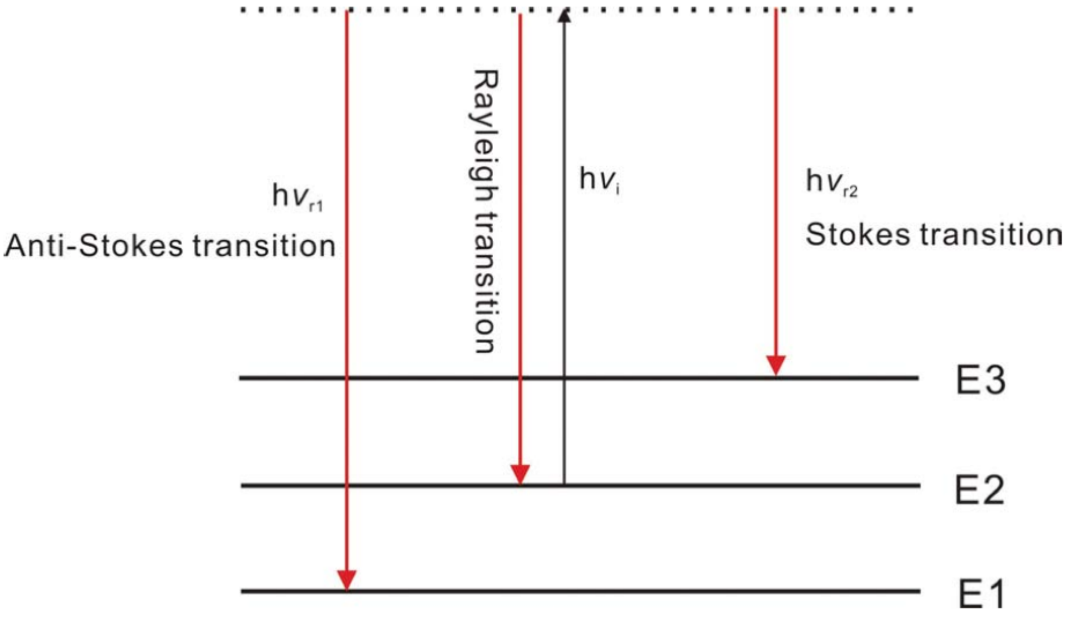

Figure 23: The schematic diagram of the Raman scattering

It can be clear seen in **Figure 23**, previously, a molecule with characteristic vibrating frequency stays on the energy state E2. It jumps to a higher visual state when a laser hits it with the energy hv. However, the emitted photon with no change in energy is called Rayleigh scattering. More than 99%

of the light is scattered in this way but a small amount of emitted photon has an energy change. When the molecules decay to the energy state E1 or E3, which are named by inelastic scattering, it refers to as Raman scattering. If it is back to E1 (hv1>hvi), it means that the emitted photon is more energetic than the incident light. Conversely, if it comes to E3 (hv2<hvi), it is demonstrated that the emitted photon is less energetic than the previous light. Also, it is well known that in terms of a molecule, the basic requirement for Raman active is the change in bond polarizability as a bond stretch. Raman spectrometer possesses the capability to be confocal image. As is shown in **Figure 24**, laser reflects off a dichroic mirror onto sample while dichroic mirror allows the long wavelength to pass. The Raman scattered light from the sample pass through the lens via a pin hole aperture , which filters out stay light or the light with no Raman scattered process. The light goes through the dichroic mirror to the beam splitter to partitions it with the detector and the visual ocular.

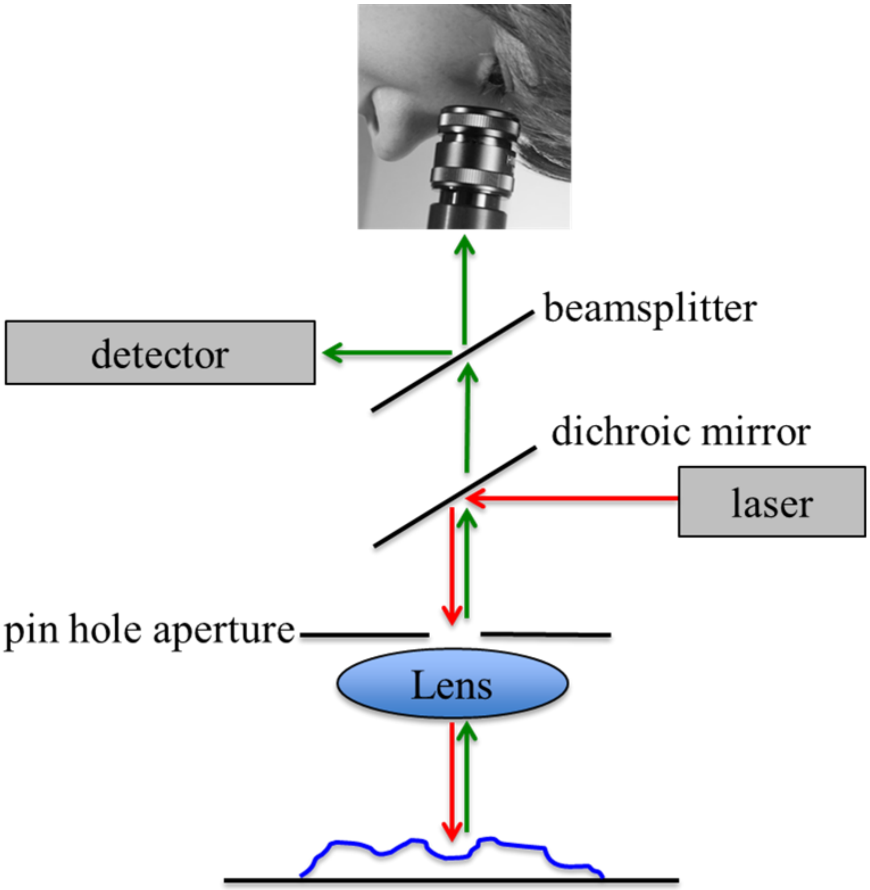

Figure 24: The schematic of laser light operation process

2.6 XPS (X-ray photoelectron spectroscopy)

XPS is a surface spectroscopic technique that is based on the photoelectric effect and is used to measure elemental component and chemical or electronic state of each element. **Figure 25** shows the photoelectric mechanism that is related to XPS. When the sample is radiated by the incident X-ray, the inner electrons with applied energy are stimulated to launch ejected photoelectron. Through this process, the kinetic energy for the electrons are known and then the binding energy is acquired, which are used for analyses the materials' electronic states and the amount of the electrons.

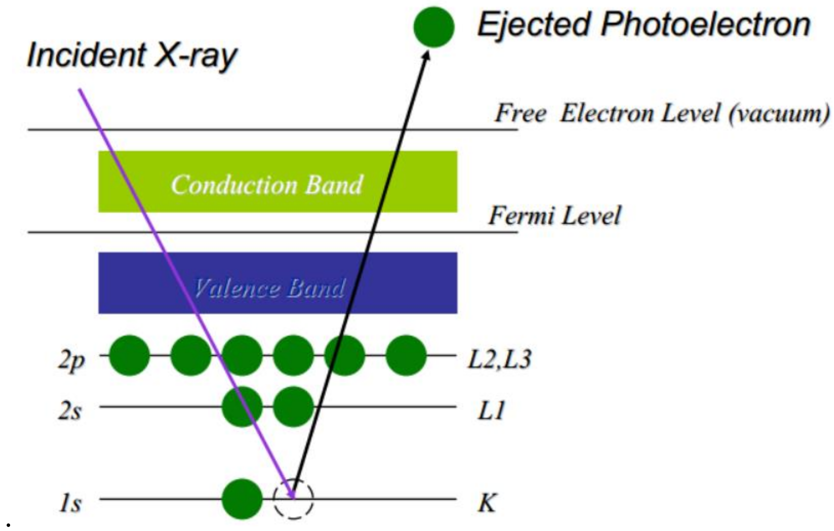

Figure 25: The diagram on the photoelectric effect

2.7 EDS (Energy –dispersive X-ray Spectroscopy)

EDS is a useful technique to elemental analysis and chemical composition analysis, which relies on the interaction of the X-ray and the sample. **Figure 26** demonstrates the principle of EDS. When X-ray is focused on the sample, the inner electrons with energy are excited and form electron holes, then the outer electrons fill the holes, which results in the energy difference between the outer shells and inner shells released by the way of X- ray . Based on this principle, the spectrum is produced, which provide the information about the number of the atoms and the composition of the samples.

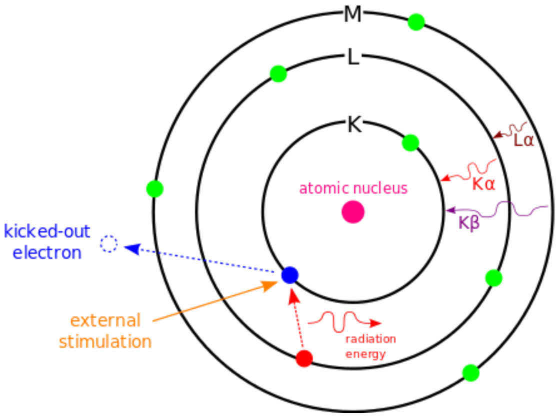

Figure 26: The illustration of EDS

Chapter 3

Hybrid Tin Sulfide Wrapped with Dual Doped Graphene for Enhanced Performance Lithium Ion Batteries

3.1 Introduction:

Recently, the demand for an energy storage device with high power and high energy density is dramatically increasing, due to the lack of fuel oil and severe environmental concern. Lithium ion battery is widely considered as optimal replacement of natural resources due to its rapid development in the area of electronic products and Eco-friendliness. Also, LIBs have exhibited excellent performance with high gravimetric and volumetric capacity, low self- charge rate. However, commercial graphite (372 mAh/g for LiC_6) as anode material cannot keep pace with the quantity demand for the energy device, which demonstrates that there should be a further investigation for increasing the capacity, stability of LIBs to meet the requirements for various fields' applications.

These days, metal chalcogenides have attracted a significant attention for researchers in the fields of energy devices such as solar cell, lithium ion batteries, supercapacitors.[90-92] Among these materials, layered metal chalcogenides have been developed in lithium ion batteries.[93] When the size of metal chalcogenides decreases to nanometer scale, it can show unique physical and chemical properties due to well- known quantum size effect and the large contact area which is beneficial to energy devices.[94] However, tin sulfide is one of the best candidates as anode electrode materials for next generation lithium ion batteries, because the specific capacity of tin sulfides is twice higher than that of commercial graphite electrodes. The following **Figure 27** demonstrates the crystal structure of tin disulfide. Tin disulfide is a CdI_2 layered structure and for unit cell, a=b=3.64 Å, c=5.87Å.[1, 95] In terms of lithium insertion/deinsertion mechanism, there should be involved two steps: conversion and lithium alloying reactions. During these steps, alloying /de-alloying process contributes to reversible capacity.[30] Firstly, it is the lithiation process for tin sulfides followed by the formation of Li_2S and sold electrolyte interface, which leads to the initial irreversible capacity. Then, the step is related to form a LixSn alloy, which contributes to reversible capacity.

Nevertheless, large volume changes for the alloy / de-alloy process during charging / discharging result in mechanical degradation of the electrodes, eventually leading to poor cycle performance.

There are several methods to improve the electrochemical performance of tin sulfides. It has been reported that incorporating tin sulfides into graphene, which provided tremendous improvements.

Graphene, a 2D dimensional layer of sp^2 hybridized carbon atoms which also used in many field has attracted more attention as a promising anode for lithium ion battery.[96] It is known that the nano - cavities between the graphene nanosheets resulting from scrolling and crumpling makes great contribution to the energy storage of LIBs.[97] Because its high conductivity and good stability, nowadays graphene is always used for modifying other materials in order to get good performance.

Here, a solvothermal method was used for synthesizing tin disulfides is introduced. Graphene oxide was employed as oxide precursor, which was used to oxidize tin stannous. Consequently, there was a formation of sulphur and nitrogen dual doped graphene with improved electrical conductivity, which is beneficial for enhancing rate performance. [98]

However, there are no publications about acquiring absolute SnS with dual doped graphene (GSN-SnS) after annealing SnS_2 with graphene (GSN-SnS_2) in lithium ion battery application, which exhibited excellent electrochemical properties. To our best knowledge, the distinctive crystal structure for SnS with large interlayer spacing (c=0.4330nm) assists the intercalation of lithium ions and restrains the volume expansion during the charging / discharging process.[99]

In this work, a fancy tactic of preparing GSN-SnS_2 via heat treatment was developed to synthesisze GSN-SnS. Tin sulfides with tuned morphology and composition were prepared which is supported by, and wrapped with graphene , whose nanostructures were prepared by solvothermal synthesis followed by controlled heat treatment. After heat treatment the hexagonal nanosheets of SnS_2 were transformed to rod-like structure with chemical transformation to stannous sulfide (SnS). The acquired GSN-SnS hybrid nanostructures showed unique properties in energy storage device for the good electrical conductivity and ion transport. Additionally, for the electrode stability, the SnS retains a crystal structure similar to the cubic tin after the convention process during the discharging /charging process , which largely helped improving the electrochemical performance, while SnS_2 formed amorphous tin.[95] Furthermore, the involved dual graphene with large surface area and flexibility also makes great contribution to enhancing the high stability. In terms of electrochemical performance, both materials have first cycle charge/discharge capacities which exceed the theoretical values. However, the heat treated material is more durable, it was able to maintain a charge capacity of ~ 870 mAh/g for more than 100 cycles and ~ 850 mAh/g after 200 cycles at the rate of 0.1 A/g. Even at higher energy density 0.5 A/g , the annealing GSN-SnS showed long cycling performance , which continued 1000 cycles and kept a nearly 85% capacity retention compared with theoretical capacity and after 1500 cycles , the capacity was still higher than 550 mAh/g .

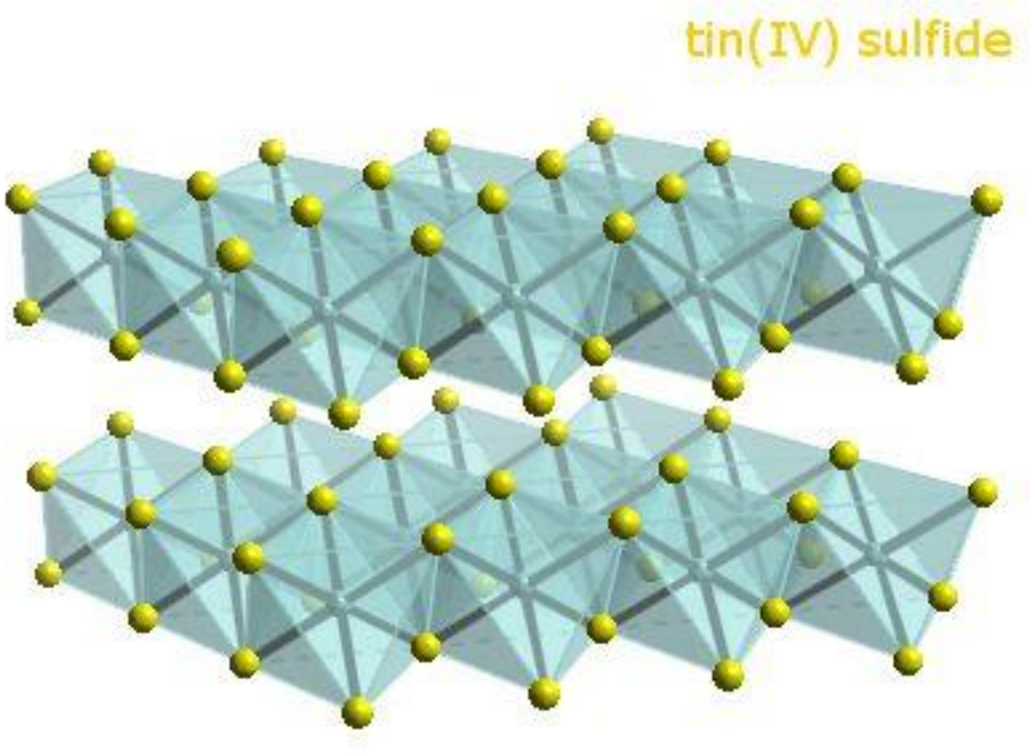

Figure 27: The crystal structure of tin disulfide

3.2 Experimental section

Materials: grapheme oxide (GO), Stannous chloride dehydrate ($SnCl_2.2H_2O$), thiourea ($CS(NH_2)_2$), ethylene glycol(EG) . All reagents were of analytical grade and used as received without any purification process.

Synthesis of GSN-SnSx nanocomposites: graphene oxide (GO) was fabricated according to previous literature procedures. To synthesize GSN-SnSx nanocomposites, a mixture of GO, ethylene glycol, $SnCl_2.2H_2O$ and thiourea was prepared. Secondly, the above suspension was transferred into a autoclave and heat the solution 10hours @ 100 °C and 10hours @ 200°C. After that, the autoclave was cooled to the room temperature, and the products were collected and filtered. Then the products were put into a freeze dry machine (Labconco Freezone 1, USA) for two nights and the material was labeled as GSN-SnS_2. After that, some of the material was brought into the furnace under the argon atmosphere.In terms of the controlled heat treatment: the time was set from room temperature to 500°C for 2 hours followed by maintaining at the same temperature for 3 hours, which was labeled as GSN-SnS. The reference experiments which only contained SnS_2, SnS, and dual graphene (GSN) were also acquired by the similar procedures.

Characterization and Electrochemical Measurement

X-ray diffraction (XRD) patterns were collected on using Ni-filtered Cu Kα radiation (λ =1.5418 Å). The morphology of the nanocomposites was observed using a field emission scanning electron microscope (FE-SEM, Zeiss Ultra Plus, UK) and high-resolution transmission electron micrographs (HR-TEM, FEIPhilipsCM 300, USA).Thermal gravimetric analysis (TGA) was carried out to explore the ratio of tin sulfides and graphene. X- Ray photoelectron spectroscopy (XPS) was also used to confirm the composition of GSN-SnS x products.

Electrochemical Evaluation : The working electrodes were fabricated by mixing 60 wt % active material, 20 wt% super P (as a carbon additive for conductivity enhancement), and 20 wt % CMC (used as a binder,2wt % CMC (sodium carboxymethyl cellulose)and PAA(poly(acrylic acid), Sigma Aldrich) with weight ratio:1:1)in water and coated on copper foil . The electrodes were treated in vacuum oven for 2 hours at 150 degrees and assembled in the gloves box (MBRAUN 10, USA) Conventional two electrode coin cells were fabricated using lithium metal(Aldrich, USA) as the counter electrode and $LiPF_6$(1 M) in ethylene carbonate/diethyl carbonate(EC/DEC, 3:7vol %) as the electrolyte. The electrochemical performances of the prepared electrodes were characterized by cyclic voltammetry (Versa Stat MC, Princeton Applied Research, USA) and galvanostatic charge−discharge (Neware, China) tests between0.1 and 3 V vs. Li/Li^+.All of the specific capacities in this study were calculated based on the mass of active materials (GSN-SnSx).

3.3 Result and discussion

The total synthesis processes were declared into two steps: firstly, it was the formation of GSN-SnS_2 by solvothermal method. Subsequently, the schematic diagram is about the chemical transition from GSN-SnS_2 to GSN-SnS shown in the **Figure 28** (bottom part). As shown in the **Figure 28** (top part) , it is clear that the GO sheets interacted with ethylene glycol through sonication .According to the previous publications, the GO sheets is negatively charged and can attract Sn^{2+} as the following equation (1) shows.[100] Then, Sn^{2+} is oxidized by GO and graphene is formed with EG as well. (eqn2, 3).[101] At the temperature of 100°C, there is no change in thiourea. At higher temperature, GSN-SnS_2 is produced (eqn6).

$Sn^{2+} + GO \longrightarrow Sn^{2+}/GO$ (1)

$GO + SnCl_2 \longrightarrow SnO_2 + HCl + G$ (2)

$GO + EG \longrightarrow G$ (3)

$CS(NH_2)_2 \longrightarrow$ no change ----100°C (4)

$GO + Tu \longrightarrow G$ (5)

$SnO_2 + G + Tu \longrightarrow SnS_2/G$ (6) -------200°C (6)

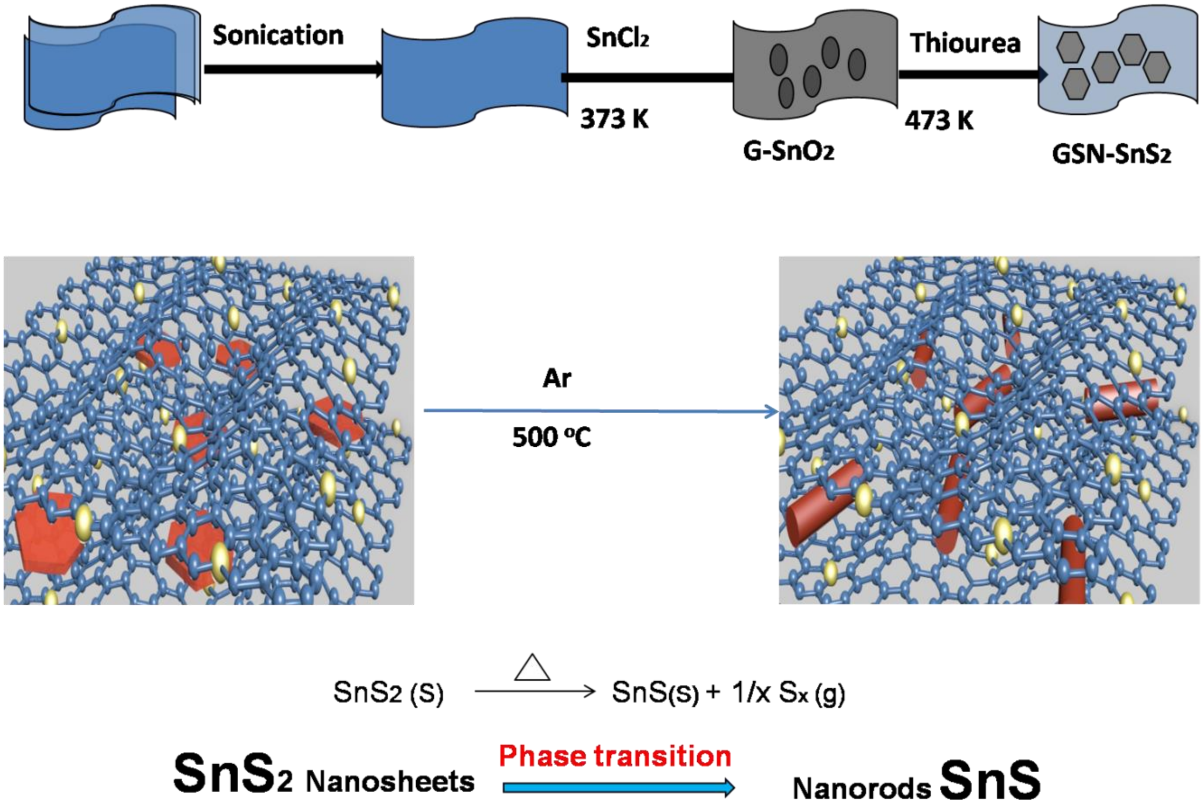

Figure 28: The schematic diagram of synthesizing process of GSN-SnS_2 and GSN-SnS.

Here, the formation of GSN-SnS using the GSN-SnS_2 having prepared was emphasized for the previous material shows better performance than the latter. The annealing process with 500 °C is used to transfer chemically from GSN-SnS_2 to GSN-SnS .It is proposed that there is an exact reaction happened in the furnace. The sulfur of SnS_2 under high temperature flees from the previous bond and the power from the high temperature drives the composite to aggregate together, resulting in the rod like GSN-SnS as the architecture shown in the **Figure 28** (bottom part).

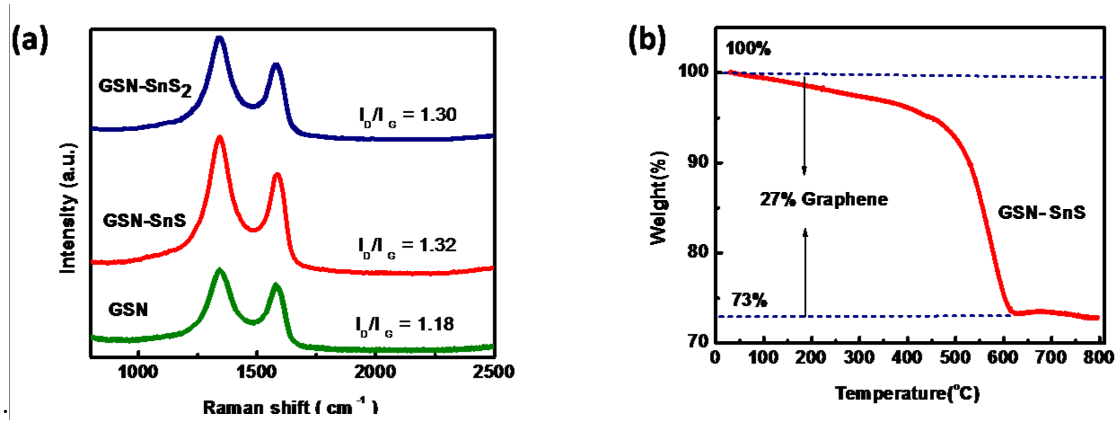

Figure 29: (a) Raman spectroscopy for GSN, GSN-SnS, GSN-SnS$_2$; (b) TGA for GSN-SnS

Figure 29(a) compares Raman spectroscopy of GSN-SnSx and GSN. In this Figure, it can be seen that a peak at around 1583 cm $^{-1}$(G band) , which is related to the vibration of graphitic layers while there is a peak at 1320 cm^{-1}(D band) which means the defects and disorder of graphitic layers.[102] The intensity ratio of D to G for GSN is determined as 1.18 and around 1.30 for GSN-SnSx. According to the previous literature shown, the intensity ratio expresses the graphitization level and defect degree of carbon based materials. Compared with GSN, it is clear that the ratio of I_D to I_G increases slightly, which is mainly for the exfoliation of graphene and the insertion of tin sulfides into graphene layers.[103]

In order to measure the content of graphene in the as- synthesized GSN-SnS material, thermogravimetric analysis (TGA) was carried out from normal temperature to 800 degrees in air (**Figure 29(b)**) From the TGA curve , the main mass decreasing at the range from 450 degrees to 600 degrees was attributed to the removal of graphene. It can be calculated the graphene occupied around 27%.

Through XRD, the whole crystal structure of GSN-SnS$_2$ (JCPDS01-1010) and GSN-SnS (JCPDS39-0354) were determined by XRD. As shown in **Figure 30 (a)** and **(b)**, it is clear that the XRD patterns of both materials are similar to that of hexagonal SnS$_2$ nanosheets and SnS nanorods. All the peaks of GSN-SnS$_2$ are fully indexed to SnS$_2$, which indicates the high purity of products. In comparison, nearly all of the strong diffraction peaks in GSN-SnSx after annealing could be indexed to the standard diffraction data of GSN-SnS. Therefore, the whole results showed that Sn^{2+} is oxidized by GO to form SnS$_2$ and heat treatment is an excellent method to react chemically to form pure GSN-SnS with the structure of nanorods.

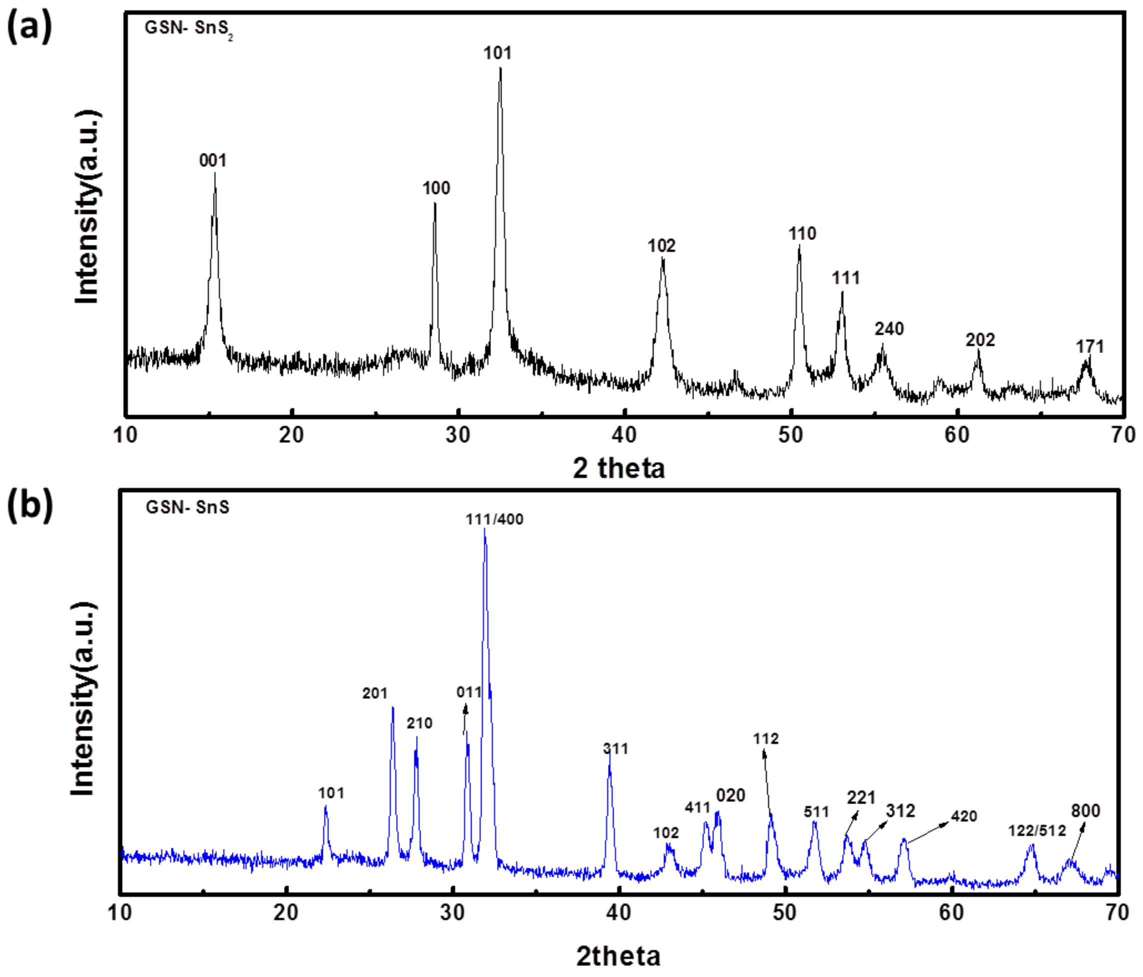

Figure 30:(a) and (b) X-ray Diffraction pattern of GSN-SnS_2 and GSN-SnS nanocomposites.

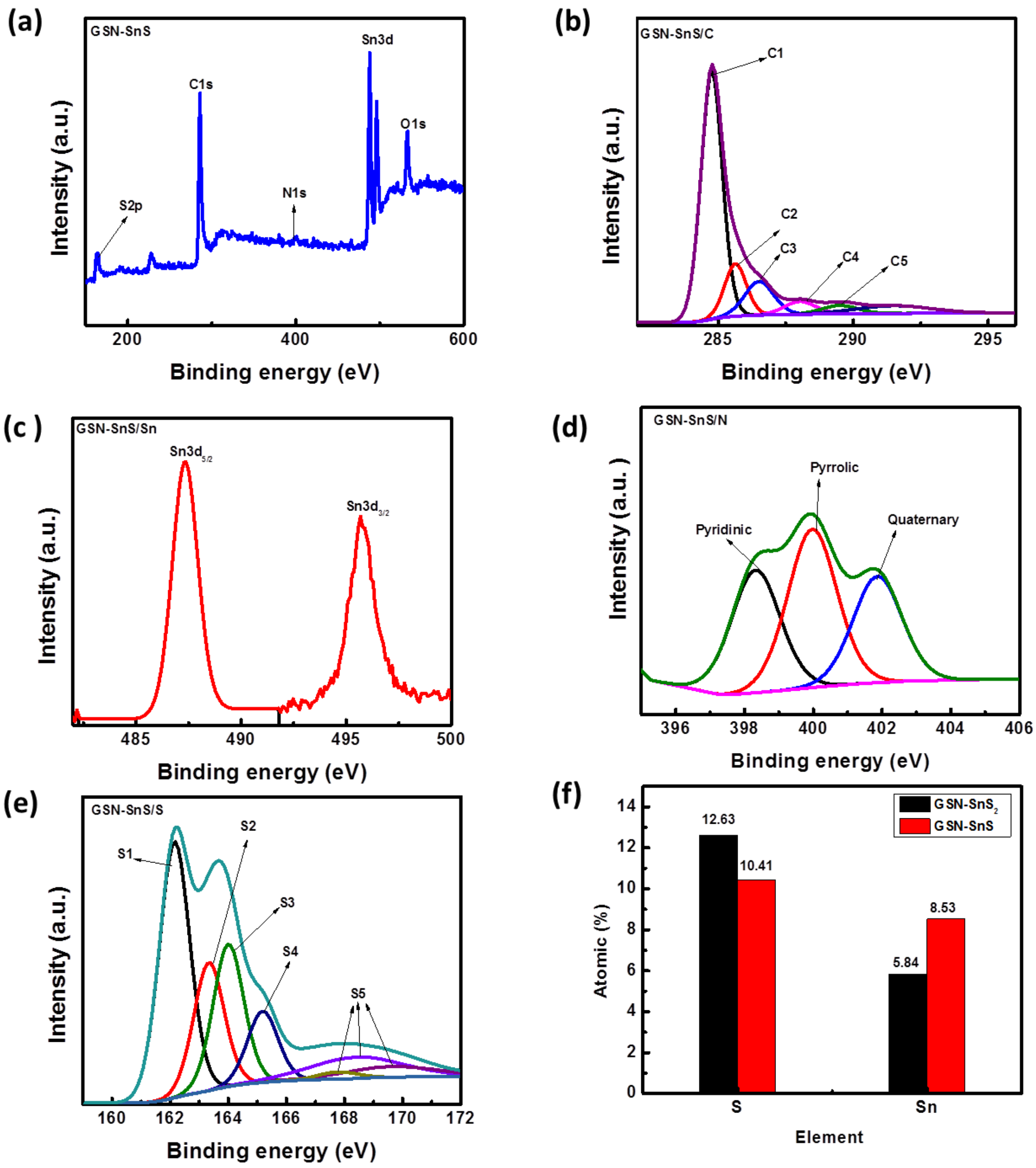

Figure 31: XPS analysis for GSN-SnS : (a) survey spectrum (b) C1s(C1 : -C-C-;C2:C-OH;C3:C-O-C;C4:C=O;C5:O-C=O) (c) Sn3d (d) N1s (e)S2p (S1:-S-Sn-;S2:-SH;S3:-C-S-C-$(2P_{3/2})$;S4:-C-S-C-$(2p_{1/2})$;S5:-SOx- (X=2,3,4)) (f) the EDS results of Sn , S for GSN-SnS, GSN-SnS$_2$.

Figure 31 shows X-ray photoelectron spectroscopy (XPS) analysis for GSNS-SnS to determine the element and valence. The survey spectrum is shown in **Figure 31(a)**. The detected elements from the sample are C1s, S2p, Sn3d, O1s and N1s.The peak for C1s is shown at 284.8 eV in **Figure 31(b)**, which represents the C-C group. It is related to the high conductivity of graphene. There are two peaks for the Sn3d XPS spectrum spectroscopy (**Figure 31(c)),** which are corresponding to $3d_{5/2}$, $3d_{3/2}$. In terms of N1s (**Figure 31(d)**), there are three characteristic peaks: binding energy 398.9eV for pyridinic, 400.1e V for pyrrolic, 401.5 eV for quaternary, which provides the direct evidence for N doped graphene.[97] As for sulphur, there are two main peaks. At 162.15 eV, it is-S-Sn–group and the S2p doublet corresponding to C-S-C which represents $S_{2P3/2}$ and $S_{2P1/2}$ spin orbit coupled peaks are located at 163.98 and 165.18eV labeled as S3 and S4,which means sulphur doped graphene.[104] At higher energy, the peaks named as S5 are related to oxygen bound to sulfur (-SOx).[104, 105]

Further, in **Figure 31(d)**, it obviously showed the comparisons of two elements for GSN-SnS_2 and GSN-SnS: S and Sn. In terms of both materials, the atom ratios for S to Sn are a little bit higher than that of pure materials: SnS：1：1, SnS_2: 2:1, which are confirmed by XRD already. These values ulteriorly provide the information about the sulphur exceeding usage for the material synthesis, which also confirm the XPS results that the there is a sulphur doping in graphene during the reaction process.

The general morphology and microstructure of both materials were shown in **Figure 32(a), (b)**. It can be seen that GSN-SnS_2 before annealing is nested in the graphene layers with the structure of nanosheets while GSN-SnS after annealing is surround by the layers shown as nanorods. A rod-like SnS is among the layers even after processing by sonication for TEM observation as shown in **Figure 32 (c)**, which indicates the strong connection between the SnS and graphene. And in **Figure 32(d)**, it shows the STEM and color mapping of C, Sn, S, which further demonstrates the homogeneous and highly efficient combination of graphene and SnS nanorods.

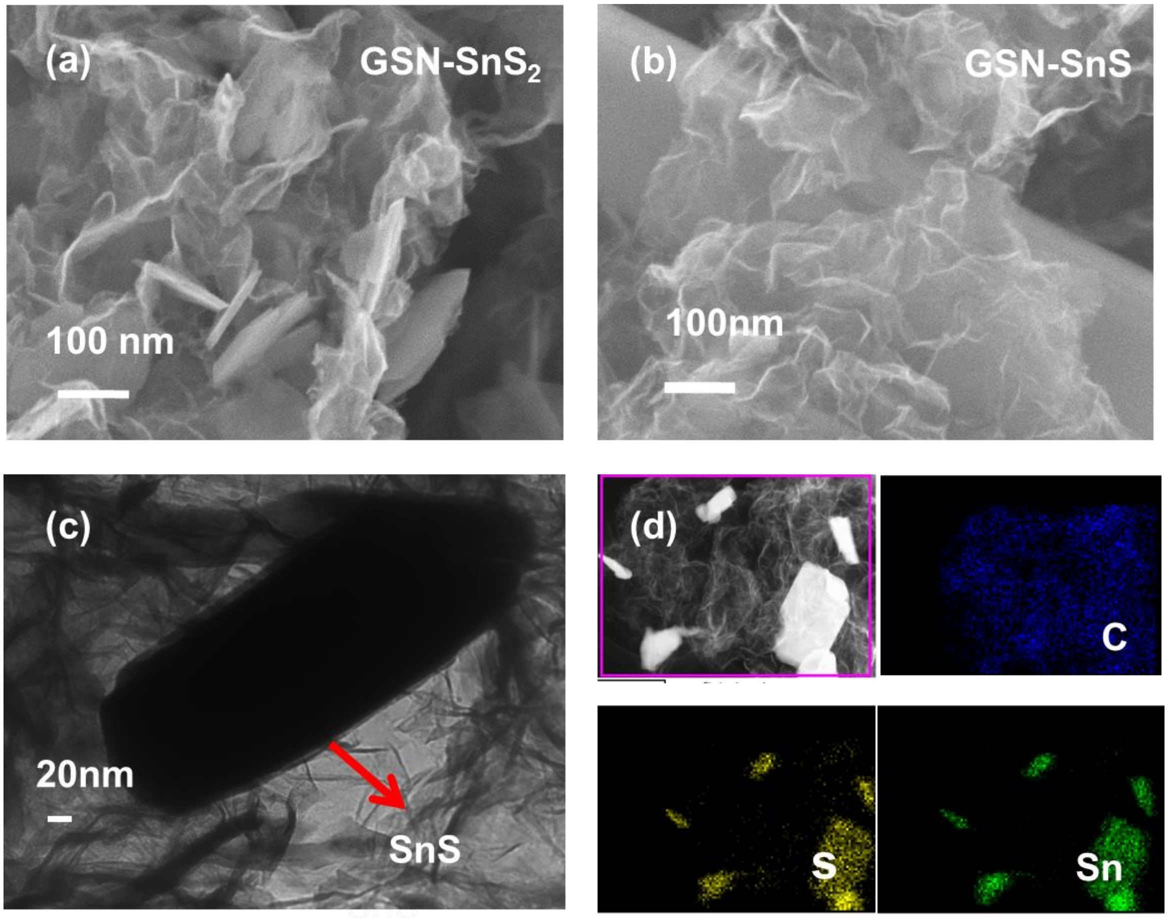

Figure 32: (a) and (b) FESEM images of GSN-SnSx at the same magnification (c) HRTEM images of GSN-SnS (d) STEM and color mapping of GSN-SnS.

Actually, graphene occupy rather significant role as supporter and morphology regulator during the whole chemical reaction procedures, which is obtained from a reduction reaction of graphene oxide. Graphene possess a layered structure with flexibility which offer accommodations for the tin sulfides to embed and prevent crystal structures to grow disorderly and unsystematically. **Figure 33** compares the SEM images of pure GSN-SnS$_2$ **(Figure 33(a))**, GSN-SnS **(Figure 33(b))**, SnS$_2$ **(Figure 33(c))** and SnS **(Figure 33(d))**. It can be noted that there is distinct change about the crystal structures' formation under the condition of the presence and the absence of graphene. It is indicating that tin sulfides are formed around the graphene layers and aligned in order which is beneficial for the insertion/ deinsertion during charging/ discharging **(Figure 33(a)** and **(b))**. **Figure 33(c)** and **(d)** introduces SEM images of tin sulfides without graphene, which shows the booming aggregation of tin sulfides nanosheets and the formation of messily bulk tin sulfide. It is suggested that graphene plays a vital role in morphology modification.

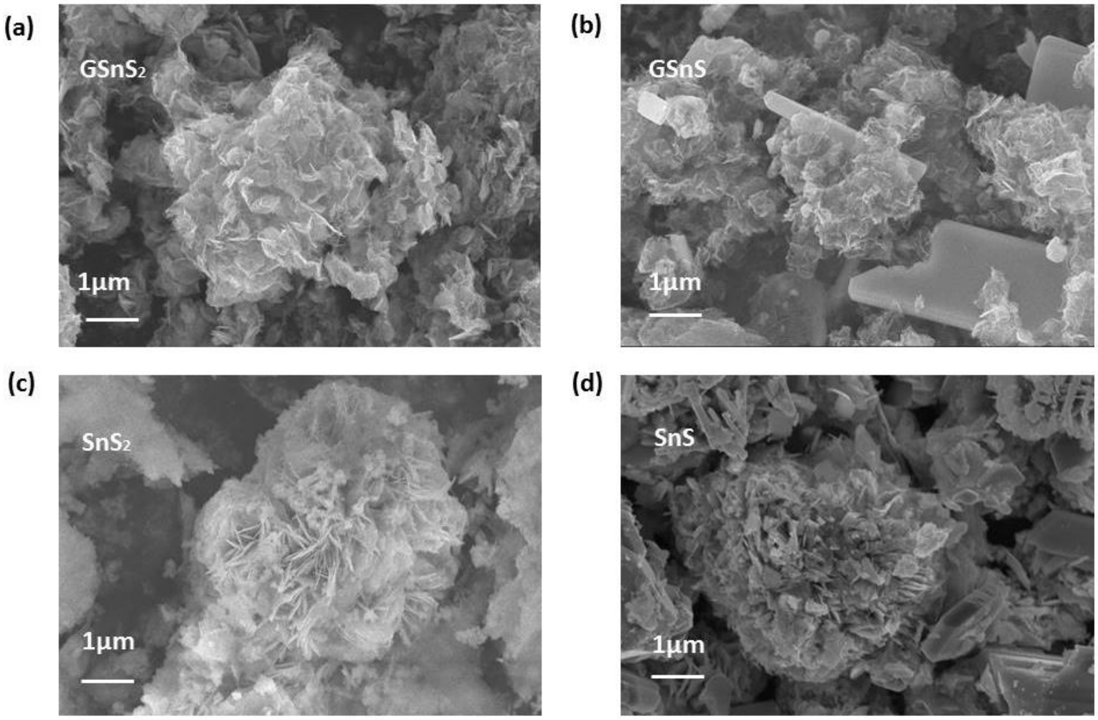

Figure 33: The SEM images of different materials: GSN-SnS_2, GSN-SnS, SnS_2, and SnS.

The lithium storage performances were investigated by galvanostatic discharge and charge processes. **Figure 34(a)** shows voltage profiles with a voltage range between 0.1 and 3V (versus Li^+) of GSN-SnS electrodes. It is demonstrated in **Figure 34(b)** that number of cycles with discharge and charge capacity of the series products that were synthesized in this study. It is shown in **Figure 34(a)** that there is a large irreversible capacity for the initial cycle. The formation of a solid electrolyte interphase(SEI), conversion reaction of SnS with Li ion, which forms Sn and Li_2S, and some unexpected reactions during charging / discharging process are attributed to the charge capacity decay for the first cycle.[106] According to the curves of the subsequent cycles, there is a sharply decrease in the loss of the irreversible capacity, which indicates that most irreversible capacity occurrs in 1st cycles. Remarkably , for the first cycle, GSN-SnS exhibits discharge and charge capacities of about 1630 and 1132 mA h /g, corresponding to a columbic efficiency of about 69.4% , which is due to the decomposition irreversibly of SnS to metallic tin that is surround by an Li_2S matrix and SEI formation . Then, the cycle efficiency is maintained at around 97% when the cycles reaches to 200 cycles (see **Figure 34(b)**) .**Figure 35** shows discharge / charge curves for GSN-$SnS_{2,}$ SnS_2, SnS, and

GSN as comparison experiments. The initial charge capacities for GSN-SnS_2, SnS_2, SnS and GSN are 1050, 752, 629, 550 mAh/g which are lower than that of GSN-SnS.As expected, GSN-SnS_2 retains lower capacity than that of GSN-SnS even though it still exceeds the theoretical capacity of SnS_2 (645 mAh/g). After more than 100 cycles, GSN-SnS can still obtain a reversible capacity of around 870 mAh/ g and even after 200 cycles, it is around 850 mAh/g while GSN-SnS_2 exhibits 700 mAh/g. In comparison, the curves of cycling performances for SnS_2 and SnS are declining all the time (**Figure 34(b)**). After 200 cycles, the capacities for SnS_2 and SnS are 200 and 300 mAh/g. This is attributed to the fact that with no graphene as supporter, the particles were agglomerated to for larger size (**Figure 33**), which provides less active sites for lithium insertion/ de –insertion process. Particularly, GSN-SnS shows better cycling performances than that of other composites. It is attributed to its theoretical capacity and a synergistic effect in the presence of doped graphene and tin based materials.

Furthermore, in terms of improved electrochemical performances, graphene plays a key role that it provides 2-dimensional electron pathway and large contact sites for tin sulfides. Graphene not only provide buffer space for the large volume change of tin sulfides but also suppress the volume change. In our work, the graphene is dual doped by sulphur and nitrogen (GSN), which acts as the attracter for tin sulfides to keep the integrity for the electrodes. It is also assumed that GSN partially contributes to specific capacity, but worth nothing. These roles of GSN can be directly supported by testing the performance of only GSN (see **Figure 34(b)**, **Figure 35(d)**). The initial cycle for graphene shows a first charge capacity of 509 mAh/g. Subsequently, the cycles show reversible capacity at 300 mAh/g for more than 100 cycles. Generally speaking, GSN-SnS_2 and GSN-SnS both demonstrate high specific capacity and acceptable cycle stability, which can be attributed to the functions of dual doped graphene in the composites.

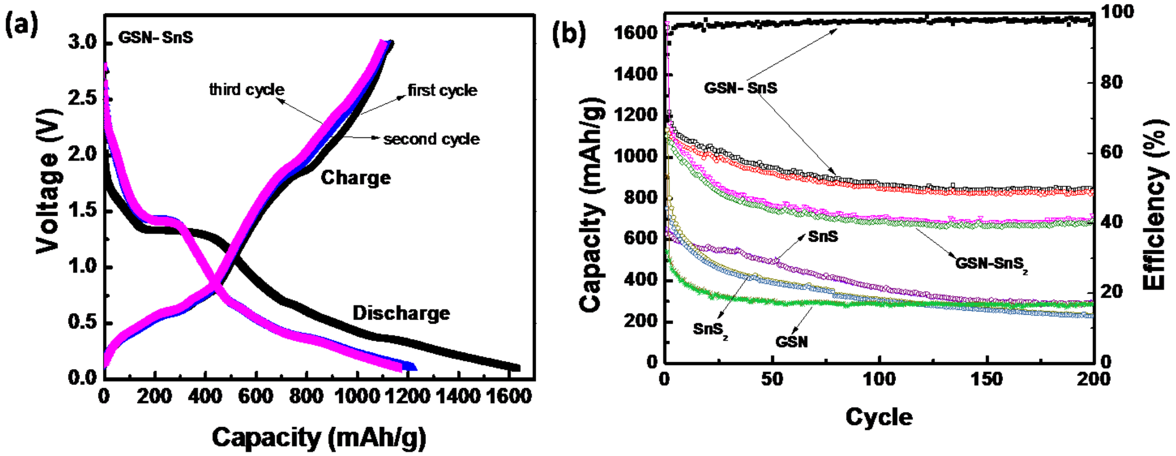

Figure 34: Galvanostatic (a) discharge and charge curves of GSN-SnS (b) discharge and charge capacity of GSN-SnS, GSN-SnS$_2$, SnS$_2$, SnS, GSN, at current rate of 0.1A/g with respect to the cycle number.

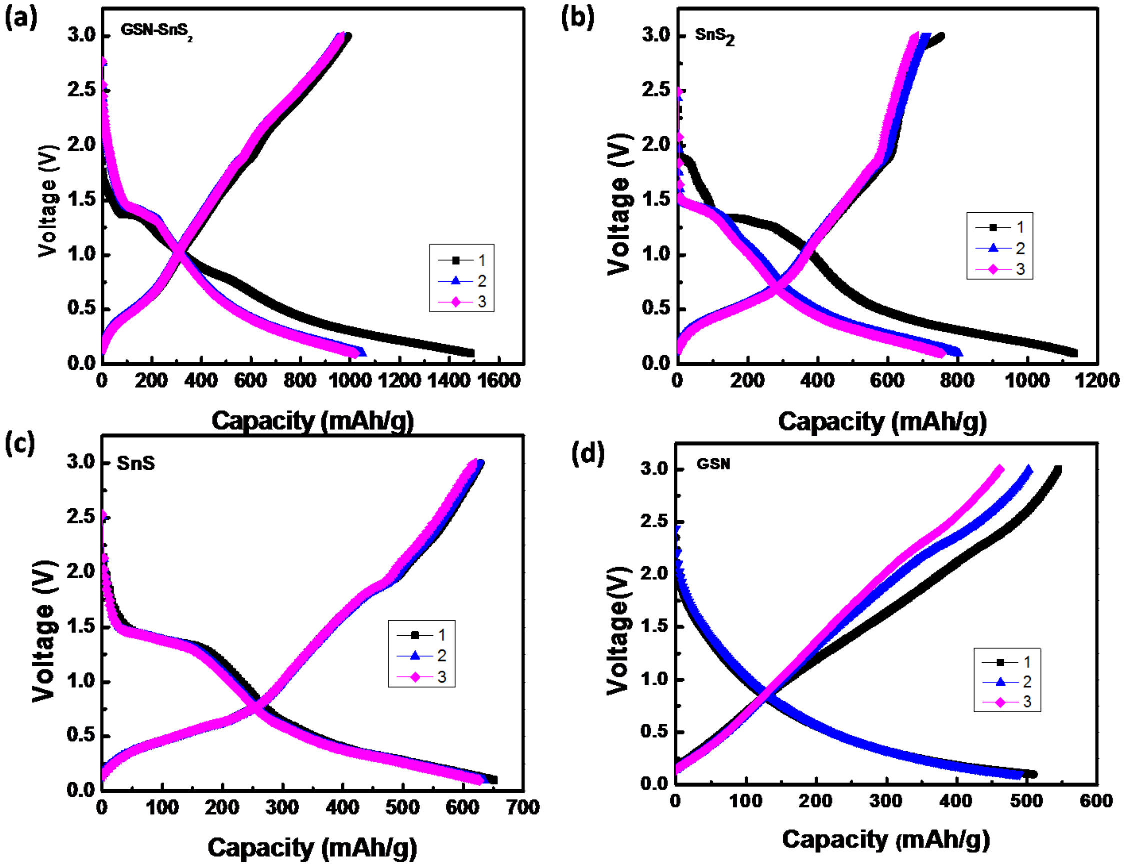

Figure 35: Galvanostatic discharge and charge curves of GSN-SnS_2, SnS_2, SnS, and GSN.

The rate permance along with cylce stability of GSN-SnS_2 andGSN-SnS were tested and shown in **Figure 36** and **Figure 37**. The test was conducted at the current densities from 100 to 1000mA/g with 10 cycles to investigate cycle stability. At current densities 0.1, 0.25 ,0.5 , 0.8, 1A/g, the capaities for GSN-SnS are 1000 , 830 , 750 , 700, 620 mAh/g respectively while GSN-SnS_2 exhibits quicker decrease in the capacity at higher current densities even though they are still better than that of SnS_2 , SnS , GSN, which show lower capacities as shown in **Figure 38(a)**. It can be seen that at the highest current densities 1000mA/g , the capacities for SnS_2 and SnS are only around 300 mAh/g even for GSN , it is only 100mAh/g . Also , **Figure 36(a)** and **Figure 37(a)** show the curves for voltage profiles for GSN-SnS_2 and GSN-SnS at different densities. Obviously , it is observed that the decreasing trend based on reversible capacities for GSN-SnS is smaller than that of GSN-SnS_2 which further expresses that excellent performances for GSN-SnS .

In order to know the stabilities for GSN-SnS_2 and GSN-SnS at higher current density , long cycles for both materials at 0.5 A/g are obtained for 1450 cycles after rate capability testing (50 cycles in the top right corner) as shown in **Figure 36**, **Figure 37**. Clearly , the stability for GSN-SnS is prominent : after 50 cycles , there is no obvious decrease in the capacity . After 1000 cycles , the capacity for GSN-SnS is maintained at 600 mAh/g , subesenquently , until 1500 cycles , it is still more than 550 mAh/g . However , compared with GSN-SnS , GSN-SnS_2 reflects a worse stability and capacity : after 500 cycles , it shows a sharp decrease in the capacity and until 1000 cycles , it is stable at around 200 mAh/g .

In order to clarify the hybrid effect on the electrochemical performance of GSN-SnS_2 and GSN-SnS, it is necessary to calculate theroratical capacities of nanocomposites . It is considered thetheroretical capacity of SnS as 782 mAh/g and for graphene as 509 mAh/g (acquired from the maximum charge capacity from **Figure 34(d)**). Based the TGA information, the mass ratio of SnS is considered as 73% while the mass ratio of graphene is deducted from 100%, which is 27%. The theoretical capacity of the mixture can be calculated by the following:

$C_{\text{theoretical for GSN-SnS}} = (C_{\text{SnS}} * \text{mass\% of SnS}) + (C_{\text{Graphene}} * \text{mass \% of Graphene}) = 782 * 0.73 + 509 * 0.27 = 707.43$ mAh/g

The observed capacity for GSN-SnS is 600 mAh/g after 1000 cycles at 0.5A/g (as computed from **Figure 36(b)**), it can be clearly demonstrated that the retention for GSN-SnS was around 85%, which further confirmed the excellent stability of this material. On performing similar calculation for GSN-SnS_2, it is suggested the mass ratio of graphene is the same as that of GSN-SnS and the theoretical capacity of GSN-SnS_2 is 645 mAh/g, then:

$C_{\text{theoretical for GSN-SnS2}} = （C_{\text{SnS2}} * \text{mass\% of SnS}) + (C_{\text{Graphene}} * \text{mass \% of Graphene}) = 645 * 0.73 + 509 * 0.27 = 607$ mAh/g

For the reversible capacity observed in **Figure 37**, it is stable at 200 mAh/g after 1500 cycles based on the current density 0.5 A/g, which means the capacity retention is only around 33%. It provides a conclusion that GSN-SnS offers superior electrochemical properties than that of GSN-SnS_2.

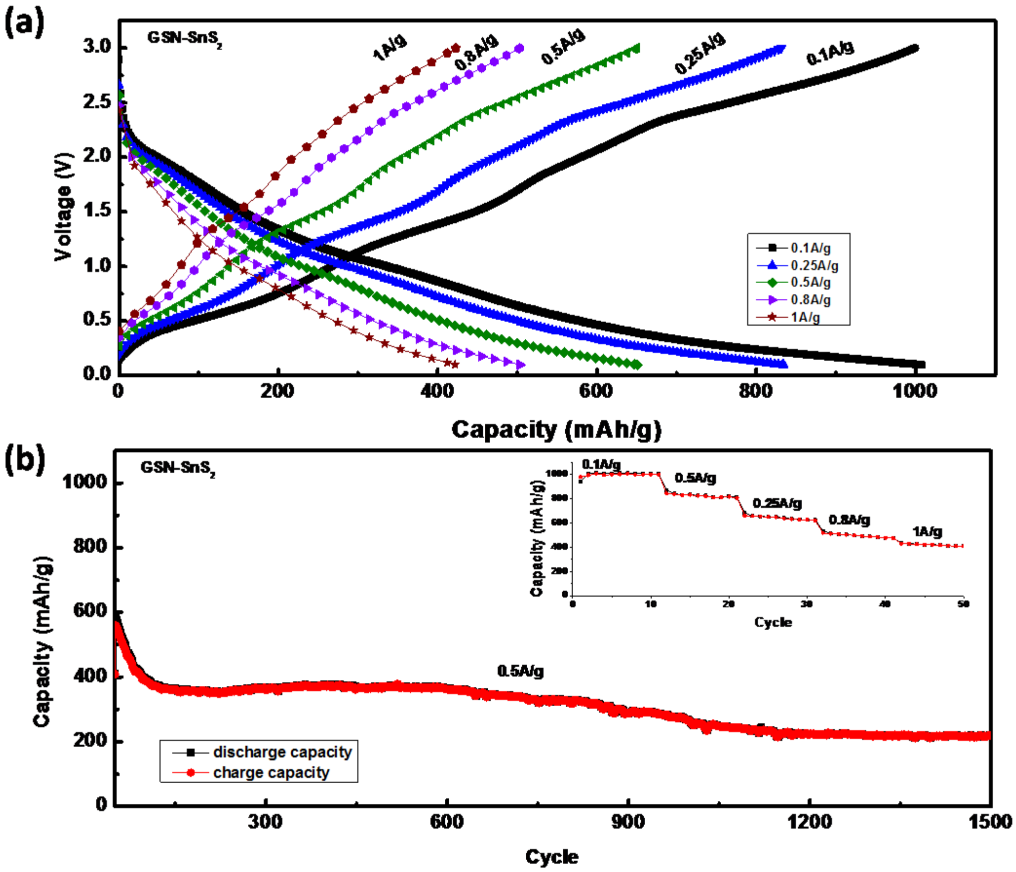

Figure 36: (a) and (b) voltage profiles for GSN-SnS$_2$ at different current densities followed by cycle stability.

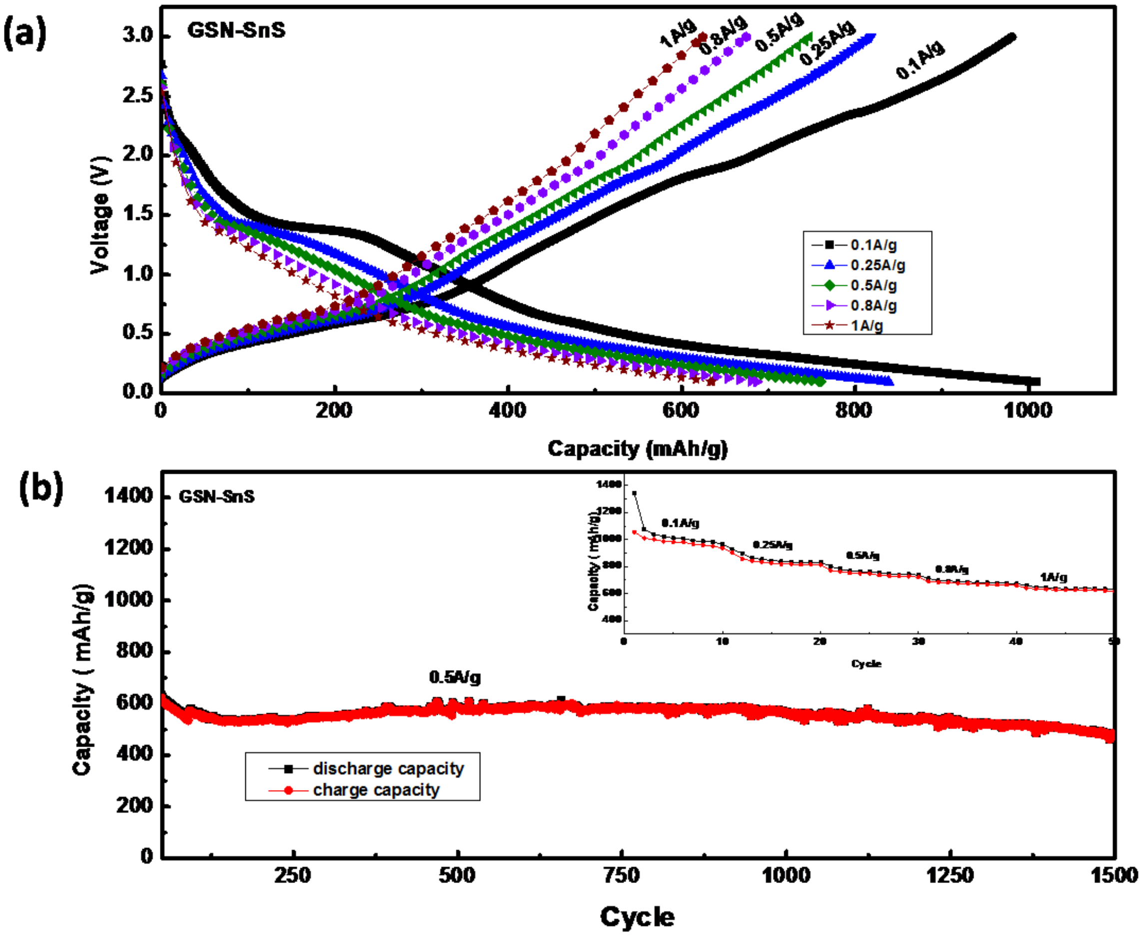

Figure 37:(a) and (b) Voltage profiles for GSN-SnS at different current densities followed by cycle stability.

The cyclic voltammogram (CV) profiles of coin cells for GSN-SnSx as anodes for LIBs were characterized for the study of electrochemical reaction mechanism. **Figure 38(b, c, d)** shows the CV curves for GSN-SnS_2, GSN-SnS and GSN nanocomposites. The Li^+ insertion/de-insertion mechanism could be proposed as the following equations[107]:

$SnSx+xLi +2e \rightarrow Sn +xLi_2S$ (equation 1)

$Sn+xLi+xe \leftrightarrow LixSn$ $(0 \leq x \leq 4.4)$ (equation 2)

For **Figure 38(b)** and **(c)**, for the first cycle , the peak in the cathodic scans at around 0.6-1.3V (a) is corresponding to decomposition of SnSx to Sn and Li_2S which may result in large irreversibility of the electrode at the first cycle as shown in equation1**,** and the second dominant peak at around 0.05V (b) is related to the formation of LixSn alloys as the following equation 2 shown.[34] And for GSN-

SnS$_2$ and GSN-SnS, the X is different. The X for SnS$_2$ is 2 while SnS is 1, which explains that why SnS$_2$ has a lower capacity than SnS.

During the anodic process, at the peak about 0.5 V(c), Sn-Li encountered a delithiation process .It is clear that there is another anodic peak at about 1.8 V, which is suggested that lithium intercalation of the GSnS$_X$ layers without phase decomposition.[108] During the continuing two cycles, there is no obvious loss of the area in the CV testing, indicating the good stability of the electrodes. As shown in **Figure 38(d)**, for the first cycle scanning of GSN, there are two reduction peaks on the cathodic side: 0.6 V, 0.1 V. At 0.6 V, it is related to the formation of solid electrolyte interphase (SEI) which corresponds to the large irreversible capacity for the first cycle. At 0.1 V, it is forming the lithium alloys. For anodic side, at 0.2 V, the peak is related to the separation of lithium alloys. [98]

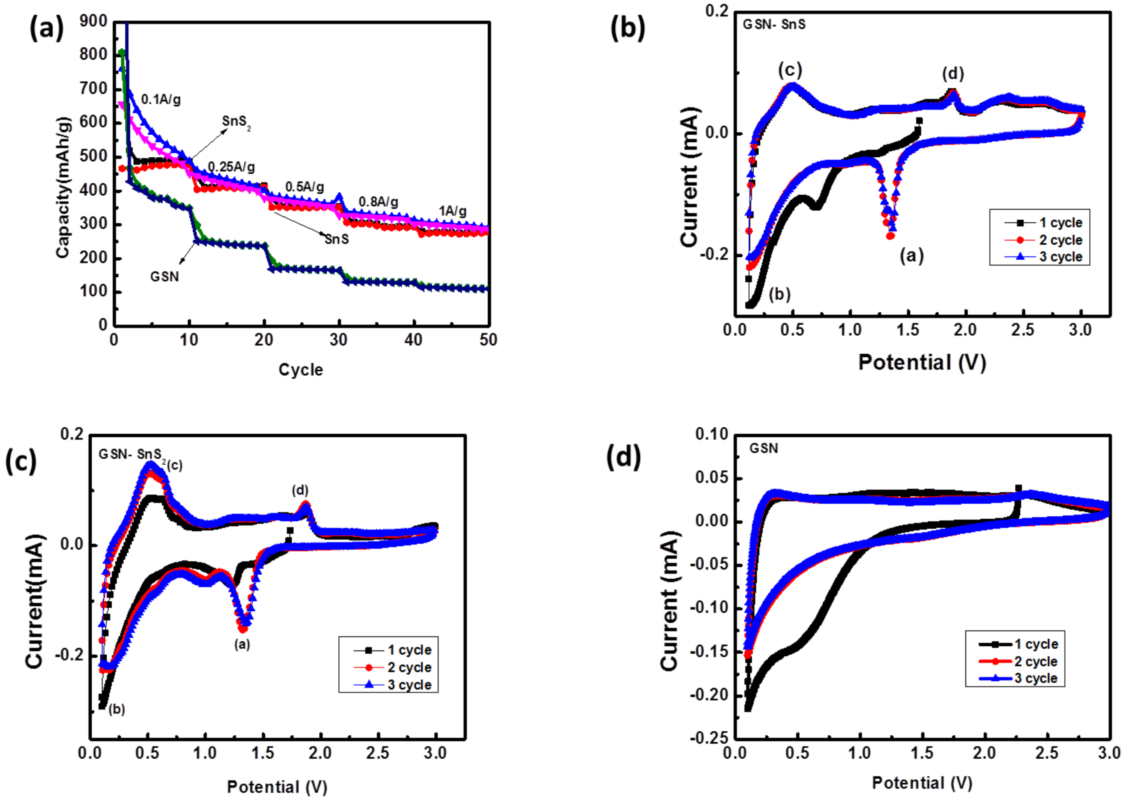

Figure 38 :(a) Rate capabilities for SnS$_2$, SnS, GSN; (b) (c) (d) the CV testing for GSN-SnS, GSN-SnS$_2$, and GSN.

To explain why GSN-SnSx nanocomposites have different features, electrochemical impedance spectroscopy (EIS) measurement for coin cells were obtained as Nyquist plots shown in

Figure 39.Compared with GSN-SnS_2 nanosheets, the after annealing material shows lower charge transfer resistance and SEI resistance.

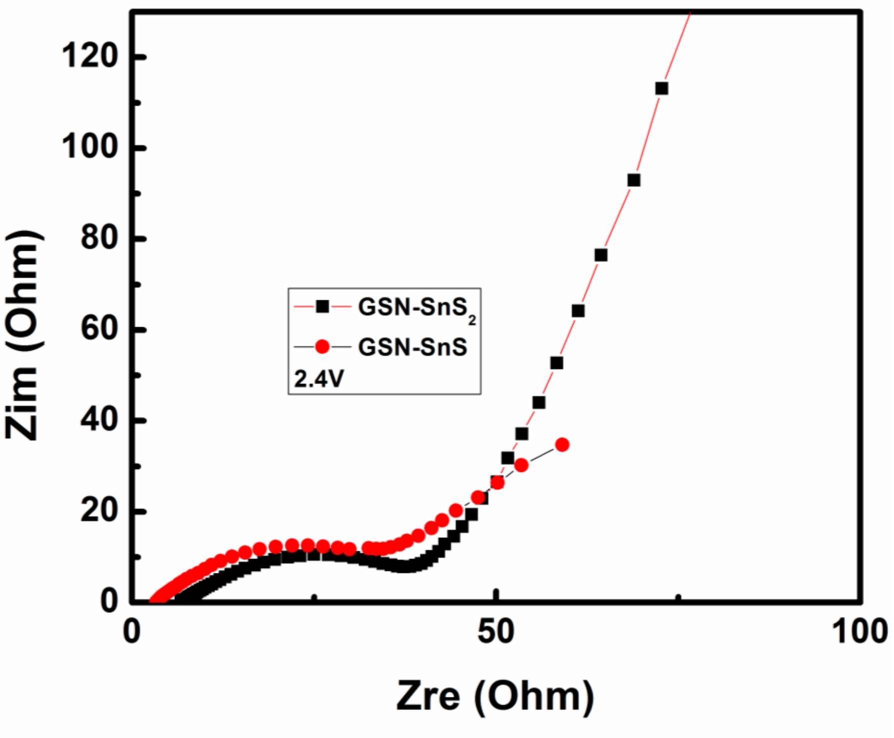

Figure 39: EIS of both materials in a frequency range of 1 × 10^6 to 1 × 10^{-1} Hz and at the amplitude of 10mV.

By combing the cyclic voltammogram illustrated in the **Figure 38**, the mechanism of GSN-SnS_2 and GSN-SnS during the discharging and charging process were explained further. During the discharging process, at the voltage point around 1.3 V, the SnS is reduced to sulphur through a conversion reaction, which is consistent with the charging / discharging profile as shown in the **Figure 40(a)** , where there is a plateau at that voltage point . For the next step, it is the reversible reaction about the lithium ions with as formed tin. As shown in the **Figure 40**, the only differences for the discharging / charging process of two batches of materials are the conversion reaction. Alpha tin with face centered structure is produced when the material is SnS while that is beta tin when the material is SnS_2. According to the literature, it can be known that alpha tin can retain crystallinity when lithiation process happens which shows better performance for lithium storage while beta tin is amorphous during charging / discharging process. [95]

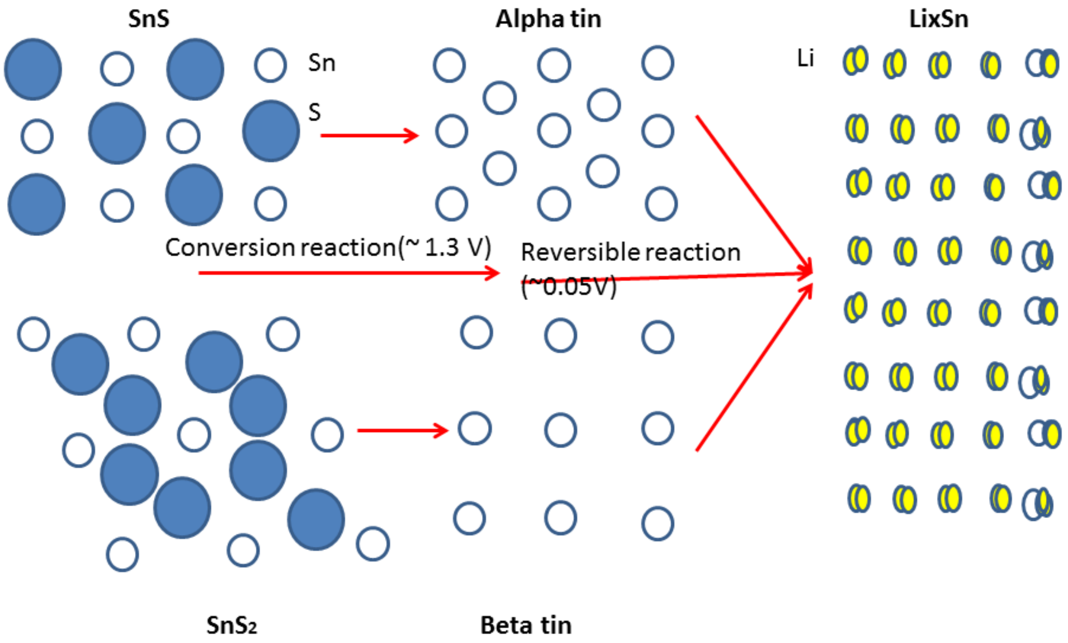

Figure 40: The schematic diagram of lithiation process for both materials.

Also, in this work, we investigated and optimized the electrode fabrication process by using the highly crossed – linked binder (sodium carboxymethyl cellulose and poly acrylic acid).

According to the **Figure 41**, it can be seen that there is a condensation reaction between the binders at 150 degrees, which forms a cross – linked structure for the electrodes that is beneficial for improving the stability of the batteries for the polymer binder shows high mechanical resistance to strain and no swelling in commercialized electrolytes which will result in no large movement.[109]

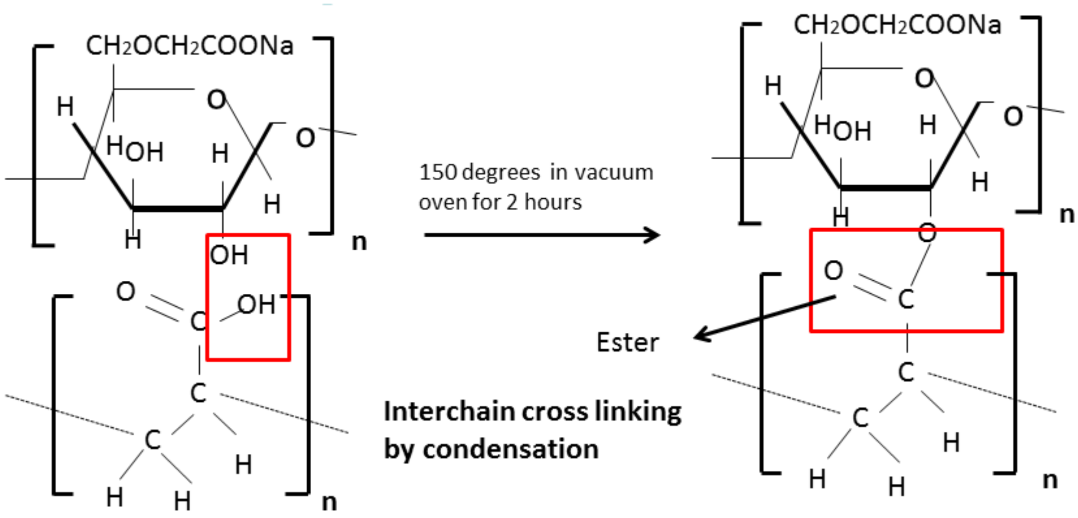

Figure 41: The scheme of chemical reaction for binders in the annealing process of electrodes for GSN-SnS_2 and GSN-SnS at 150 degrees.

Chapter 4

Conjugate polyacrylonitrile: a binder and conducting medium for highly stable anode material for lithium ion batteries based on SnS_2/Graphene nanocomposites

4.1 Introduction

The excessive consumption of natural fossil fuel leads to a vital role as renewable energy storage devices for applications in electric vehicles, portable laptops. Traditionally, graphite is employed as anode material with 372 mAh/g, which cannot satisfy tremendous demand for the advance of new technology. In terms of lithium ion battery, nowadays, it requires a new type of anode electrode materials with high energy density, reliable safety as well as low fabrication cost for practical development.[3, 110-113] Based on the high theoretical capacity of 645 mAh/g, tin disulfide is one of the best candidates. However, there are two main challenges for tin disulfides: the formation of Solid electrolyte interphase resulting low columbic efficiency for the first cycle and large volume expansion leading to rapid capacity loss during charging / discharging process.[114]

To confine volume expansion, an effective method to tailor the nanostructure and buffer the mechanical strain is combing SnS_2 with conductive matrix.[115, 116] Graphene with large surface area,[117] superior mechanical strength and excellent electronic transport[118, 119] is considered as an ideal conductive supporter for tin disulfides. It can be used for modifying the size of tin disulfides, which prevents tin disulfides from aggregation that has a negative effect on the lithium transport and reduce the active sites for lithium utilization.[114] It has been reported that SnS_2 nanostructures with graphene has shown improved electrochemical performance.[120, 121] These nanocomposites are intending to enhance batteries' cycle stability and improve the current efficiency.

Further, polymeric binder is likely to be significant in the design of electrodes 'fabrication. In fact, polymeric binder after heat treatment either carbonization or curing can rearrange the electrode surface, which is supposed to provide an elastic accommodation for volume expansion leading to improve the stability. Additionally, the covalent linkages between the binder and the active materials can ease the mechanical damage resulted from volume expansion. It has been reported that this tragedies are used to maintain the electrodes integrity for tin based materials.[122] A recent report shows by using polyvinylpyrrolidone (PVP) as carbon precursor to synthesis uniform Sn/ C composites performing high rate capability.[123] A facile solid state reaction for successfully synthesizing SnS_2/C has provided a unique concept to exert the function of polymer fully.[124] Actually, these processes are sophisticated and tedious for the synthesis of active materials and until now, there is not a highlighted electrochemical performance for tin disulfides based on this methodology. Instead, it may lead to excessive cost for the preparation of electrodes.

In this work, a safe and economical method is presented for post – treatment of SnS_2 /G made by solvothermal method to achieve high performance. The low temperature heat treatment (LTHT) engineers the electrode structure, which has the following advantages: the curing of polymer provides the conductive addictive; the heat treated electrodes are attributed to the enhanced electrode integrity. To our knowledge, polyacrilonitrile (PAN) is a conductive polymer and the glass transition temperature is 90 degrees. After this temperature, there is an improvement in elasticity of PAN, which is useful for lithium ion batteries. Also, the mechanical rearrangement for the electrodes after heat treatment leads to a more compact structure, which effectively reduces the access of electrolyte to electrode's voids. To some extent, it eases the negative effect of SEI, which makes a contribution to the improvement of cycle efficiency for the first cycle. In this report, the composites for SnS_2/G with polymer binder after LTHT exhibits improved performance: after 150 cycles, at current density of 0.25A/g, the capacity is stable at 1000mAh/g and the coulombic efficiency is still 100%.

Also, a new reaction mechanism is proposed. Normally, the reaction for SnS_2 during charging/ discharging process is two steps: SnS_2 +2Li $\Leftrightarrow$2 Li_2S +Sn (1) Sn+Li $\Leftrightarrow$$Li_{4.4}Sn$ (2).[107] It is reported that the first step contributes to irreversible capacity while the second step is attributed to reversible capacity. However the reversible capacity of SnS_2/G is twice higher than the calculation based on the traditional reaction mechanism of SnS_2 (the theoretical capacity is 645mAh/g). Then, it is believed that the content of Li_2S in the first step also provides reversible capacity. It is confirmed by cycling voltammetry (CV).

4.2 Methods

4.2.1 Preparation of SnS_2/G

Graphene oxide (GO) was fabricated according to previous literature procedures. To synthesize SnS_2/G nanocomposites, a mixture of GO, ethylene glycol, $SnCl_2.2H_2O$ and thiourea was prepared. Secondly, the above suspension was transferred into an autoclave and heats the solution 10hours @ 100 °C and 10hours @200°C. After that, the autoclave was cooled to the room temperature, and the products were collected and filtered. Then the products were put into a freeze dry machine (Labconco Freezone 1, USA) for two nights and l the material was labeled as SnS_2 /G.

4.2.2 Electrode fabrication

Electrodes for lithium ion battery testing were fabricated by using as- prepared active materials. The working electrodes contain 70% SnS_2/G and 30% polyacrylonitrile (PAN) as a binder. The slurry is mixed by grinding for 30 minutes then coated on Cu foil. The average mass loading of SnS_2-G on the electrodes is around 0.8 mg. The electrodes were dried in convection oven at 333K for 1 hour, which were followed by the vacuum oven at 353K for overnight. Then electrodes were dealed by heat treatment as the below shown. More reference experiment was prepared with only graphene and PAN as the same ratio.

4.2.3 Low temperature heat treatment

Electrodes were placed in vacuum oven and kept at temperature at 80 degrees, 150 degrees for 5 hours. And a batch of electrodes were heated up to 500 degrees for 2 hours then followed by holding for 3 hours in the furnace under the gas flow of 140 SCCM Ar. And they are named by SnS_2/G/PAN/80^o C, SnS_2/G/PAN/150^o C SnS_2/G/PAN/500^o C.

4.2.4 Electrochemical measurements

2023- Type coin half cells were fabricated in an argon filled glove box and lithium metal as counter electrode. The separator for separating the two electrodes was made from polypropylene. And $LiPF_6$ (1 M) in ethylene carbonate/diethyl carbonate (EC/DEC, 3:7vol %) was employed as electrolyte. The voltage range for Galvanostatic charge/ discharge test was 0.1 to 3 V versus Li^+ /Li with different current densities based on NEWARE BTS – CT 3008 (Newware Technology ,Ltd .,Shenzhen , China) . Cyclic voltammetry (CV) were performed on VMP3 potentiostat / galvanostat (Bio-Logic LLC, Knoxville, TN) by using the voltage range from 3 to 0.1 V at a scanning rate 0.1 mV/s.

4.2.5 Material Characterization

X-ray diffraction (XRD) patterns were collected on using Ni-filtered Cu Kα radiation (λ =1.5418 Å). The morphology of the nanocomposites was observed using a field emission scanning electron microscope (FE-SEM, Zeiss Ultra Plus, and UK).Thermal gravimetric analysis (TGA) was carried out to explore the ratio of tin disulfides and graphene.

4.2.6 Results and Discussion

The synthesis process of SnS_2/G is based on solvothermal methodology by employing graphene oxide as oxidizer. It consists of two steps: at lower temperature, it is the formation of SnO_2/G and there is a transformation from SnO_2 to SnS_2 at higher temperature.

In order to confirm the component of the composites for the pre -synthesized materials and the electrodes combing SnS_2/G with PAN followed by heat treatment at different temperatures, XRD results are teste and shown in **Figure 42**. **Figure 42(a)** represents the peaks for SnS_2/Gcan be indexed to hexagonal SnS_2 (JCPDS No. 01-1010), which indicates that the pure SnS_2 has been obtained. After heat treatment at 80, 150 degrees, the XRD of the electrodes **(Figure 42b, c)** expresses the active material in the electrodes is SnS_2 with no change. **Figure 42(d)** introduces the analysis of XRD after 500 degrees. It is observed that the peaks is mainly matched with that of SnS (JCPDS No. 39-0354), which means there is a chemical reaction between SnS_2 and SnS.

To verify the morphology of SnS_2 /G, the SEM image in **Figure 43(a)** illustrates that hexagonal SnS_2 nanosheets are wrapped with graphene layers. The SEM images in **Figure 43(b, c, d)** show the surface morphology of the electrodes with heat treatment at various temperatures with the same magnification. It can be observed that SnS_2/G/PAN/150 ^{o}C in **Figure 43(c)** shows the large microparticles of graphene sheets (2~ 7 micrometer) sandwiching the SnS_2 particles with limited interfacial voids (**Figure 44**), which restricts the entrance of the electrolyte to the inner of the electrodes and then minimize the SEI formation. It is advantageous for the improvement of the columbic efficiency for the first cycle. The graphene sheets enhance the conductivity and render them elastically, which result in combonding the stress for the volume expansion during lithiation and delithiation. Consequently, this leads to more stable and higher reversible capacity. In comparison, it is clear that the structure of SnS_2/G/PAN/80 ^{o}C electrodes is not compact as SnS_2/G/PAN/150 ^{o}C, which is attributed to the lower temperature heat treatment. In terms of SnS_2/G/PAN/500 ^{o}C, PAN is totally carbonization and partially thermal degradation at high temperature, which does not provide elasticity for the electrode. And at 500 degrees, there is a chemically phase transition from SnS_2 to SnS based on XRD, which deepens the collapse of the electrodes. As shown in **Figure 43(d)**, the electrode breaks down with disorder voids, which provides opportunities for the formation of SEI. It is predicted that SnS_2/G/PAN/500 ^{o}C has worst durability while SnS_2/G/PAN/150 ^{o}C has the best stability.

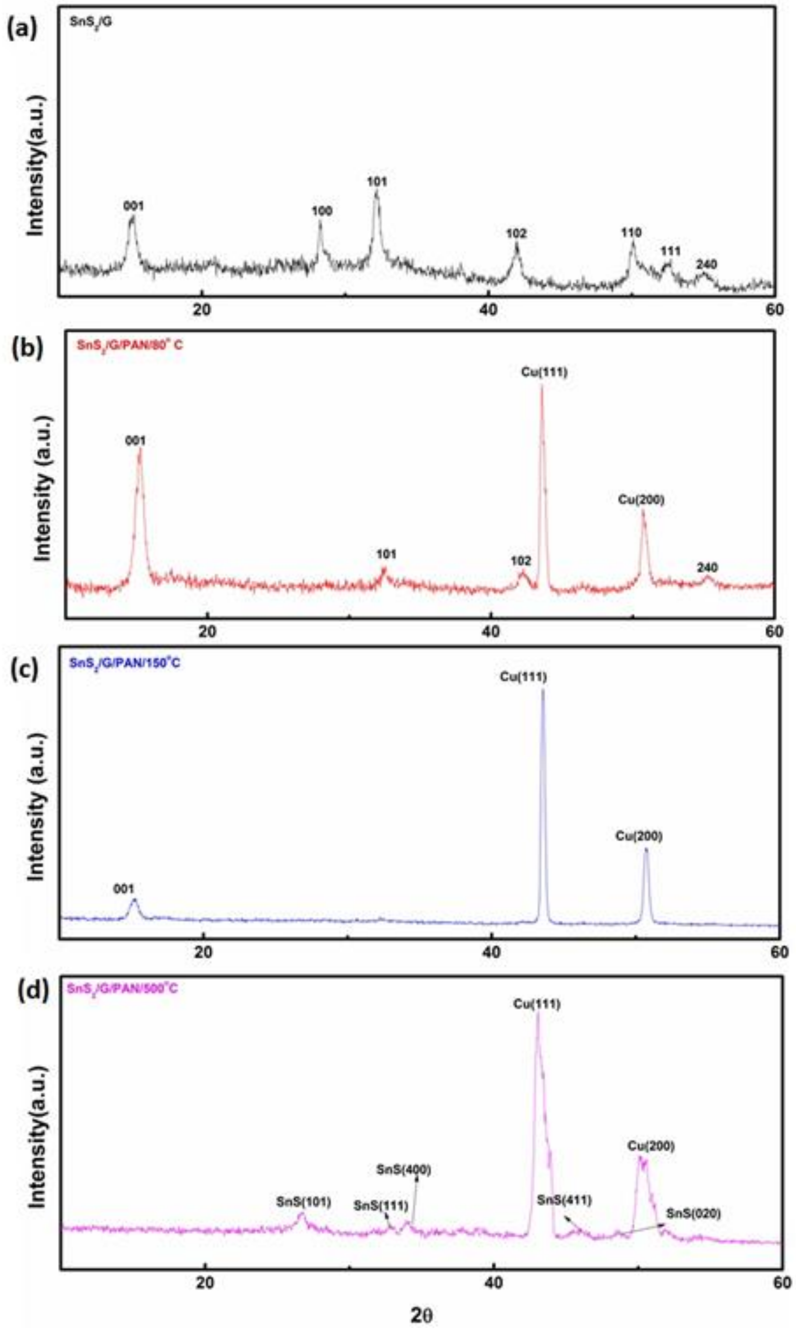

Figure 42: XRD analysis of SnS_2/G, SnS_2/G/PAN/80^{o}C, SnS_2/G/PAN/150 ^{o}C, SnS_2/G/PAN/500^{o}C.

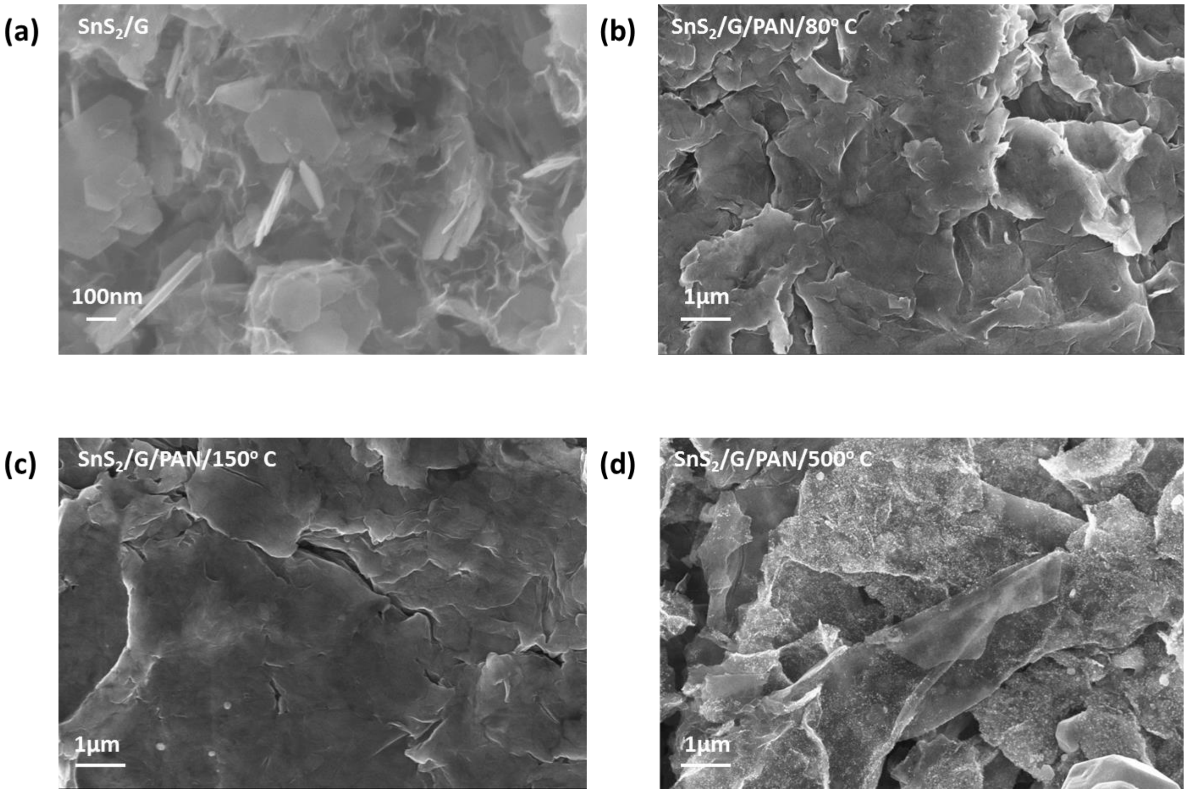

Figure 43:(a) SEM micrographs for SnS_2 /G active materials; (b) (c) (d) SEM images of the electrode surfaces before and after heat treatment (80, 150, 500 degrees).

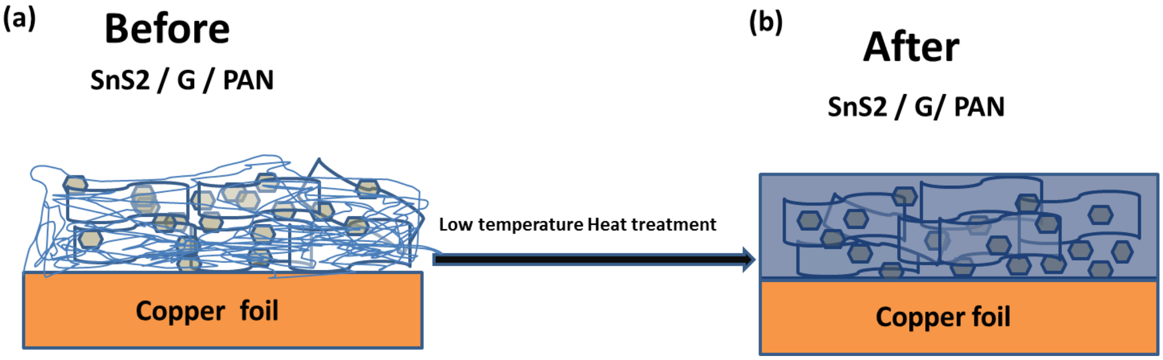

Figure 44: (a) and (b): Schematic of electrode surface before and after LTHT.

The content of SnS_2 in nanocomposites was determined by TGA, which was performed in air from room temperature to 800 degrees **(Figure 45).** It can be observed that there are two main sharp decreasing temperature regions. One is from 200 to 450 degrees, which is attributed to the oxidization of SnS_2. It is all known that there is a 17.5% loss in weight. The range from 450 to 800 degrees is mainly due to the decomposition of graphene. It can be finally calculated that graphene is occupied 19.5%. The remaining SnS_2 is deducted by 100%, which is 80.5%, respectively. It can be suggested that there is a high weight percentage of tin disulfides nanosheets as active material in the composites.

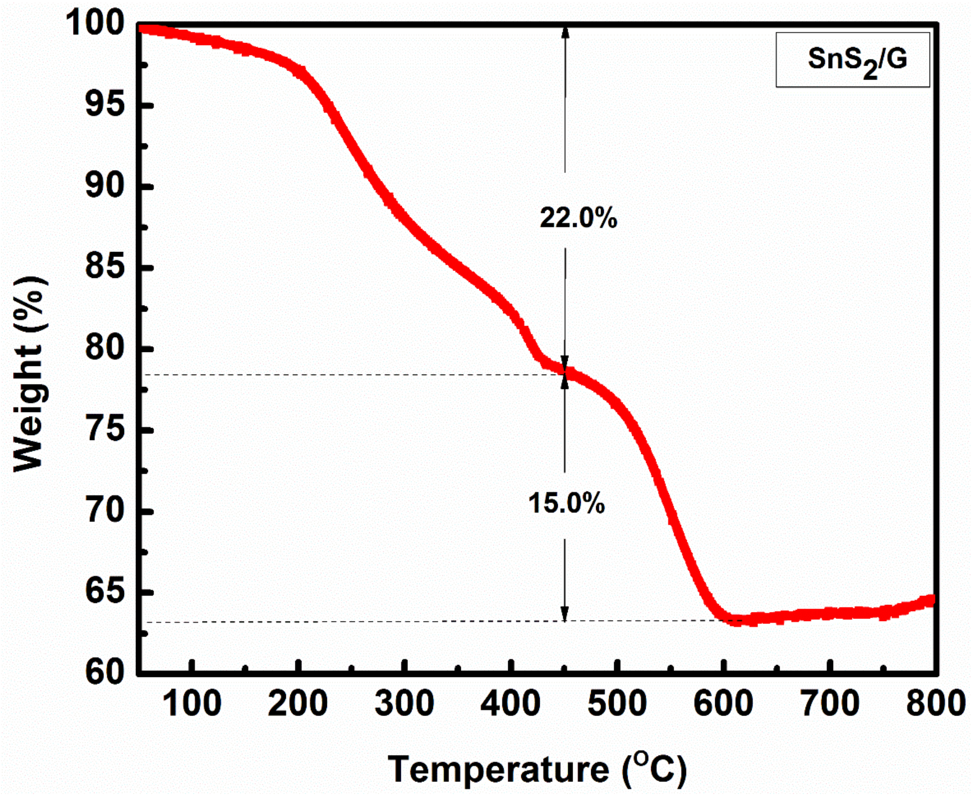

Figure 45: TGA analysis of SnS_2/G.

In order to demonstrate the potential application of SnS_2/G prepared by graphene oxide and stannous chemicals, a round of electrochemical testings was utilized to determine the performance in lithium ion batteries. SnS_2/G was dispersed as active material and PAN as binder, which was deposited on a copper current collector followed by controllable heat treatment. Then, the coin cells were assembled in glove box, which were tested on galvanostatic charge/discharge cycling, cyclic voltammetry (CV) and electrochemical impedance spectroscopy (EIS).

Figure 46 introduces the voltage profile for SnS_2/G/PAN with heat treatment (80 °C, 150 ° C, 500 ° C and graphene/PAN with heat treatment (150°C) at low current 0.1A/g and a voltage range of 3 to 0.1 V. In **Figure 46(b)** **(**SnS_2/G/PAN/150 °C**)**, there is a plateau at 1.3 V, which corresponds to the expected behavior of the formation of metallic tin and lithium sulfide. The discharge capacity for the first cycle is 1517mAh/g with a columbic efficiency of 79%, which is attributed to the formation of solid electrolyte interphase (SEI) even though it has shown a high reversible capacity. In comparison, **Figure 46(a, c, d)** illustrates the voltage profiles for SnS_2/G/ PAN/ 80 ^oC , SnS_2/G/ PAN/ 500 ^oC, Graphene/ PAN/ 150 ^oC , which shows that the first cycle discharge capacities and columbic efficiencies are 1273 mAh/g and 79% , 1461 mAh/g and 79%, 657 mAh/g and 71% , respectively .The cycle test is depicted in **Figure 47(a)** at a low current density 0.1 A/g for SnS_2/G/PAN with heat treatment (80 ^oC (reference), 150 ^{o} C, 500 ^{o} C) and graphene /PAN (150^oC) .

It is clearly observed that the capacity for SnS_2/G/PAN/150 ^oC maintains at 1200 mAh/g after 60 cycles and there is no apparent shaking in the capacity change for the 60 cycles with a columbic efficiency of 100% except for the first cycle, which is attributed to the functionality of graphene and PAN with low temperature heat treatment. Graphene layers with flexibility provide enough space for volume expansion of SnS_2/G and electron pathway. In addition, PAN with a low temperature heat treatment which is higher than glass transition temperature, is soften and flowing in the electrodes when the temperature reaches 150 ^{o} C, which results in a physical change in the interior electrode that the binder distribution is more homogenous. After cooling down, the curing of PAN leads to a more plastic polymer. The whole process is beneficial to maintain the integrity of the electrode, which further improves the cycling stability. In **Figure 47(a)**, the curve for SnS_2/G/PAN/500 oC as reference also shows high capacity after 60 cycles with 1000 mAh/g while it is not a straight line. At 500 degrees, there is a partially – pyrolyzing the PAN binder, which has a negative effect on the battery stability. Further, graphene does as small contribution to the total capacity even though it was stable at 230 mAh/g from **Figure 47(a)**. As shown in **Figure 47(b)**, a higher current density 0.25A/g for SnS_2/G/PAN with different temperature heat treatments was tested. SnS_2/G/ PAN/ 150 ^oC still exhibits superior cycling performance in terms of capacity and durability than that of SnS_2/G/ PAN/ 80 ^oC, SnS_2/G/ PAN/ 500^o C. Obviously, after 14 cycles, the reversible capacity for SnS_2/G/ PAN/ 150 ^oC is retained at ~ 1020mAh/g and after more than 150 cycles, there is no remarkable loss in capacity. Even after 250 cycles, the capacity loss compared with 1020mAh/g is 120mAh/g and the columbic efficiency for SnS_2/G/ PAN/ 150 ^oC is close to 100% except for the first cycle. For SnS_2/G/ PAN/ 80 ^oC, it is a decreasing curve, which remains a capacity of 320mAh/g. It demonstrates the structure of the electrode for SnS_2/G/ PAN/ 80 ^oC is a challenge for lithium insertion / de-insertion at high current density. Even though the cycling capability of SnS_2/G/ PAN/ 500^o C is better than that of SnS_2/G/ PAN/ 80 ^oC, it leads to a declining in the capacity and stability. After 100 cycles, the capacity is 700 mAh/g, while after 250 cycles; it decreases to 643 mAh/g which is still higher than that of SnS_2/G/ PAN/ 80 ^oC. After 300 degrees, PAN begins to carbonize and there is a phase transition chemically from SnS_2 to SnS. Until 500 degrees, the carbonization of PAN is completely finished and there is partial thermal decomposition, which represents the destruction of the elastic network structure. Also, there is a formation of SnS at 500 degrees. Both leads to the breakdown of the electrodes, which explains the instability of the battery.

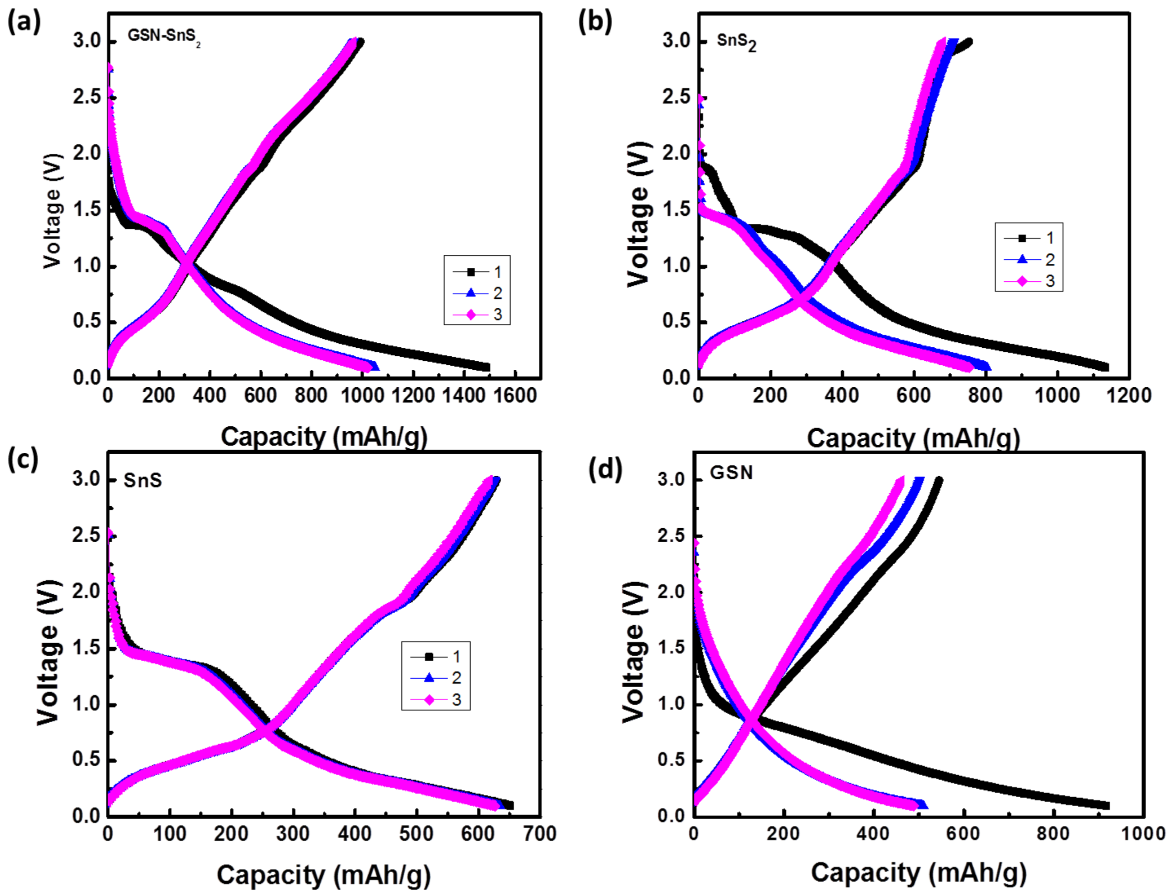

Figure 46 : (a) (b) (c) (d) Voltage profiles for coin cells containing SnS_2/G/PAN with heat treatment (80 °C (reference), 150 ° C, 500 ° C and graphene/PAN with heat treatment (150°C, reference) cycled at 0.1A/g .

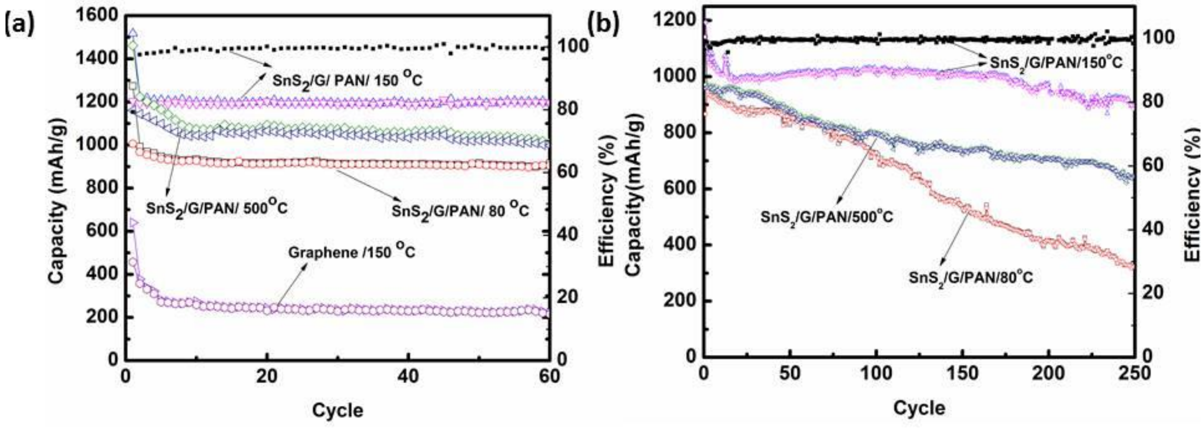

Figure 47:(a) and (b) The comparison sof the cycle capability of SnS$_2$/G/PAN with heat treatment (80 °C (reference), 150 ° C, 500 ° C and graphene/PAN with heat treatment (150°C, reference) at 0.1A/g and 0.25 A/g.

The rate capabilities of SnS$_2$/G/ PAN/ 80 °C, SnS$_2$/G/ PAN/ 150 °C, SnS$_2$/G/ PAN/ 500 °C are shown in **Figure 48**, **Figure 49**, and **Figure 50**. **Figure 49** reveals the excellent kinetics of SnS$_2$/G/ PAN/ 150 °C electrodes at different currents up to 1A/g. The capacities for SnS$_2$/G/ PAN/ 150 °C at current densities 0.1 A/g, 0.25 A/g, 0.5 A/g, 0.8 A/g, and 1 A/g are 1207, 1085, 992, 919, 880 mAh/g, respectively. Moreover, the curing structure enables a high current cycling, where a capacity of about 830 mAh/g after 100 cycles and 650 mAh/g after 200 cycles. On the other hand, the similar electrodes by replacing the heat treatment temperature 80 degrees and 500 degrees gives rate capability as comparisons are shown in **Figure 48** and **Figure 49**. For SnS$_2$/G/ PAN/ 80°C, the capacities at 0.1 A/g, 0.25 A/g, 0.5 A/g, 0.8 A/g, and 1 A/g are 1000, 957,917,880,850 mAh/g, which is lower than that of SnS$_2$/G/ PAN/ 150°C. And SnS$_2$/G/ PAN/ 500°C provide a more significant distinction.

Figure 50 introduces the capacities at 0.1 A/g, 0.25 A/g, 0.5 A/g, 0.8 A/g, and 1A/g are 948, 802, 632,500, 415mAh/g and in the following cycles, the capacity fades sharply to be stable at around 300 mAh/g.

Figure 51 shows the curves for cycling capability at even a higher current density 1.2 A/g after 10 cycles at 0.1 A/g for SnS$_2$/G/ PAN/150°C and SnS$_2$/G/ PAN/500°C. It can be concluded that after 200 cycles for SnS$_2$/G/PAN/150°C the capacity reaches to 600 mAh/g while for SnS$_2$/G/ PAN/500°C, it is only 200 mAh/g, which is attributed to the degradation of the electrode structure leading to the instability in SEI structure.

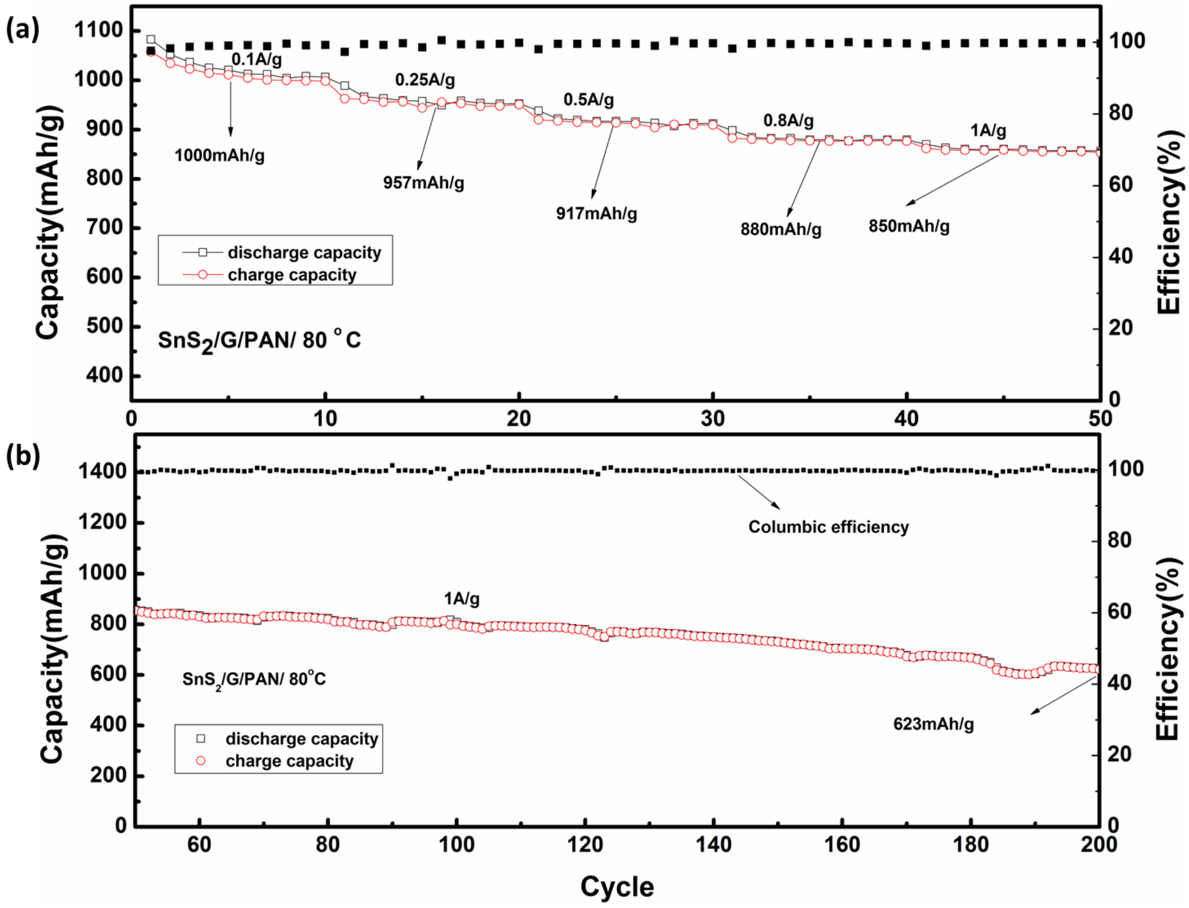

Figure 48: (a) (b) Rate capability of SnS_2/G/PAN with heat treatment (80 ^{o}C (reference),) followed by cycling capability.

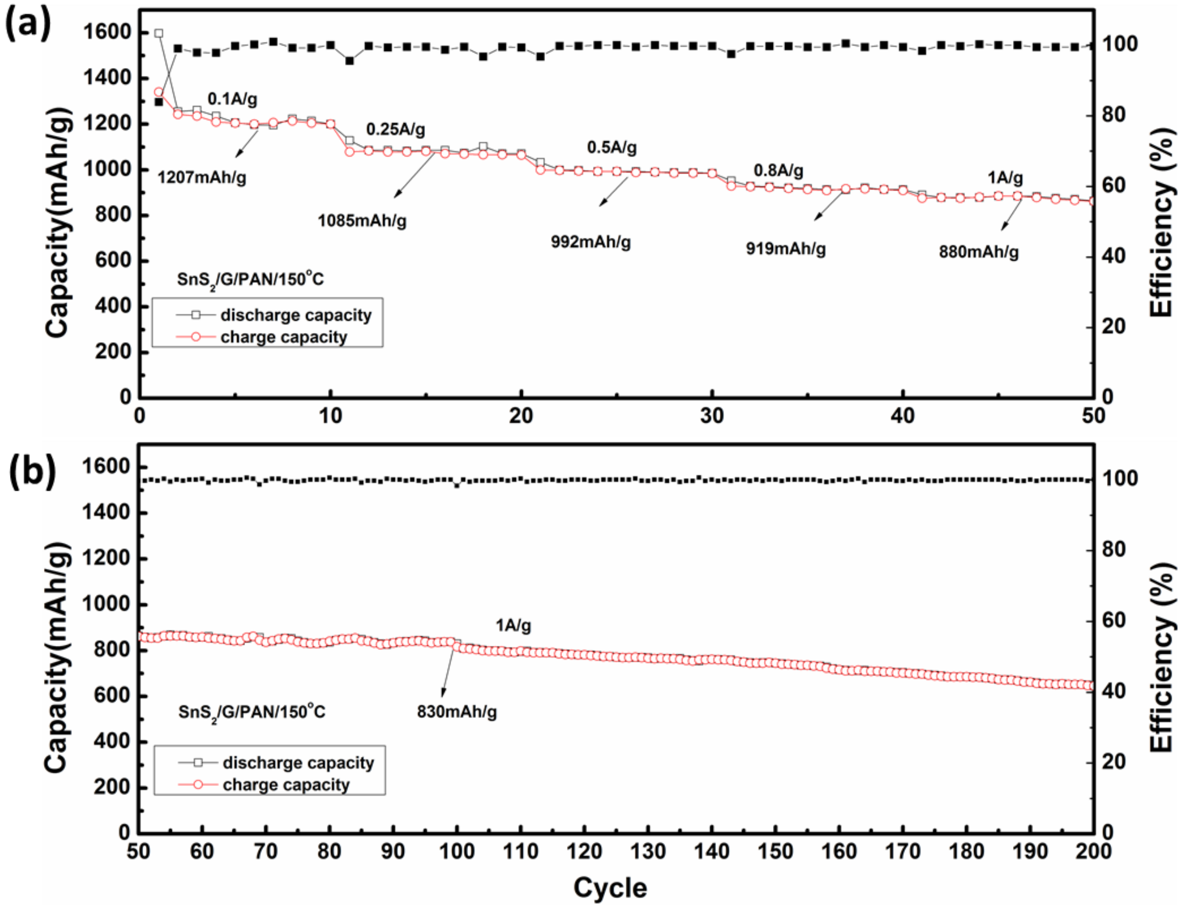

Figure 49: (a) (b) Rate capability of SnS_2/G/PAN with heat treatment (150 °C) followed by cycling capability.

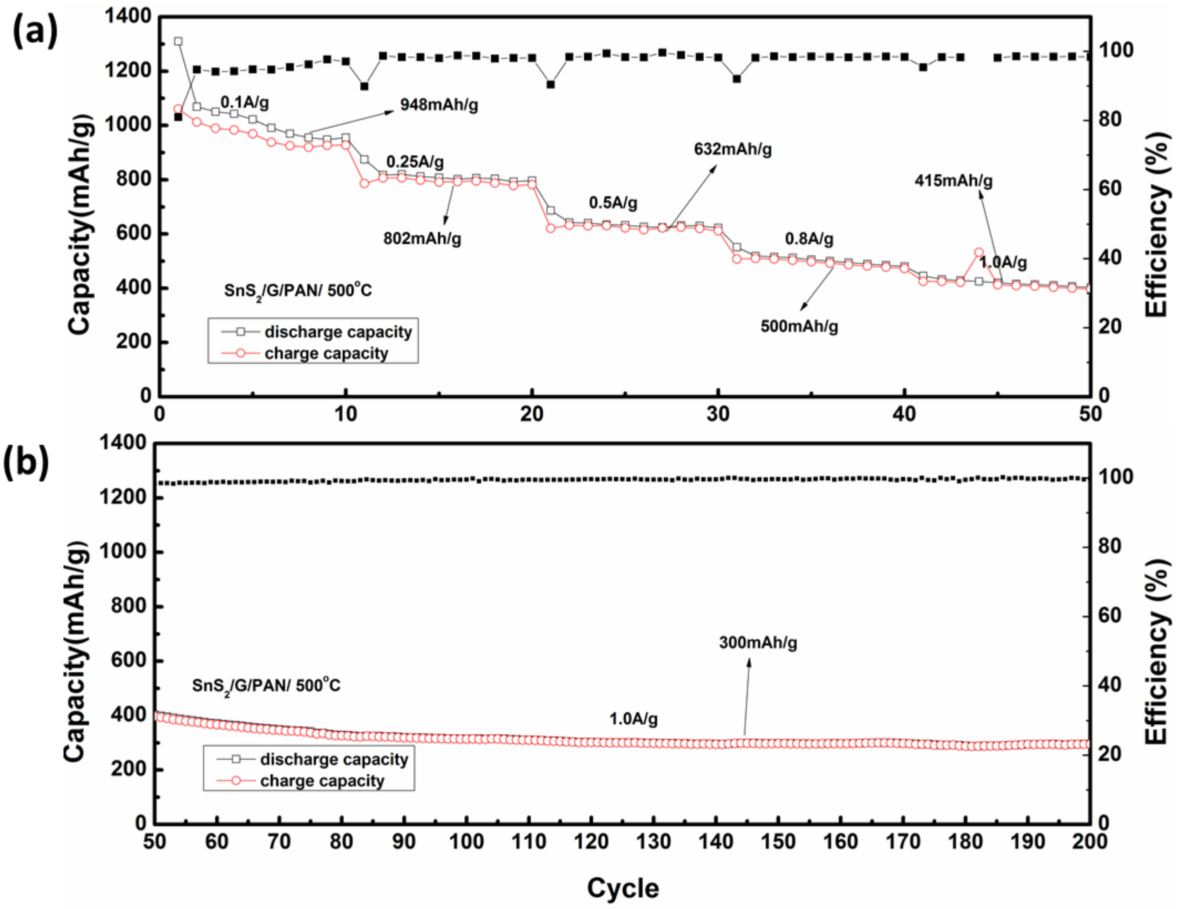

Figure 50: (a) (b) Rate capability of SnS$_2$/G/PAN with heat treatment (500 ^{o} C) followed by cycling capability

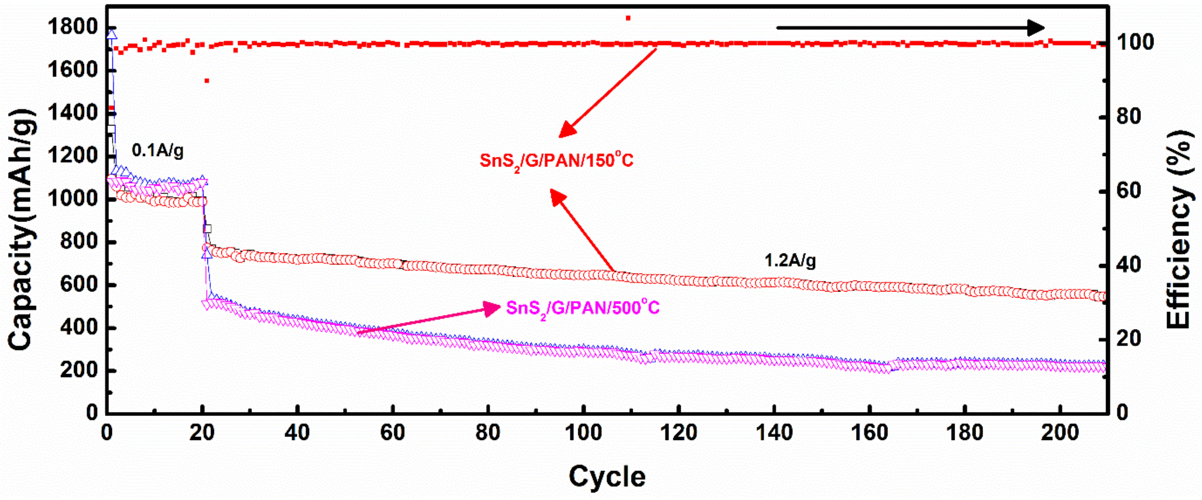

Figure 51: Cycling capability of SnS_2/G/PAN with heat treatment (150 °C, 500 °C) at high current density after 10 cycles at 0.1 A/g for SnS_2/G/PAN.

To understand the real battery performance of SnS_2/G, it is necessary to calculate the theoretical capacity for these hybrid composites. Firstly based on the traditional reaction mechanism, the theoretical capacity of SnS_2 is 645 mAh/g. Also, the capacity for graphene is considered as 457 mAh/g, which is estimated from the maximum charge capacity from **Figure 47d** .The percentage of graphene is 19.5% from TGA and SnS_2 occupies 80.5%. Then the theoretical capacity for SnS_2/G is obtained as the following shown:

$C_{\text{theoretical for SnS2/G}}$ = （C_{SnS2} * mass% of SnS_2) + (C_{Graphene}* mass % of Graphene) = 645* 0.805 + 457* 0.195= 608 mAh/g

However, the theoretical capacity is less than the observed ones (stable charge capacity observed in **Figure 47**) which are almost twice higher than this value: 1200 and 1020 mAh/g. It is pointed to a new reaction mechanism. Previous literature has shown that Li_2S are active in electrochemical performance.[125, 126] In this case, taking Li_2S into consideration, there should be a reversible capacity for Li_2S which represents a theoretical capacity for SnS_2 of 1231 mAh/g. [107, 127]Builted on this principle, there are increase in the theoretical capacities for SnS_2.[33] The theoretical capacity for SnS_2/G is the below shown:

$C_{\text{theoretical for SnS2/G}}$ = （C_{SnS2} * mass% of SnS_2) + (C_{Graphene}* mass % of Graphene) = 1231* 0.805 + 457* 0.195= 1079 mAh/g

This value gives a reasonable explanation for higher charge capacities of SnS_2 /G than traditional theoretical capacity. And it is proposed that the sulphur in SnS_2/G/PAN/150°C is totally reversibly reacted with lithium ions during the charging/discharging process (**Figure 47**).

To further approve the new mechanism for chemical reactions, cyclic voltammetry for SnS_2/G/PAN/150°C is used to explain the detailed procedure for lithium insertion and de- insertion as shown in **Figure 52**. During the first cycle, there are two reduction peaks at 1.26 V, 0.1 V. At 1.26 V, it is attributed to the decomposition of SnS_2, the formation of Li_2S. At 0.1 V, it means the alloy of lithium ions with metallic tin and the lithium storage for graphene layers. During the anodic sweep, the peak at 0.5 V represents the delithtiation of lithium alloy .There are another two peaks at 1.8, 2.2 V. The peak at 1.8 V is proposed the delithtiation of lithium sulfide and at 2.2 V, which is assigned the transformation from lithium sulfide to poly sulfides. These five peaks (two cathodic peaks and 3 anodic peaks) are unchanged from the second cycle,which is suggested the good stability of SnS_2/G/PAN/150 °C. The peak at 1.8 V in the anodic side is believed the delithiation of lithium sulfide and there is no loss in current compared with the first cycle, which confirms the proposal that the total sulphur in SnS_2/G/150 °C contributes to the reversible capacity.

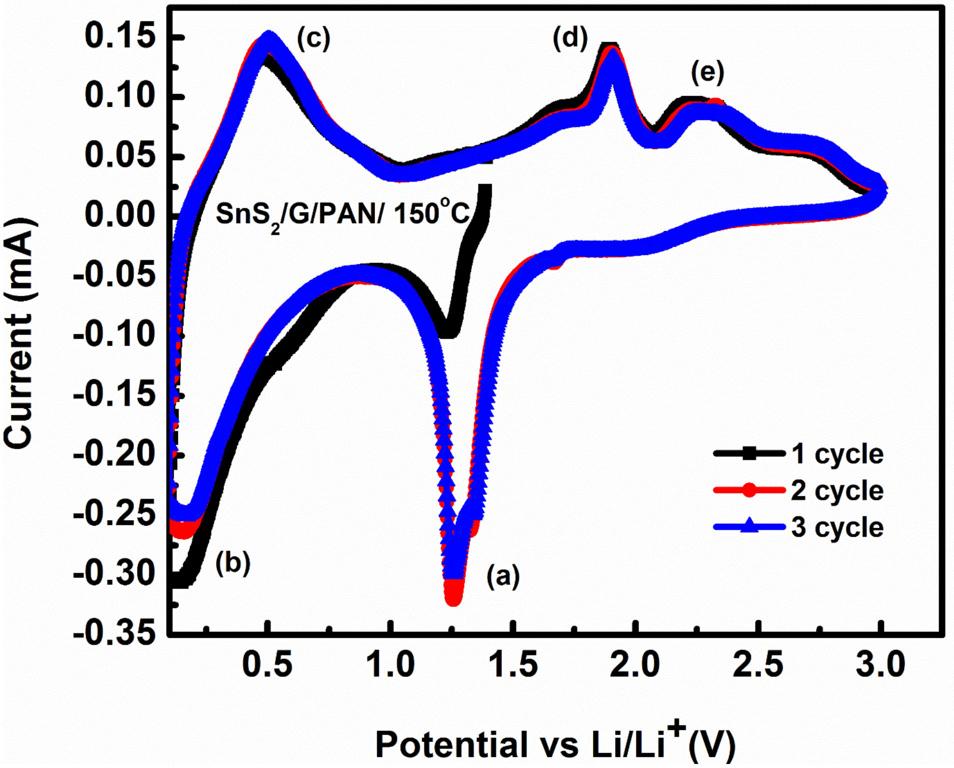

Figure 52: Cyclic voltammetry testing for SnS_2/G/PAN/150°C in a voltage range from 3 to 0.1V vs. Li/Li^+ at a scanning rate 0.1mV/s.

To understand the reason that the high rate capability of SnS_2/G/PAN/150°C, Nyquist plots were tested in a frequency range 1×10^{6} to 1×10^{-1} Hz and at the amplitude of 10mV after finishing 10 cycles with voltage 2.4V. It is shown in **Figure 53**, at high frequency range, there are two semicircles for SnS_2/G/PAN/150°C and SnS_2/G/PAN/500°C electrodes, which suggests the charge transfer resistance (Rct) and SEI resistance (R_{SEI}). In the low frequency range, the inclined curves are clearly observed, which demonstrates the Warburg impedance. It can be seen that the radius of SnS_2/G/PAN/150°C is smaller than that of SnS_2/G/PAN/500°C, which indicates lower Rct and R_{SEI} of SnS_2/G/PAN/150°C. This result matches the rate capabilities trend between these two types of electrodes.

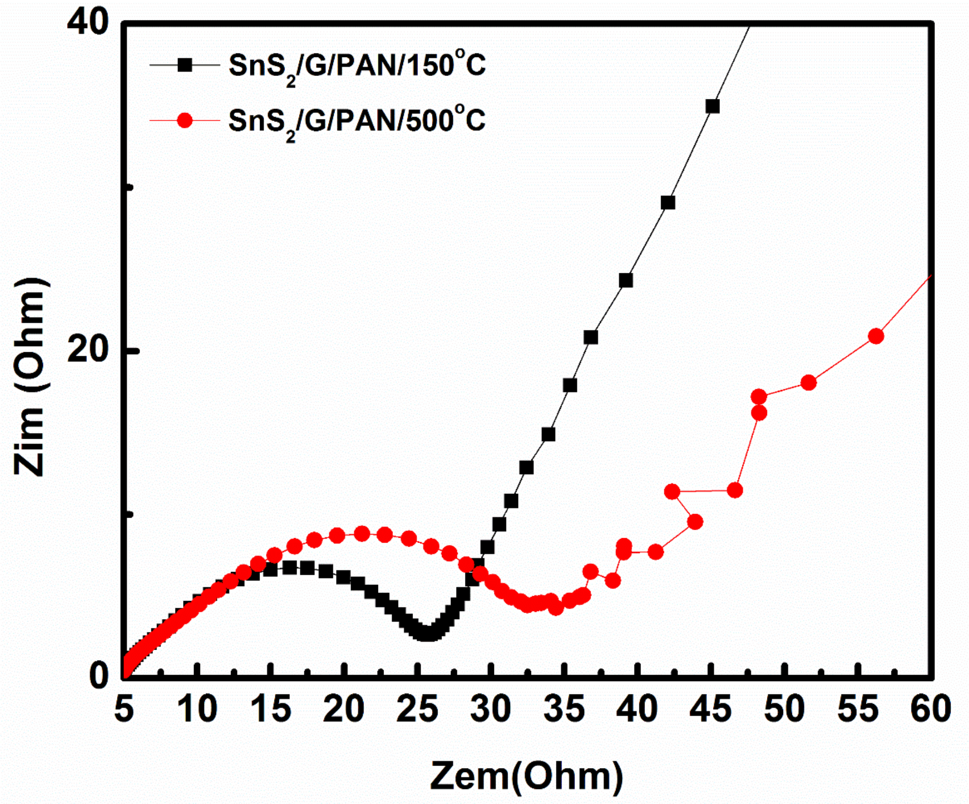

Figure 53: Electrochemical impedance spectroscopy (EIS) plots for SnS_2/G/PAN/150°C andSnS_2/G/PAN/500°C in a frequency range 1×10^6 to 1×10^{-1} Hz and at the amplitude of 10 mV after finishing 10 cycles with voltage 2.4 V.

Conclusion:

In this work, graphene is commonly used to improve the stability of SnS_2 nanostructures and PAN is unitized to optimize the electrode structure. Three temperatures for heat treatment are applied in the as- prepared electrodes: 80 degrees (normal drying temperature as comparison), 150 degrees (higher than the glass transition temperature PAN), 500 degrees (the temperature after carbonization of PAN and the phase transition temperature for SnS_2 to SnS). It is observed that SnS_2/G/PAN/150°C shows excellent electrochemical performance for the cooperation between PAN and graphene, which enhance the stability, and the function of sulphur in composites, which contributes to high capacity. More importantly, a unique reaction mechanism links the LIBs and lithium sulphur batteries, which open a new time for the investigation of metal sulfides material.

Chapter 5

Summary and Future work

5.1 Summary for tin based materials

Tin sulfides with graphene were prepared to investigate the electrochemical performances as anodes in lithium ion batteries. Initially, tin ion precursors were oxidized by graphene oxides and transferred to tin disulfides nanosheets. After that, it was annealed at controllable temperature to obtain tin sulfide nanorods chemically. In terms of initial capacity, cycle stability and rate capability, GSN-SnS demonstrates the best performance which is superior to the conventional graphite. It is observed that GSN-SnS shows around 1500 cycling performance which is considered as the longest cycles for tin sulfide materials compared with published papers. At the same time, the promising performance for GSN-SnS is attributed to the graphene layer, which provides the space for volume expansion. With the remarkable rate capability and cycle stability, the GSN-SnS composite is referred as highly promising anode electrode materials for next generation lithium ion batteries.

Additionally, the second work is focused on the design of the electrode based on the SnS_2/G synthesized by solvothermal method. Binder plays a significant role in this project. PAN works as polymer binder and conductive addictive, which mixed with active material followed by different temperature annealing. It is seen that SnS_2/G/PAN/150^oC with the rearrangement of the electrode exhibits the optimal performance, which is stable at 1200 mAh/g at 0.1 A/g and 1020 mAh/g at 0.25 A/g. It is attributed to the advantages of the flexible graphene. Also, the recombination of PAN with SnS_2 provides a beneficial room for the electron path. Moreover, from this study, a new mechanism is proposed and proved, which creates a bridge between lithium ion battery and sulphur battery. It also benefits the research on the reaction principle on metal chalcogenides as anode materials.

5.2 Future work

For future work, it is suggested as the following:

1. In terms of tin based material, it is meaningful to propose tin nanoparticles as anode for LIBs due to a high theoretical capacity for tin .Tin nanoparticles (<10nm) will decreases the negative effect on the large volume expansion, resulting in the enhanced stability.
2. For the research on the anode material, silicon is more interesting in practical applications for the highest theoretical capacity. Nevertheless, silicon has low conductivity, large volume expansion and the formation of SEI, which leads to a capacity fading. It is proposed that

combining commercial silicon nanoparticle with carbon nanotubes and cyclized PAN, which may introduce a robust new design for silicon electrodes.

3. Sulphur batteries are popular as cathode materials with the highest theoretical capacity, which is the optimal choice for cathode materials in silicon based batteries. There are three challenges for sulphur as cathode: low conductivity, the dissolution of sulphur in electrolyte, large volume expansion. It is suggested that synthesizing sulphur with conductive material. Then lilitiating the silicon electrode, assembling into full battery will lead to a jump in the improvement in the energy density.

References

1. Gao, M.-R., et al., *Nanostructured metal chalcogenides: synthesis, modification, and applications in energy conversion and storage devices.* Chemical Society Reviews, 2013. **42**(7): p. 2986-3017.
2. Arico, A.S., et al., *Nanostructured materials for advanced energy conversion and storage devices.* Nat Mater, 2005. **4**(5): p. 366-377.
3. Tarascon, J.M. and M. Armand, *Issues and challenges facing rechargeable lithium batteries.* Nature, 2001. **414**(6861): p. 359-367.
4. Armand, M. and J.M. Tarascon, *Building better batteries.* Nature, 2008. **451**(7179): p. 652-657.
5. Martin, C., *Driving change in the battery industry.* Nat Nano, 2014. **9**(5): p. 327-328.
6. WHITTINGHAM, M.S., *Electrical Energy Storage and Intercalation Chemistry.* Science, 1976. **192**(4244): p. 1126-1127.
7. Kasavajjula, U., C. Wang, and A.J. Appleby, *Nano- and bulk-silicon-based insertion anodes for lithium-ion secondary cells.* Journal of Power Sources, 2007. **163**(2): p. 1003-1039.
8. Yamada, A., S.C. Chung, and K. Hinokuma *Optimized LiFePO4 for Lithium Battery Cathodes.* Journal of The Electrochemical Society, 2001. **148**(3): p. A224-A229.
9. Yi, T.-F., et al., *Recent development and application of Li4Ti5O12 as anode material of lithium ion battery.* Journal of Physics and Chemistry of Solids, 2010. **71**(9): p. 1236-1242.
10. Yang, Z., et al., *Enabling renewable energy—and the future grid—with advanced electricity storage.* JOM, 2010. **62**(9): p. 14-23.
11. Armstrong, G., et al., *TiO2(B) Nanowires as an Improved Anode Material for Lithium-Ion Batteries Containing LiFePO4 or LiNi0.5Mn1.5O4 Cathodes and a Polymer Electrolyte.* Advanced Materials, 2006. **18**(19): p. 2597-2600.
12. Xiong, S., et al., *Characterization of solid electrolyte interphase on lithium electrodes cycled in ether-based electrolytes for lithium batteries.* Journal of Electroanalytical Chemistry, 2014. **719**(0): p. 122-126.
13. Zhang, S.S., *A review on electrolyte additives for lithium-ion batteries.* Journal of Power Sources, 2006. **162**(2): p. 1379-1394.
14. Ciosek Högström, K., et al., *Impact of the flame retardant additive triphenyl phosphate (TPP) on the performance of graphite/LiFePO4 cells in high power applications.* Journal of Power Sources, 2014. **256**(0): p. 430-439.
15. Etacheri, V., et al., *Challenges in the development of advanced Li-ion batteries: a review.* Energy & Environmental Science, 2011. **4**(9): p. 3243-3262.
16. Wu, H. and Y. Cui, *Designing nanostructured Si anodes for high energy lithium ion batteries.* Nano Today, 2012. **7**(5): p. 414-429.
17. Dahn, J.R., et al., *Mechanisms for lithium insertion in carbonaceous materials.* Science, 1995. **270**(5236): p. 590-598.
18. Flandrois, S., et al., *Intercalation compounds of graphite with nickel chloride: synthesis, structure, and mechanism of intercalation.* Synthetic Metals, 1981. **3**(1–2): p. 1-13.
19. Derrien, G., et al., *Nanostructured Sn–C Composite as an Advanced Anode Material in High-Performance Lithium-Ion Batteries.* Advanced Materials, 2007. **19**(17): p. 2336-2340.

20. Zhang, W.-M., et al., *Tin-Nanoparticles Encapsulated in Elastic Hollow Carbon Spheres for High-Performance Anode Material in Lithium-Ion Batteries.* Advanced Materials, 2008. **20**(6): p. 1160-1165.
21. Hassoun, J., et al., *A New, Safe, High-Rate and High-Energy Polymer Lithium-Ion Battery.* Advanced Materials, 2009. **21**(47): p. 4807-4810.
22. Xu, Y., J. Guo, and C. Wang, *Sponge-like porous carbon/tin composite anode materials for lithium ion batteries.* Journal of Materials Chemistry, 2012. **22**(19): p. 9562-9567.
23. Idota, Y., et al., *Tin-Based Amorphous Oxide: A High-Capacity Lithium-Ion-Storage Material.* Science, 1997. **276**(5317): p. 1395-1397.
24. Kim, H., et al., *Scalable Functionalized Graphene Nano-platelets as Tunable Cathodes for High-performance Lithium Rechargeable Batteries.* Sci. Rep., 2013. **3**.
25. Winter, M. and J.O. Besenhard, *Electrochemical lithiation of tin and tin-based intermetallics and composites.* Electrochimica Acta, 1999. **45**(1–2): p. 31-50.
26. Lee, K.T., Y.S. Jung, and S.M. Oh, *Synthesis of Tin-Encapsulated Spherical Hollow Carbon for Anode Material in Lithium Secondary Batteries.* Journal of the American Chemical Society, 2003. **125**(19): p. 5652-5653.
27. Kim, I.-s., G.E. Blomgren, and P.N. Kumta, *Sn/C Composite Anodes for Li-Ion Batteries.* Electrochemical and Solid-State Letters, 2004. **7**(3): p. A44-A48.
28. Yu, Y., et al., *Tin Nanoparticles Encapsulated in Porous Multichannel Carbon Microtubes: Preparation by Single-Nozzle Electrospinning and Application as Anode Material for High-Performance Li-Based Batteries.* Journal of the American Chemical Society, 2009. **131**(44): p. 15984-15985.
29. Goodenough, J.B. and K.-S. Park, *The Li-Ion Rechargeable Battery: A Perspective.* Journal of the American Chemical Society, 2013. **135**(4): p. 1167-1176.
30. Li, H., et al., *Nano-alloy anode for lithium ion batteries.* Solid State Ionics, 2002. **148**(3–4): p. 247-258.
31. Xu, X., et al., *Nanostructured transition metal sulfides for lithium ion batteries: Progress and challenges.* Nano Today, 2014. **9**(5): p. 604-630.
32. Magasinski, A., et al., *High-performance lithium-ion anodes using a hierarchical bottom-up approach.* Nat Mater, 2010. **9**(4): p. 353-358.
33. Zhang, M., et al., *Graphene oxide oxidizes stannous ions to synthesize tin sulfide-graphene nanocomposites with small crystal size for high performance lithium ion batteries.* Journal of Materials Chemistry, 2012. **22**(43): p. 23091-23097.
34. Luo, B., et al., *Two dimensional graphene-SnS2 hybrids with superior rate capability for lithium ion storage.* Energy & Environmental Science, 2012. **5**(1): p. 5226-5230.
35. Cai, J., Z. Li, and P.K. Shen, *Porous SnS Nanorods/Carbon Hybrid Materials as Highly Stable and High Capacity Anode for Li-Ion Batteries.* ACS Applied Materials & Interfaces, 2012. **4**(8): p. 4093-4098.
36. Xu, J., et al., *Cathode materials for next generation lithium ion batteries.* Nano Energy, 2013. **2**(4): p. 439-442.
37. Winter, M. and R.J. Brodd, *What Are Batteries, Fuel Cells, and Supercapacitors?* Chemical Reviews, 2004. **104**(10): p. 4245-4270.
38. Cheng, F., et al., *Template-Directed Materials for Rechargeable Lithium-Ion Batteries†.* Chemistry of Materials, 2008. **20**(3): p. 667-681.

39. Nishi, Y., *The development of lithium ion secondary batteries.* The Chemical Record, 2001. **1**(5): p. 406-413.
40. Bhardwaj, T., et al., *Enhanced Electrochemical Lithium Storage by Graphene Nanoribbons.* Journal of the American Chemical Society, 2010. **132**(36): p. 12556-12558.
41. Yazami, R. and P. Touzain, *A reversible graphite-lithium negative electrode for electrochemical generators.* Journal of Power Sources, 1983. **9**(3): p. 365-371.
42. Clarke, R. and C. Uher, *High pressure properties of graphite and its intercalation compounds.* Advances in Physics, 1984. **33**(5): p. 469-566.
43. Inaba, M., *SECONDARY BATTERIES – LITHIUM RECHARGEABLE SYSTEMS – LITHIUM-ION | Negative Electrodes: Graphite*, in *Encyclopedia of Electrochemical Power Sources*, J. Garche, Editor 2009, Elsevier: Amsterdam. p. 198-208.
44. Peled, E., et al., *Improved Graphite Anode for Lithium ‐ Ion Batteries Chemically: Bonded Solid electrolyte interphase and Nanochannel Formation.* Journal of The Electrochemical Society, 1996. **143**(1): p. L4-L7.
45. Basu, S., et al., *Synthesis and properties of lithium-graphite intercalation compounds.* Materials Science and Engineering, 1979. **38**(3): p. 275-283.
46. Cui, G., et al., *A Germanium–Carbon Nanocomposite Material for Lithium Batteries.* Advanced Materials, 2008. **20**(16): p. 3079-3083.
47. Holzapfel, M., et al., *A new type of nano-sized silicon/carbon composite electrode for reversible lithium insertion.* Chemical Communications, 2005(12): p. 1566-1568.
48. Cui, G., et al., *A novel germanium/carbon nanotubes nanocomposite for lithium storage material.* Electrochimica Acta, 2010. **55**(3): p. 985-988.
49. Kim, H.S., K.Y. Chung, and B.W. Cho, *Electrochemical properties of carbon-coated Si/B composite anode for lithium ion batteries.* Journal of Power Sources, 2009. **189**(1): p. 108-113.
50. Zuo, P. and G. Yin, *Si–Mn composite anodes for lithium ion batteries.* Journal of Alloys and Compounds, 2006. **414**(1–2): p. 265-268.
51. Zheng, Y., et al., *Nano-porous Si/C composites for anode material of lithium-ion batteries.* Electrochimica Acta, 2007. **52**(19): p. 5863-5867.
52. Zhang, X.N., et al., *Si–Si3N4 composites as anode materials for lithium ion batteries.* Solid State Ionics, 2007. **178**(15–18): p. 1107-1112.
53. Thackeray, M.M., et al., *Lithium insertion into manganese spinels.* Materials Research Bulletin, 1983. **18**(4): p. 461-472.
54. Lazzari, M. and B. Scrosati, *A Cyclable Lithium Organic Electrolyte Cell Based on Two Intercalation Electrodes.* Journal of The Electrochemical Society, 1980. **127**(3): p. 773-774.
55. Wu, H., et al., *Stable cycling of double-walled silicon nanotube battery anodes through solid-electrolyte interphase control.* Nat Nano, 2012. **7**(5): p. 310-315.
56. Youn, D.-Y., et al., *Facile Synthesis of Highly Conductive RuO2-Mn3O4 Composite Nanofibers via Electrospinning and Their Electrochemical Properties.* Journal of The Electrochemical Society, 2011. **158**(8): p. A970-A975.
57. Wang, J.-G., et al., *Synthesis and electrochemical performance of MnO2/CNTs–embedded carbon nanofibers nanocomposites for supercapacitors.* Electrochimica Acta, 2012. **75**(0): p. 213-219.

58. Hashem, A.M., et al., *Table sugar as preparation and carbon coating reagent for facile synthesis and coating of rod-shaped MnO2.* Journal of Alloys and Compounds, 2010. **497**(1–2): p. 300-303.
59. Han, H., et al., *Nitridated TiO2 hollow nanofibers as an anode material for high power lithium ion batteries.* Energy & Environmental Science, 2011. **4**(11): p. 4532-4536.
60. Ryu, W.-H., et al., *Electrochemical performance of a smooth and highly ordered TiO2 nanotube electrode for Li-ion batteries.* Electrochimica Acta, 2012. **61**(0): p. 19-24.
61. Poizot, P., et al., *Nano-sized transition-metal oxides as negative-electrode materials for lithium-ion batteries.* Nature, 2000. **407**(6803): p. 496-499.
62. Dhanabalan, A., *Tin oxide based composites derived using electrostatic spray deposition technique as anodes for lithium-ion batteries*, 2012, Florida International University: Ann Arbor. p. 112.
63. Goriparti, S., et al., *Review on recent progress of nanostructured anode materials for Li-ion batteries.* Journal of Power Sources, 2014. **257**(0): p. 421-443.
64. Zhao, X., C.M. Hayner, and H.H. Kung, *Self-assembled lithium manganese oxide nanoparticles on carbon nanotube or graphene as high-performance cathode material for lithium-ion batteries.* Journal of Materials Chemistry, 2011. **21**(43): p. 17297-17303.
65. Ammundsen, B. and J. Paulsen, *Novel Lithium-Ion Cathode Materials Based on Layered Manganese Oxides.* Advanced Materials, 2001. **13**(12-13): p. 943-956.
66. Li, C., et al., *Cathode materials modified by surface coating for lithium ion batteries.* Electrochimica Acta, 2006. **51**(19): p. 3872-3883.
67. Fergus, J.W., *Recent developments in cathode materials for lithium ion batteries.* Journal of Power Sources, 2010. **195**(4): p. 939-954.
68. Shi, Y., et al., *Graphene wrapped LiFePO4/C composites as cathode materials for Li-ion batteries with enhanced rate capability.* Journal of Materials Chemistry, 2012. **22**(32): p. 16465-16470.
69. Wu, X.-L., et al., *Carbon-Nanotube-Decorated Nano-LiFePO4 @C Cathode Material with Superior High-Rate and Low-Temperature Performances for Lithium-Ion Batteries.* Advanced Energy Materials, 2013. **3**(9): p. 1155-1160.
70. Lung-Hao Hu, B., et al., *Graphene-modified LiFePO4 cathode for lithium ion battery beyond theoretical capacity.* Nat Commun, 2013. **4**: p. 1687.
71. Yang, S., P.Y. Zavalij, and M. Stanley Whittingham, *Hydrothermal synthesis of lithium iron phosphate cathodes.* Electrochemistry Communications, 2001. **3**(9): p. 505-508.
72. Chen, J. and M.S. Whittingham, *Hydrothermal synthesis of lithium iron phosphate.* Electrochemistry Communications, 2006. **8**(5): p. 855-858.
73. Patoux, S., et al., *High voltage nickel manganese spinel oxides for Li-ion batteries.* Electrochimica Acta, 2008. **53**(12): p. 4137-4145.
74. Lin, B., et al., *LiMn2O4 nanoparticles anchored on graphene nanosheets as high-performance cathode material for lithium-ion batteries.* Journal of Solid State Chemistry, 2014. **209**(0): p. 23-28.
75. Wang, D., et al., *[small beta]-MnO2 as a cathode material for lithium ion batteries from first principles calculations.* Physical Chemistry Chemical Physics, 2013. **15**(23): p. 9075-9083.

76. Mizushima, K., et al., *LixCoO2 (0<x<-1): A new cathode material for batteries of high energy density.* Materials Research Bulletin, 1980. **15**(6): p. 783-789.
77. Amatucci, G.G., J.M. Tarascon, and L.C. Klein, *CoO2, The End Member of the Li x CoO2 Solid Solution.* Journal of The Electrochemical Society, 1996. **143**(3): p. 1114-1123.
78. Whittingham, M.S., *Lithium Batteries and Cathode Materials.* Chemical Reviews, 2004. **104**(10): p. 4271-4302.
79. Malik, R., et al., *Particle Size Dependence of the Ionic Diffusivity.* Nano Letters, 2010. **10**(10): p. 4123-4127.
80. Chung, S.-Y., J.T. Bloking, and Y.-M. Chiang, *Electronically conductive phospho-olivines as lithium storage electrodes.* Nat Mater, 2002. **1**(2): p. 123-128.
81. Tarascon, J.M., et al., *Synthesis Conditions and Oxygen Stoichiometry Effects on Li Insertion into the Spinel LiMn2 O 4.* Journal of The Electrochemical Society, 1994. **141**(6): p. 1421-1431.
82. Thackeray, M.M., *Manganese oxides for lithium batteries.* Progress in Solid State Chemistry, 1997. **25**(1–2): p. 1-71.
83. Yonemura, M., et al., *Synthesis, structure, and phase relationship in lithium manganese oxide spinel.* Journal of Materials Chemistry, 2004. **14**(13): p. 1948-1958.
84. Du Pasquier, A., et al., *Mechanism for Limited 55°C Storage Performance of Li1.05Mn1.95 O 4 Electrodes.* Journal of The Electrochemical Society, 1999. **146**(2): p. 428-436.
85. Ohzuku, T., S. Takeda, and M. Iwanaga, *Solid-state redox potentials for Li[Me1/2Mn3/2]O4 (Me: 3d-transition metal) having spinel-framework structures: a series of 5 volt materials for advanced lithium-ion batteries.* Journal of Power Sources, 1999. **81–82**(0): p. 90-94.
86. Sigala, C., et al., *Positive electrode materials with high operating voltage for lithium batteries: LiCryMn2 − yO4 (0 ⩽y ⩽1).* Solid State Ionics, 1995. **81**(3–4): p. 167-170.
87. Arillo, M.A., et al., *Structural characterisation and physical properties of LiMMnO4 (M=Cr, Ti) spinels.* Solid State Sciences, 2005. **7**(1): p. 25-32.
88. Fang, H., et al., *High performance LiNi0.5Mn1.5O4 cathode materials synthesized by a combinational annealing method.* Electrochemistry Communications, 2007. **9**(5): p. 1077-1082.
89. Mukai, K., et al., *The gradient distribution of Ni ions in cation-disordered Li[Ni1/2Mn3/2]O4 clarified by muon-spin rotation and relaxation ([small mu]SR).* RSC Advances, 2013. **3**(29): p. 11634-11639.
90. Gewirth, A.A. and M.S. Thorum, *Electroreduction of Dioxygen for Fuel-Cell Applications: Materials and Challenges.* Inorganic Chemistry, 2010. **49**(8): p. 3557-3566.
91. Gao, M.-R., J. Jiang, and S.-H. Yu, *Catalysis: Solution-Based Synthesis and Design of Late Transition Metal Chalcogenide Materials for Oxygen Reduction Reaction (ORR) (Small 1/2012).* Small, 2012. **8**(1): p. 12-12.
92. Feng, Y. and N. Alonso-Vante, *Nonprecious metal catalysts for the molecular oxygen-reduction reaction.* physica status solidi (b), 2008. **245**(9): p. 1792-1806.
93. Hwang, H., H. Kim, and J. Cho, *MoS2 Nanoplates Consisting of Disordered Graphene-like Layers for High Rate Lithium Battery Anode Materials.* Nano Letters, 2011. **11**(11): p. 4826-4830.
94. Lai, C.-H., M.-Y. Lu, and L.-J. Chen, *Metal sulfide nanostructures: synthesis, properties and applications in energy conversion and storage.* Journal of Materials Chemistry, 2012. **22**(1): p. 19-30.

95. Im, H.S., et al., *Phase Evolution of Tin Nanocrystals in Lithium Ion Batteries.* ACS Nano, 2013. **7**(12): p. 11103-11111.
96. Su, Y., et al., *Low-temperature synthesis of nitrogen/sulfur co-doped three-dimensional graphene frameworks as efficient metal-free electrocatalyst for oxygen reduction reaction.* Carbon, 2013. **62**(0): p. 296-301.
97. Wang, Y., et al., *Nitrogen-Doped Graphene and Its Application in Electrochemical Biosensing.* ACS Nano, 2010. **4**(4): p. 1790-1798.
98. Yun, Y.S., et al., *Effects of sulfur doping on graphene-based nanosheets for use as anode materials in lithium-ion batteries.* Journal of Power Sources, 2014. **262**(0): p. 79-85.
99. Zhou, T., et al., *Enhanced Sodium-Ion Battery Performance by Structural Phase Transition from Two-Dimensional Hexagonal-SnS2 to Orthorhombic-SnS.* ACS Nano, 2014. **8**(8): p. 8323-8333.
100. Zhang, M., et al., *Fast synthesis of SnO2/graphene composites by reducing graphene oxide with stannous ions.* Journal of Materials Chemistry, 2011. **21**(6): p. 1673-1676.
101. Liu, S., et al., *Synthesis of self-assembled 3D flowerlike SnS2 nanostructures with enhanced lithium ion storage property.* Solid State Sciences, 2010. **12**(5): p. 712-718.
102. Ferrari, A.C., et al., *Raman Spectrum of Graphene and Graphene Layers.* Physical Review Letters, 2006. **97**(18): p. 187401.
103. Lin, W., et al., *Microwave Makes Carbon Nanotubes Less Defective.* ACS Nano, 2010. **4**(3): p. 1716-1722.
104. Yang, Z., et al., *Sulfur-Doped Graphene as an Efficient Metal-free Cathode Catalyst for Oxygen Reduction.* ACS Nano, 2012. **6**(1): p. 205-211.
105. Yang, S., et al., *Efficient Synthesis of Heteroatom (N or S)-Doped Graphene Based on Ultrathin Graphene Oxide-Porous Silica Sheets for Oxygen Reduction Reactions.* Advanced Functional Materials, 2012. **22**(17): p. 3634-3640.
106. Yin, J., et al., *SnS2@reduced graphene oxide nanocomposites as anode materials with high capacity for rechargeable lithium ion batteries.* Journal of Materials Chemistry, 2012. **22**(45): p. 23963-23970.
107. Kim, T.-J., et al., *Novel SnS2-nanosheet anodes for lithium-ion batteries.* Journal of Power Sources, 2007. **167**(2): p. 529-535.
108. Kim, H.S., et al., *Electrochemical behavior of carbon-coated SnS2 for use as the anode in lithium-ion batteries.* Electrochimica Acta, 2009. **54**(13): p. 3606-3610.
109. Koo, B., et al., *A Highly Cross-Linked Polymeric Binder for High-Performance Silicon Negative Electrodes in Lithium Ion Batteries.* Angewandte Chemie International Edition, 2012. **51**(35): p. 8762-8767.
110. Hassan, F.M., et al., *Sn/SnO2 embedded in mesoporous carbon nanocomposites as negative electrode for lithium ion batteries.* Electrochimica Acta, 2013. **87**(0): p. 844-852.
111. Liao, J.-Y., et al., *Multifunctional TiO2–C/MnO2 Core–Double-Shell Nanowire Arrays as High-Performance 3D Electrodes for Lithium Ion Batteries.* Nano Letters, 2013. **13**(11): p. 5467-5473.
112. Machado, B.F. and P. Serp, *Graphene-based materials for catalysis.* Catalysis Science & Technology, 2012. **2**(1): p. 54-75.
113. Liao, J.-Y., et al., *Hierarchical Li4Ti5O12-TiO2 composite microsphere consisting of nanocrystals for high power Li-ion batteries.* Electrochimica Acta, 2013. **108**(0): p. 104-111.

114. Liu, S., et al., *Preferential c-Axis Orientation of Ultrathin SnS2 Nanoplates on Graphene as High-Performance Anode for Li-Ion Batteries.* ACS Applied Materials & Interfaces, 2013. **5**(5): p. 1588-1595.
115. Yella, A., et al., *Synthesis of Fullerene- and Nanotube-Like SnS2 Nanoparticles and Sn/S/Carbon Nanocomposites.* Chemistry of Materials, 2009. **21**(12): p. 2474-2481.
116. Rui, X., H. Tan, and Q. Yan, *Nanostructured metal sulfides for energy storage.* Nanoscale, 2014. **6**(17): p. 9889-9924.
117. Zhu, Y., et al., *Microwave assisted exfoliation and reduction of graphite oxide for ultracapacitors.* Carbon, 2010. **48**(7): p. 2118-2122.
118. Zhu, Y., et al., *Exfoliation of Graphite Oxide in Propylene Carbonate and Thermal Reduction of the Resulting Graphene Oxide Platelets.* ACS Nano, 2010. **4**(2): p. 1227-1233.
119. Lee, C., et al., *Measurement of the Elastic Properties and Intrinsic Strength of Monolayer Graphene.* Science, 2008. **321**(5887): p. 385-388.
120. Wu, Q., et al., *One-pot synthesis of three-dimensional SnS2 hierarchitectures as anode material for lithium-ion batteries.* Journal of Power Sources, 2013. **239**(0): p. 89-93.
121. Sathish, M., et al., *Ultrathin SnS2 Nanoparticles on Graphene Nanosheets: Synthesis, Characterization, and Li-Ion Storage Applications.* The Journal of Physical Chemistry C, 2012. **116**(23): p. 12475-12481.
122. Hassan, F.M., et al., *Engineered Si Electrode Nanoarchitecture: A Scalable Postfabrication Treatment for the Production of Next-Generation Li-Ion Batteries.* Nano Letters, 2014. **14**(1): p. 277-283.
123. Xu, Y., et al., *Uniform Nano-Sn/C Composite Anodes for Lithium Ion Batteries.* Nano Letters, 2013. **13**(2): p. 470-474.
124. Wang, J., et al., *Solid-State Fabrication of SnS2/C Nanospheres for High-Performance Sodium Ion Battery Anode.* ACS Applied Materials & Interfaces, 2015.
125. Wang, J., et al., *Sulfur Composite Cathode Materials for Rechargeable Lithium Batteries.* Advanced Functional Materials, 2003. **13**(6): p. 487-492.
126. Ji, L., et al., *Graphene Oxide as a Sulfur Immobilizer in High Performance Lithium/Sulfur Cells.* Journal of the American Chemical Society, 2011. **133**(46): p. 18522-18525.
127. Yang, Y., et al., *New Nanostructured Li2S/Silicon Rechargeable Battery with High Specific Energy.* Nano Letters, 2010. **10**(4): p. 1486-1491.